Copyright Warning & Restrictions

The copyright law of the United States (Title 17, United States Code) governs the making of photocopies or other reproductions of copyrighted material.

Under certain conditions specified in the law, libraries and archives are authorized to furnish a photocopy or other reproduction. One of these specified conditions is that the photocopy or reproduction is not to be "used for any purpose other than private study, scholarship, or research." If a, user makes a request for, or later uses, a photocopy or reproduction for purposes in excess of "fair use" that user may be liable for copyright infringement,

This institution reserves the right to refuse to accept a copying order if, in its judgment, fulfillment of the order would involve violation of copyright law.

Please Note: The author retains the copyright while the New Jersey Institute of Technology reserves the right to distribute this thesis or dissertation

Printing note: If you do not wish to print this page, then select "Pages from: first page # to: last page #" on the print dialog screen

NJIT New Jersey's Science & Technology University

The Van Houten library has removed some of the personal information and all signatures from the approval page and biographical sketches of theses and dissertations in order to protect the identity of NJIT graduates and faculty.

ABSTRACT

TOWARDS QUALITY BY DESIGN (QbD) OF PHARMACEUTICAL ORAL FILMS LOADED WITH POORLY WATER-SOLUBLE DRUGS

by
Eylul Cetindag

Oral films are an emerging drug delivery dosage form with numerous advantages such as ease of handling, the possibility to circumvent the first-pass metabolism, better patient compliance, capability for continuous manufacturing, and as a platform for personalized medicine. As films are different from other final dosages by their dimensions and their matrix form, further research is required to better understand the impact of excipient and drug on product performance to assure a consistent and good quality product. Therefore, this dissertation aims to contribute towards the processability and manufacturability of films by examining the impact of the materials and processes. First, the effect of solvent, and cellulosic polymers on solution-cast film critical quality attributes (CQAs) is investigated. The recrystallization of the drug is observed after processing and affected by its solubility in the solvent more than the polymer type. The CQAs are greatly impacted by the extent of drug recrystallization. An inversely linear correlation is found between recrystallization and supersaturation performance. Most interestingly, the films with low initial crystallinity do not guarantee stability, and uncontrolled recrystallization and poor time stability appear to be unavoidable for solution-cast films. Next, a long-standing challenge of bioavailability enhancement of the films loaded with a poorly water-soluble drug at high drug loadings is investigated via two different techniques: slurry and solution casting.

Unfortunately, the solubility enhancement advantage of solution casting is negated by uncontrolled drug recrystallization. Thus, slurry-cast films are found to potentially outperform solution-cast films for dissolution performance at high drug loadings (> 10 wt%) and provide a stability advantage. Another unsolved formulation problem, the combined effect of particle size and loading of a poorly water-soluble drug on slurry cast film CQAs, is investigated next. The results confirm the hypothesis that as particle size decreases, the increased number of particles in the film changes the structure of the polymer matrix. Altered matrix adversely impacts the dissolution rate as a function of drug loading due to enhanced mechanical properties. Towards practical aspects such as manufacturability, drying of films, one of the most important pharmaceutical film process steps, is investigated to identify the impact of critical process parameters (CPPs). The CPPs for different drying modes (convection, conduction, and IR) are assessed through drying kinetics analysis. The effect of humidity on the drying rate is found to be as strong as air velocity along with temperature, and IR lamp power. In addition, the importance of solid-state characterization for process optimization is revealed. Towards product quality testing and assurance, Near-IR Spectroscopy is successfully evaluated for in-line monitoring of the thickness of poorly water-soluble drug-loaded polymeric films. Drug particle size and surface modification via dry coating of the drug particles are identified as key parameters that impact product quality, including film thickness and its variation. A major outcome is that smaller and/or dry coated particles lead to more uniform films as well as enabling better prediction of the thickness.

TOWARDS QUALITY BY DESIGN (QbD) OF PHARMACEUTICAL ORAL FILMS LOADED WITH POORLY WATER-SOLUBLE DRUGS

by
Eylul Cetindag

A Dissertation
Submitted to the Faculty of
New Jersey Institute of Technology
in Partial Fulfillment of the Requirements for the Degree of
Doctor of Philosophy in Chemical Engineering

Department of Chemical and Materials Engineering

August 2021

Copyright © 2021 by Eylul Cetindag

ALL RIGHTS RESERVED

.

APPROVAL PAGE

**TOWARDS QUALITY BY DESIGN (QbD)
OF PHARMACEUTICAL ORAL FILMS LOADED WITH POORLY WATER-SOLUBLE DRUGS**

Eylul Cetindag

Dr. Rajesh N. Davé, Dissertation Advisor — Date
Distinguished Professor of Chemical and Materials Engineering, NJIT

Dr. Ecevit A. Bilgili, Committee Member — Date
Associate Professor of Chemical and Materials Engineering, NJIT

Dr. Kathleen McEnnis, Committee Member — Date
Assistant Professor of Chemical and Materials Engineering, NJIT

Dr. Xiaoyang Xu, Committee Member — Date
Associate Professor of Chemical and Materials Engineering, NJIT

Dr. Rodolfo J. Romanach, Committee Member — Date
Professor of Chemistry, University of Puerto Rico at Mayagüez (UPRM), Puerto Rico

BIOGRAPHICAL SKETCH

Author: Eylul Cetindag

Degree: Doctor of Philosophy

Date: August 2021

Undergraduate and Graduate Education:

- Doctor of Philosophy in Chemical Engineering,
  New Jersey Institute of Technology, Newark, NJ, 2021

- Master of Science in Micro and Nano Technology,
  TOBB University of Economy and Technology, Ankara, Turkey, 2015

- Bachelor of Science in Food Engineering,
  Hacettepe University, Ankara, Turkey, 2012

Major: Chemical Engineering

Publications:

Cetindag, Eylul, Guluzar Gorkem Buyukgoz, Prarthana Manoj Rajai, Francis J. Garvey, Rodolfo J. Romañach, Rajesh N. Davé.“In-line Thickness Analysis via Near-IR Spectroscopy on Strip Films Loaded with Surface-Modified Poorly Water-Soluble Drug” In preparation.

Cetindag, Eylul, Rajesh N. Davé. “Effect of Particle Size and Drug Loading on Critical Quality Attributes of Polymeric Films Loaded with Poorly Water-Soluble Drug” In preparation.

Cetindag, Eylul, John Pentangelo, Lu Zhang, Honghao Lin, and Rajesh N. Davé. "Comparison of Solution Film and Slurry Films: Surface Modified Micronized Drug Particles, Nanoparticles, Amorphous Drug at High Drug Loadings." In preparation.

Dave, Rajesh N., Lu Zhang, Guluzar Gorkem, and Eylul Cetindag. "Compositions and Methods for Preparing Polymeric Films Loaded with Uniformly Distributed Drug Particles." U.S. Patent Application 16/150,931, issued February 16, 2021.

Cetindag, Eylul, John Pentangelo, Thierry Arrieta Cespedes, and Rajesh N. Davé. "Effect of Solvents and Cellulosic Polymers on Quality Attributes of Films Loaded with a Poorly Water-Soluble Drug." Carbohydrate Polymers (2020): 117012.

Patki, Manali, Richa Vartak, Joseph Jablonski, Sonia Mediouni, Tasneem Gandhi, Yige Fu, Eylul Cetindag, Rajesh Dave, Susana T. Valente, and Ketan Patel. "Efavirenz Nanomicelles Loaded Vaginal Film (EZ film) for Preexposure Prophylaxis (PrEP) of HIV." Colloids and Surfaces B: Biointerfaces (2020): 111174.

Naseri, Alireza T., Eylul Cetindag, Ecevit Bilgili, and Rajesh N. Davé. "A Predictive Transport Model for Convective Drying of Polymer Strip Films Loaded with a BCS Class II Drug." European Journal of Pharmaceutics and Biopharmaceutics 137 (2019): 164-174.

Naseri, Alireza T.*, Eylul Cetindag*, Joseph Forte, Ecevit Bilgili, and Rajesh N. Davé. "Convective Drying Kinetics of Polymer Strip Films Loaded with a BCS Class II Drug." AAPS PharmSciTech 20, no. 2 (2019): 40. (*Authors contributed equally to this work.)

To my family

ACKNOWLEDGMENT

I would like to extend my sincere gratitude to my dissertation advisor, Dr. Rajesh N. Davé, for his continuous guidance, encouragement throughout my research, and financial support from his grant from the National Science Foundation (NSF EEC-0540855) and the National Institute of Health (NIH- U01FD005521). I am truly grateful for his advice and for doing everything in his power to enable me to grow and succeed as a Ph.D. student and beyond. I offer thanks to Dr. Ecevit A. Bilgili, Dr. Kathleen McEnnis, Dr. Xiaoyang Xu, and Dr. Rodolfo Romañach for accepting to serve on my committee and offering helpful suggestions. I would also like to extend special thanks to Dr. Bilgili for facilitating collaboration with his milling equipment.

I am grateful for financial support through teaching assistantships from Department of Chemical and Materials Engineering. Special thanks to the department chair, Dr. Lisa Axe for her support.

I would like to extend acknowledgment to the following members of our group for their direct involvement in my research: Guluzar Gorkem Buyukgoz, Lu Zhang, Kuriakose Kunnath, Mahbubur Rahman, Liang Chen, Kai Zheng, Sangah Kim, Meng Li, Gulenay Guner, Siddharth Tripathi, Zhixing Lin, Ruosong Dong, John Pentangelo, Joseph Forte, Prarthana Manoj Rajai, Thierry Arrieta Cespedes, Intisar Chowdhury, and Francis J. Garvey.

Finally, I would like to express my deepest gratitude to my family. To my husband, Semih, for his unique support throughout my graduate studies and life, my mother, Sema, and my grandmother, Sabahat, for their endless love and

support at every stage of my life, and everyone else who has supported me throughout my life. I would not have been able to accomplish what I have without you, and I promise to continue to make you proud!

TABLE OF CONTENTS

Chapter			Page
1	INTRODUCTION		1
	1.1	Background Information	1
	1.2	Objective	6
	1.3	Dissertation Outline	7
2	EFFECT OF SOLVENTS AND CELLULOSIC POLYMERS ON QUALITY ATTRIBUTES OF FILMS LOADED WITH A POORLY WATER-SOLUBLE DRUG		8
	2.1	Introduction	8
	2.2	Materials	13
	2.3	Methods	13
		2.3.1 Polymer solution preparation	13
		2.3.3 Casting and drying	17
	2.4	Characterization	17
		2.4.1 Solubility	17
		2.4.2 Morphology	18
		2.4.3 Extent of recrystallization	18
		2.4.4 Content uniformity	19
		2.4.5 Mechanical properties	20
		2.4.6 Dissolution under sink conditions	20
		2.4.7 Dissolution under non-sink conditions	21
		2.4.8 Stability	21
	2.5	Results and Discussion	22
		2.5.1 Morphology	22

TABLE OF CONTENTS
(Continued)

Chapter **Page**

2.5.2 Extent of recrystallization 24

2.5.3 Content uniformity 28

2.5.4 Mechanical properties 30

2.5.5 Dissolution under sink conditions 32

2.5.6 Dissolution under non-sink conditions 35

2.5.7 Stability 37

2.6 Conclusions 39

3 EFFECT OF CASTING TECHNIQUES ON CQAS OF FILMS LOADED WITH POORLY WATER-SOLUBLE DRUGS 41

3.1 Introduction 41

3.2 Materials 44

3.3 Methods 45

3.3.1 Preparation of micronized coated drug powders 45

3.3.2 Preparation of drug nanosuspensions 45

3.3.3 Preparation of films loaded with fenofibrate 46

3.3.4 Crystallinity of fenofibrate in the film 49

3.3.5 Redispersion of particles from dried films 50

3.3.6 Content uniformity 50

3.3.7 Mechanical properties 51

3.3.8 Dissolution under sink conditions 52

3.4 Results and Discussion 52

3.4.1 Crystallinity of fenofibrate in the film 52

TABLE OF CONTENTS
(Continued)

Chapter **Page**

3.4.2 Redispersion of particles from dried films 55

3.4.3 Content uniformity 60

3.4.4 Mechanical properties 61

3.4.5 Dissolution under sink conditions 63

3.5 Conclusions 66

4 EFFECT OF PARTICLE SIZE AND DRUG LOADING OF API ON CRITICAL QUALITY ATTRIBUTES OF THE FILM 68

4.1 Introduction 68

4.2 Materials 72

4.3 Methods 73

4.3.1 Preparation of pre-milled drug powder 73

4.3.2 Preparation of drug suspensions 73

4.3.3 Preparation of polymer solution and precursors 74

4.3.4 Casting & drying 74

4.4 Characterization 75

4.4.1 The particle size of FNB in suspension and after redispersed from dry films 75

4.4.2 Content Uniformity 75

4.4.3 Morphology 76

4.4.4 Mechanical properties 77

4.4.5 Dissolution profiles 77

4.4.6 Curve fitting and analysis of dissolution curves 78

4.5 Results and Discussion 79

TABLE OF CONTENTS
(Continued)

Chapter **Page**

4.5.1 Particle size of FNB in suspension and after redispersed from dry films 79

4.5.2 Content uniformity 82

4.5.3 Morphology 84

4.5.4 Mechanical properties 85

4.5.5 Dissolution profiles 87

4.6 Conclusions 96

5 EFFECT OF PROCESS PARAMETERS ON THE FILMS LOADED WITH POORLY WATER-SOLUBLE DRUG: DRYING 97

5.1 Introduction 97

5.2 Materials 99

5.3 Methods 100

5.3.1 Preparation of micronized-coated drug 100

5.3.2 Preparation of precursor 100

5.3.3 Drying of films 101

5.3.4 Thermo-gravimetric analysis (TGA) and Differential scanning calorimetry (DSC) 103

5.3.5 Mechanical properties 104

5.4 Results and Discussion 104

5.4.1 Drying kinetics: process parameters 104

5.4.2 Characterization of the films 109

5.4.3 Thermal analysis of films loaded with drug 110

5.4.4 Mechanical analysis of films loaded with drug 112

TABLE OF CONTENTS
(Continued)

Chapter **Page**

5.5 Conclusions 113

6 IN-LINE THICKNESS ANALYSIS VIA NEAR-IR SPECTROSCOPY ON STRIP FILMS LOADED WITH SURFACE-MODIFIED POORLY WATER-SOLUBLE DRUG 114

6.1 Introduction 114

6.2 Materials 117

6.3 Methods 118

6.3.1 Preparation of coated and uncoated micronized drug powders 118

6.3.2 Preparation of films loaded with drug 118

6.3.3 Uniformity of the films loaded with drug 119

6.3.4 Re-dispersion of drug particles from the dried films 120

6.3.5 Imaging of dried films loaded with drug 120

6.3.6 In-line Near-IR (NIR) Spectroscopy data acquisition and analysis 121

6.4 Results and Discussion 124

6.4.1 Uniformity of films loaded with drug 124

6.4.2 The particle size of drug powders and after re-dispersion of drug particles from the dried films 127

6.4.3 Imaging of dried films loaded with drug 128

6.4.5 Development of the NIR calibration model and prediction 136

6.5 Conclusions 140

7 OVERALL CONCLUSIONS AND FUTURE WORK 141

7.1 Conclusions 141

TABLE OF CONTENTS
(Continued)

Chapter **Page**

7.2 Future Work 144

APPENDIX A SOLUTION CAST FILM PREPARATION 146

APPENDIX B PREVENTION OF RE-CRYSTALLIZATION VIA BI-LAYER FILMS 152

B.1 Material and Methods 152

B.2 Results and Discussion 155

B.3 Conclusions 162

APPENDIX C SOLUTION VS SLURRY CASTING 163

APPENDIX D EFFECT OF PARTICLE SIZE 165

APPENDIX E IN-LINE THICKNESS ANALYSIS 169

REFERENCES 171

LIST OF TABLES

Table		Page
1.1	Summary of Critical Quality Attributes and Related Process Parameters and Material Attributes	5
2.1	Solubility of Fenofibrate (FNB) in Pure Solvents and Their Mixtures	14
2.2	Formulation Compositions	16
2.3	Extent of Recrystallizations in Solution Cast Films Computed from DSC Thermograms (n=3)	27
2.4	Drug Content Uniformity for Various 10% FNB Loaded Films	30
3.1	Formulation Compositions of Films Prepared via Different Casting Methods	47
3.2	Formulation Names, Processing Conditions and Particle Sizes of FNB Before Mixing with Polymer Solution	55
3.3	Particle Size Distribution of Re-Dispersed Particles from Dry Films	58
3.4	Relative Standard Deviation (RSD) Values of Drug per Area and Acceptance Values (AV) of Films Loaded with FNB	61
4.1	Formulation Compositions of the Dry Films	75
4.2	Formulation Names, Processing Conditions and Particle Sizes of FNB Suspensions	80
4.3	Relative Standard Deviation (RSD) Values of Drug Per Area and Acceptance Values (AV)	83
4.4	Fitting Parameters of Dissolution Models Used for Dissolution Profiles of FNB Loaded Films with Varying Drug Loading and Particle Size	92
5.1	Composition of Wet and Dry Films	101
5.2	Experimental Conditions in the Drying Chamber	102
5.3	Fitting Parameters for Drying Curves of Films Dried with Conduction and Convection Heating	106
6.1	Compositions of Films Loaded with Drug	119
6.2	Particle Size Distribution of Dry Powders and Re-Dispersed Particles from Dry Films	127

LIST OF TABLES
(Continued)

Table		Page
6.3	Statistics of PLS Models for the Prediction of the Thickness (Films Loaded with 30 wt% FNB)	137
6.4	Thickness Predictions Using Selected PLS Models for Corresponding API(s) in the Film	138
A.1	Statistical Analysis of Dissolution Profiles of HPMC Films under Sink Conditions	151
A.2	Statistical Analysis of Dissolution Profiles of HPC Films under Sink Conditions	151
B.1	Viscosity of Polymer Solutions Used as A Second Layer	156
B.2	DSC Thermograms of Coated and Uncoated Films	159
B.3	Drug Content Uniformity of Uncoated and Coated Films	160
C.1	Statistical Analysis of Dissolution Profiles of Films Loaded with FNB at Varying Drug Loadings	164
D.1	Particle sizes of Redispersed FNB from Films	165
D.2	Statistical Analysis of Dissolution Profiles of Films Loaded with FNB at Varying Particle Size and Drug Loadings	166
E.1	Statistics of PLS Models Developed Using Different Pre-Processing Methods (Films Loaded with 30 wt% AR-FNB)	169

LIST OF FIGURES

Figure		Page
2.1	Optical images of HPMC (a-d) and HPC (e-g) films loaded with 10% fenofibrate. (a) Ace-HPMC (b) EtOH-HPMC (c) MeOH-HPMC (d) Slurry-HPMC (e) Ace-HPC (f) EtOH-HPC (g) Slurry-HPC.	23
2.2	DSC thermograms of films made using different solvents; (a) HPMC films (b) HPC films.	25
2.3	Crystallinity in freshly made 10% FNB loaded HPMC and HPC films versus solubility of FNB in the corresponding solvents. Fitted trend-line based on a power-law function.	28
2.4	Mechanical properties of placebo and 10% FNB loaded HPMC and HPC films.	32
2.5	Film dissolution profiles under sink conditions, (a) HPMC-E15 (b) HPC-L (arrows indicate decreasing FNB solubility).	34
2.6	Film dissolution profiles under non-sink conditions, (a) HPMC-E15 (b) HPC-L (arrows indicate decreasing FNB solubility).	36
2.7	Correlation between AUC of non-sink dissolution profiles and crystallinity.	37
2.8	Dissolution profiles under sink conditions for fresh and 1-year-old 10% FNB loaded solution cast films; Ace-HPMC, EtOH-HPMC and MeOH-HPMC.	39
3.1	Optical images of Solution films loaded with a) 10% b) 20% c) 30% and d) 40% FNB.	53
3.2	a) DSC thermograms of Solution cast films with varying drug loadings b) Extent of recrystallizations in solution cast films computed from thermograms.	54
3.3	Particle size distribution of re-dispersed particles from dry films with varying drug loadings and different preparation methods.	56
3.4	Mechanical properties of films prepared with different methods and having varying drug loads.	63
3.5	Dissolution profiles of films prepared with different methods loaded with varying preparation methods at fixed drug loadings, 10 - 40 wt%.	65

LIST OF FIGURES
(Continued)

Figure		Page
4.1	Particle sizes of redispersed FNB from films, i.e., d_{10}, d_{50}, and d_{90}. Dashed lines indicate the primary particle size.	81
4.2	SEM images of cross-sectional area of films loaded with particles with a) 10% of 160 nm FNB b) 25% of 160 nm FNB c) 40% of 160 nm FNB d) 40% of 400 nm FNB e) 40% of 700 nm FNB and f) 40% of 15 µm FNB	84
4.3	Mechanical properties of films loaded with FNB in varying sizes and drug loadings a) Tensile strength b) Young's Modulus c) Elongation at break. Arrows show the direction of change.	86
4.4	Dissolution profiles of suspensions containing drug particles with varying sizes.	87
4.5	Dissolution profiles of the films loaded with FNB in varying sizes with a) 2.5% b) 10% c) 25% and d) 40% drug loading.	88
4.6	Dissolution analysis with respect to total surface area of FNB a) drug loading and b) particle size grouping.	95
5.1	Schematic of drying setup	102
5.2	Drying curves at different temperatures and air velocity with a casting thickness of a) 0.3 mm b) 0.5mm. Symbols represent experimental data points while lines are the fitted modified model.	105
5.3	Drying curves under varying infrared lamp power and forced convection presence.	107
5.4	Drying curves of films dried at 40 °C and varying dew points.	108
5.5	Drying curves of films loaded with different drugs.	109
5.6	Drying curves of films loaded with 10% MC-FNB at varying drying conditions.	110
5.7	DSC thermograms of films dried at varying conditions.	111
5.8	Mechanical properties of dried films at varying conditions.	112
6.1	Schematic for manufacturing and detection steps.	122

LIST OF FIGURES
(Continued)

Figure		Page
6.2	Relative standard deviation (RSD) values of a) film thickness and b) drug amount per area c) drug loading%.	125
6.3	SEM images of top surfaces of films loaded with 30% a) AR-FNB b) ARC-FNB c) MUC-FNB and d) MC-FNB.	128
6.4	Cross-sectional optical images of films loaded with 30% a) AR-FNB b) ARC-FNB c) MUC-FNB and d) MC-FNB (scale bars represents 100 µm) (top surface of the film faces upwards).	129
6.5	Pre-treatment (1st derivative) applied and averaged NIR spectra belonging to films with varying thickness, loaded with 30% MC-FNB.	130
6.6	PCA score plots for NIR spectra belonging films loaded with 30% a) AR-FNB b) ARC-FNB c) MUC-FNB and d) MC-FNB.	131
6.7	PCA score plots for NIR spectra belonging films loaded with 30% a) AR-FNB or MUC-FNB b) ARC-FNB or MC-FNB c) AR-FNB or ARC-FNB and d) MUC-FNB or MC-FNB.	133
6.8	PCA score plots for NIR spectra belonging films loaded with 30% MC-FNB a) Belt speed grouping b) Dry film thickness grouping.	135
A.1	Optical images of 10% FNB (in dry film) loaded HPMC precursors prepared with 1:1 (a and d), 1:2 (b and e), and 1:4 (c and f) ratios of w:Ace (a, b, and c) w:EtOH (d, e, and f) solvent mixtures. Scale bars on the images represents 400 µm.	148
A.2	Drying of the HPMC films made with 1:4 (water:ethanol) at different temperatures.	149
A.3	Dissolution profiles under sink conditions - 10 % FNB loaded solution casting films made of HPMC and HPC-L (a) 1:4 (w:Ace), (b) 1:4 (w:EtOH), and (c) Slurry.	150
A.4	Dissolution profiles under non-sink conditions for 10% FNB loaded solution casting films made of HPMC and HPC-L.	151
B.1	The 2nd derivative of Raman spectra during drying of the film.	157
B.2	Optical images of cross-section of the films loaded with FNB a) Slurry b) Uncoated Solution film c) Coated Solution film.	158

LIST OF FIGURES
(Continued)

Figure **Page**

B.3 Particle size distribution of re-dispersed particles from dry films with varying drug loadings and different preparation methods. 159

B.4 Dissolution profiles under non-sink conditions for 10% FNB loaded films coated with 5% polymer solution. 161

B.5 Dissolution profiles under non-sink conditions for 10% FNB loaded films coated with 8% polymer solution. 161

C.1 Dissolution profiles of films prepared with different methods loaded with varying drug loadings, 10%, 20%, 30% and 40% FNB. 163

D.1 Dissolution analysis with respect to total surface area of FNB a) drug loading and b) particle size grouping. 168

E.1 PCA score plots for NIR spectra belonging films loaded with 30% AR-FNB a) Reduced (1304-1651 nm) and b) Full spectral range (908-1676 nm) were used. 170

CHAPTER 1

INTRODUCTION

1.1 Background Information

Oral films are relatively new dosage forms that have attracted the attention of many researchers [1, 2]. They can be defined as a thin polymeric film loaded with an active pharmaceutical ingredient (API) which dissolves and leads targeted therapeutic effect [3]. Depending on the site of application in the mouth (buccal and sublingual areas), the drug can be absorbed orally and bypasses the first-pass metabolism, leading to increased bioavailability [1]. Having this advantage, buccal and sublingual type oral films can be a better alternative for the drugs requiring intravenous administration, such as insulin or vaccines [4-6]. Aside from patient compliance and improved bioavailability, oral films possess other advantages such as flexible dosing and easiness to be incorporated into continuous manufacturing. In addition to these advantages, oral films are believed to play a key role in the reduction of time and the cost of manufacturing [7]. Moreover, a single formulation can be adjusted for different dosages considering a dispenser to arrange a desired amount of film. Through precision dispensing; the time and costs of packaging and manufacturing of several dosages will be significantly reduced [8] while giving flexibility to the practitioners in terms of supplying accurate prescriptions for varying ages and weights.

Considering their attractive features, oral films are promising dosage forms, particularly given the growing interest in personalized medicine expanding the

research from the scientific and engineering design aspects. Despite considerable research, much work remains towards better standardization from materials to processing perspectives [2].

Oral films can be prepared by hot-melt extrusion (HME) [9-19], solution casting [20-26], and slurry casting [27-32] which are commonly used techniques for oral films. The films prepared by HME are subjected to elevated temperatures during processing. HME processing results in films loaded with amorphous or molecularly dispersed drugs, facilitating increased solubility, particularly for poorly water-soluble drugs. However, high temperatures may cause degradation of the drug. In addition, the thickness of most films produced via HME is either too high (300 μm) or thinner (70-120 μm) with a standard deviation of at least 10 μm. These are not acceptable features since thickness is the most important parameter in terms of product quality attributes and patient compliance. Most importantly, drug content is strongly dependent on the thickness of the film.

In another film preparation method, solution casting, the drug is designed to be amorphous similar to the HME process. In solution casting, the drug is dissolved in the polymer solution before casting unlike the heating in HME. If the drug is poorly water-soluble, an organic solvent must be used in the polymer solution to dissolve the drug. In the opposite case, if the drug is water-soluble, there is no need for an organic solvent. In the polymer solution, the drug dissolves and becomes amorphous, but as the solvent is evaporated the drug particles tend to recrystallize during the drying process which is the major issue for both HME and solution casting methods. Recrystallization of the drug during storage is quite

possible even if initially a crystal-free fresh film is obtained. For this reason alone, optimization of the formulation and selecting the process parameters must be performed meticulously. Each time when there is a change in the formulation such as polymer type, drug, excipient, the process parameters must be optimized again. In contrast to these techniques, slurry casting is a robust process delivering predictable and stable product quality. In slurry casting, the polymer solution is prepared using water as the solvent and the poorly water-soluble drug is directly added resulting in a suspension. Due to the usage of suspension, this method is called slurry casting. Since the drug is not dissolved, formulation optimization does not depend on the drug as much as in HME or solution casting methods. In the scope of this dissertation, films made with both solution and slurry casting will be analyzed.

There are many studies related to the effect of critical material attributes (CMAs) and process parameters (CPP) on the critical quality attributes (CQAs) of the films [24, 33-36]. Yet, a general framework towards design space and control systems is missing for film manufacturing to assure good product quality. Product quality is of importance in every different type of manufacturing, but it is critically important in the pharmaceutical industry as pharmaceutical products must meet very specific needs. There is an approach called Quality by Design (QbD) in pharmaceutical development to ensure the fulfillment of CAQs' needs and have better control of the product qualities by the design itself [37]. QbD includes predefined objectives, emphasizing product and processes by understanding process control steps to gain better control of any process to ensure the consistent

yield and high-quality products [38]. In this approach, the first challenge is defining a target product quality profile and objectives. These predefined quality performance criteria are followed by the design and development of products and manufacturing processes in accordance with these quality profiles. Moreover, in this approach identifying critical quality attributes, process parameters, and sources of variability is of great importance to assure the production of consistent and reliable quality over the production time [38]. The last step of QbD, ensuring the defined product quality, can be achieved by implementing Process Analytical Technology (PAT) into the manufacturing system. PAT offers process control by timely measurements and helps to intervene in case of failure in the system.

QbD approach is not necessarily a new concept in pharmaceutical drugs. It has been investigated and established for the tablets by many researchers as it was reviewed by Lionberger et al. [39]. However, for oral films, one of the main missing parts in drug development is a well-defined roadmap for a reliable QbD approach. Having this incentive, Visser et al. prematurely tried to apply the QbD approach to films [40]. In their study, tensile strength, elongation at break, Young's modulus, and disintegration time consists of the main CQAs. Also, for the CQAs, they defined an upper or lower bound for these parameters. However, for design purposes, a well-defined range should be constituted rather than bounds. Implementation of these CQAs in QbD of oral films is more appropriate not only in the identification of sources of fails but also for higher quality design and experimental layouts. Besides this study [40], current literature lacks a comparison for the effects of CQAs on QbD performances in films.

Table 1.1 Summary of Critical Quality Attributes and Related Process Parameters and Material Attributes

CRITICAL QUALITY ATTRIBUTES	***PROCESS PARAMETERS***	***MATERIAL ATTRIBUTES***
Dose Uniformity, Stability, Appearance, Residual Water Content, Organoleptic Characterization, Physical Strength, Drug release profile	**Mixing** Batch: Type and geometry of mixer, mixing time, mixer load level, impeller speed, solids loading, mixing temperature Continuous: Screw geometry, feed rate of ingredients, screw rotation rate, Solids loading, Mixing temperature **Defoaming** Method of defoaming, defoaming time **Casting** Feed die type and geometry, gravity vs. pressurized feed, feed rate **Drying & Sampling** Drying equipment type and geometry, feed type (slurry vs. solvent), feed rate, feed moisture content, types of drying and heat transfer modes , roller speed, zone temperatures, irradiation flux, inlet air flow rate, temperature, humidity, roller substrate type, drying (residence) time, film temperature, exhaust air temperature and humidity, punch type/size	**Film Formers** MW, viscosity in water, water solubility, film forming capability, toxicity, taste, cost, hydrophobicity, gel formation, solubility in organic solvents, swelling **Plasticizers** Compatibility with polymer, impact on T_g **Active Pharmaceutical Ingredient** Water solubility, MW, melting point, logP, particle size, BCS class **Stabilizers/surfactants** Surface tension, adsorption, toxicity, irritation, hydrophilic-lipophilic balance (HLB), tendency to promote foaming, may promote Ostwald ripening

Table 1.1 depicts the most important CQAs with projected CPPs and critical material attributes CMAs. It should be noted that implementing the analysis of these parameters would allow creating design space which is the key missing factor in oral film designs. In the following chapters, the current status of oral films is described within the perspective of attributes presented in Table 1.1. The related literature about the CMAs and CPPs in pharmaceutical film manufacturing is reviewed in the following chapters. In these chapters, certain formulation and process parameters were analyzed in terms of relevant CQAs to identify CMAs and CPPs for pharmaceutical film manufacturing.

1.2 Objective

Due to its many advantages (explained in Section 1.1), oral films loaded with the drug have taken the attention of many researchers. There are extensive studies especially about the effect of material attributes on the CQAs of the films. Yet, a general framework towards design space is missing for every step of manufacturing. To understand the effect of formulation and process parameters on the CQAs of the films which will help to create a design space later, the following scientific questions are raised:

- How do different solvents affect CQAs of the films i.e., crystallinity, mechanical properties, dissolution, content uniformity?
- How does the solubility of API in selected solvents affect the stability of films?
- How does the recrystallization kinetics change with drug loading?
- How do particle loading and size affect the dissolution?

- Do the drying modes i.e., conduction, convection, or radiation, affect CQAs (i.e., final moisture, crystallinity, mechanical properties) of the films?
- How the casting thickness affect the drying kinetics?
- How do engineered particles affect the film thickness?

Throughout this dissertation, the questions above will be addressed by systematic analysis of CMAs and CPPs. In addition to these, in Chapter 7, PAT will be introduced into the analysis of CQAs of the drug-loaded films.

1.3 Dissertation Outline

This dissertation comprises eight chapters. Chapter 1 starts with a general review of the introduction to pharmaceutical films. A more detailed related literature review is included at the beginning of each chapter. Chapter 2 analyzes the effect of solvent and polymer on the properties of solution cast films. Chapter 3 investigates the effectiveness of different casting techniques, i.e., solution casting and slurry casting, in terms of dissolution rate. Chapter 4 explores the effect of particle size and drug loading on the dissolution enhancement of film loaded with a crystalline drug. In Chapter 5, the process parameters in the drying of drug-loaded films are examined. Chapter 6 introduced the Process Analytical Tools integration into the continuous film manufacturing to detect and analyze the thickness. Chapter 7 presents the general conclusions of this dissertation and anticipated future work.

CHAPTER 2

EFFECT OF SOLVENTS AND CELLULOSIC POLYMERS ON QUALITY ATTRIBUTES OF FILMS LOADED WITH A POORLY WATER-SOLUBLE DRUG

2.1 Introduction

Oral films are an emerging dosage form for drug delivery due to their numerous advantages. Some of the significant advantages of films include ease of handling, capability for continuous manufacturing, the possibility to bypass the first-pass metabolism leading to increased bioavailability [4-6], patient compliance in particularly for pediatrics, geriatrics and dysphagia patients [1, 2] and personalized medicine taking advantage of precision dispensing and flexible dosing capability [8]. Commonly adopted techniques for oral films are solventless casting, i.e., hot-melt extrusion (HME) [9-11, 13-19], and solvent casting including solution [20-26] and slurry casting [27-32, 36, 41]. These techniques can be used to enhance the bioavailability of BCS (Biopharmaceutics Classification System) Class II active pharmaceutical ingredients (APIs) by increasing the dissolution rate. Two major approaches to enhance the dissolution rate in films are: increasing the solubility of the API by forming amorphous solid dispersions, which can be accomplished through HME or solution casting, or by using nano or low micro-sized API particles and preserving their large surface area through slurry casting as it can be explained by Noyes-Whitney equation [42]:

$$\frac{dC}{dt} = kA\left(C_s - C\right) \tag{2.1}$$

in which C_s is the solubility of the API, C is the concentration at a time "t", A is the total surface area over which dissolution occurs, and k the is solute transfer coefficient.

In this chapter, the solution casting approach is investigated by examining the effect of solvents on the dissolution rate and other critical quality attributes (CQAs) for cellulosic films loaded with a poorly water-soluble drug. The main goal is to identify which CQAs in addition to the API crystallinity and form could be impacted by the solvent and assess the extent of the impact as compared to the impact of the polymer and other key formulations parameters.

In solution casting, API is solubilized using an organic solvent and it is hoped that upon drying, the API is in an amorphous state within polymer matrix [20, 22-24], while in slurry casting API is crystalline, hence it has solubility limitation due to crystalline nature. Solution casting offers a highly promising option due to its potential for facilitating higher solubility and supersaturation during dissolution alleviating the solubility limitation of slurry casting. Unfortunately, recrystallization becomes a major challenge for solution casting [21-23, 43, 44]. It must be addressed by optimizing the materials used in the formulation as well as processing parameters because they can all significantly impact the properties and stability of the film product. However, in most studies to-date, the solid-state of the API in the film was either not considered or it was not well characterized [21, 22, 24, 44-46].

As discussed previously, the API is likely to recrystallize in the film prepared via solution casting. Therefore, a representative API based on its crystallization tendency needs to be selected. Several API properties affect the crystallization tendency of the molecules. These include thermal properties such as the melting and glass transition temperatures, enthalpy, entropy, molecular weight and rotatable bonds [47, 48], and surface diffusion coefficient [49]. It was reported that higher molecular weight, number of rotatable bonds, more complex structure, lower enthalpy and entropy, and higher T_g decreases the crystallization tendency [47, 48]. In addition, high, intermediate, or low crystallization tendency categories have been proposed based on a detailed experimental analysis via solvent evaporation of a large group of organic molecules based on their glass-forming ability [47] and undercooled melt techniques [48]. Accordingly, for solvent evaporation, which is the most relevant to solution casting for films, the classification included 39 APIs as fast, 23 APIs as intermediate, and 31 APIs as slow or non-crystallizers [47]. Unfortunately, such classification is dependent on the solvent used [47]. Further, it has been reported that even slow crystallizers may have poor time stability [50], and in general most amorphous glasses tend to crystallize in time [51-53]. While it is not possible to account for all aspects of the intrinsic crystallization tendency of the selected API for the current study, one from an intermediate crystallizer category, Fenofibrate (FNB), is considered. Doing so assures that its behavior represents about 2/3rd of the APIs that could be classified as intermediate or fast crystallizers [47]. In addition, significant previous work on film formation with FNB via slurry casting is available as a baseline [27, 29, 30].

Several studies have focused on understanding the effect of the polymer in solution casting for the films [23-26]. However, studies on the effect of solvent selection are very limited. Among these, Preis et al. discussed solvent suitability but only characterized the precursors [25]. Moreover, the visible appearance was the only characterization for the precursors which is not a quantitative technique. Pattnaik et al. studied the effect of solvent on the crystallinity of ondansetron in the film but did not analyze the effect on dissolution rates or mechanical properties of the films [54]. Considering these examples from the existing literature, solution casting appears to be implemented for oral film production without an adequate understanding of the effect of solvent on the solid-state of the API and other key quality attributes including dissolution.

Two other solvent evaporation methods, spin coating and spray drying [55, 56] may provide insights into solvent selection. Although these two techniques differ from solution casting in the final product form, time and mode of drying, and the relative amounts of drug and polymer, they all require preparation of a precursor solution that includes polymer and drug dissolved in a suitable solvent [57]. Spray drying studies showed that solvent may significantly influence the properties of the resulting dispersion i.e., particle size, glass transition temperature, dissolution rate, supersaturation level [58-62]. A general conclusion from these studies is that the solvent selection may influence the morphology and size of the particles and as a result, related dissolution profiles. Mugheirbi et al. examined the effect of the solvents on the polymer conformation using the films prepared via spin-coating [63]. It was concluded that even the smallest change in

solvent and evaporation rate could drastically affect the film matrix. Likewise, it is expected that the solvent system used in oral film preparation via solution casting would significantly affect the film matrix. Consequently, the film matrix would have an impact on the thermal properties (i.e., T_g), mechanical properties and the stability and release of the drug [1]. In addition, because the films are used as final dosage form, unlike spray-dried powders where additional additives and formulation development may help mitigate some of the negative effects from solvents, the effect of solvent is expected to play even more crucial role in film product development.

Consequently, the main objective of this study was to investigate the impact of different solvents in conjunction with the film-forming polymer on the CQAs of the films produced via solution casting. The effect of solvents was experimentally examined on two widely used cellulosic polymers [64], i.e., hydroxypropyl methylcellulose E15 (HPMC E15) and hydroxypropyl cellulose (HPC, L grade). Fenofibrate (FNB) was used as a model BCS class II model drug and four different organic solvents, ethanol (EtOH), methanol (MeOH), acetone (Ace) and dichloromethane (DCM) were used in binary solvent systems. Key critical attributes of the films prepared using different solvents were measured, such as the film morphology and the FNB recrystallization, the content uniformity, film mechanical properties, and dissolution profiles, including supersaturation potential. These results were analyzed to assess the hypothesis that, significant drug recrystallization as a function of solvent and polymer can be expected,

impacting key film properties, including drug supersaturation during dissolution for solution-cast films.

2.2 Materials

Fenofibrate (FNB, Jai Radhe Sales) as a model BCS Class II drug, low molecular weight (MW) hydroxypropyl methylcellulose (HPMC; Methocel E15 Premium LV, M_w ~40 000, 12-18 *cP*; The Dow Chemical Company, Midland, MI) and hydroxypropyl cellulose (HPC, L grade, M_w ~140 000, 6-10 *cP*; donated by Nisso America Inc, New York, NY, USA) as film formers and glycerin (Sigma-Aldrich, Saint Louis, MO) as plasticizer were used. Ethanol (Alfa-Aesar, anhydrous, HPLC grade), methanol (VWR, ACS), acetone (Honeywell, Burdick & Jackson, ACS/HPLC) and dichloromethane (Sigma-Aldrich, anhydrous) were used as received.

2.3 Methods

2.3.1 Polymer solution preparation

Hydroxypropyl methylcellulose (HPMC) and hydroxypropyl cellulose (HPC) are commonly used as a film former pharmaceutical products [20, 23-26, 29, 30, 65, 66]. Therefore, these cellulosic polymers were selected as film formers in this study. HPMC and HPC both have cellulose backbone with different levels of methoxyl and/or hydroxypropyl substitutions. HPMC used is E15 LV grade having average MW of 40 000 Da, viscosity of 12-18 *cP* (2% in water), and degree of substitution (DS) of 1.9 (methoxyl) and 0.23 (hydroxypropyl) [67]. HPC used is L

grade having average MW of 140 000 Da, viscosity of 6-10 *cP* (2% in water), and degree of substitution of 2.2 (hydroxypropyl) [68].

Table 1.1 Solubility of Fenofibrate (FNB) in Pure Solvents and Their Mixtures

Solvent	***Solubility of FNB (g/L)***
Methanol	43.1
Ethanol	38.6
Acetone	353.3
Dichloromethane (DCM)	617.2
1:4 (water:methanol)	11.6
1:4 (water:ethanol)	23.7
1:4 (water:acetone)	156.4
1:1 (DCM:ethanol)	535.7
Water	0.1 mg/L [69]

Ethanol (EtOH), methanol (MeOH), acetone (Ace), and dichloromethane (DCM) were chosen as solvents allowing to examine a wide solubility range (Table 1.1) for the model poorly water-soluble drug (FNB). It is noted that the usage of DCM in pharmaceutical products should be limited according to FDA guidance for industry [70]. However, its alcoholic mixture is a good solvent for the polymers used, HPMC and HPC, as well as the drug, FNB. This allowed for preparing one of the formulations without any water in the solvent system, DCM:EtOH mixture, selected for research purpose. A binary organic solvent mixture including water is

needed to dissolve both HPMC and FNB due to the solubility limitation of HPMC. As a result of a preliminary study, 1:4 (water / organic solvent) ratio was selected to further analyze (Details may be found in Appendix A).

Formulations were given abbreviated names indicating polymer and solvent used (Table 1.2). These names were used throughout the manuscript for the sake of brevity. Polymer solutions prepared with HPMC E15 contained 10% (wt%) polymer, 3.3% (wt%) plasticizer while HPC-L solutions contained 20% (wt%) polymer, 1% (wt%) plasticizer and the rest were the solvent mixture.

The composition of HPMC E15 solutions was adapted from Zhang et al [30] and HPC-L solutions were adjusted considering viscosities and peelability of the films. Details may be found in the Appendix A. To prepare a polymer solution in a binary solvent mixture for both HPMC E15 and HPC-L, the required amounts of organic solvent and deionized water were added to a glass jar with magnetic stirring and heated together. Upon reaching 30 ˚C, the plasticizer, glycerin, was added to the binary solution and stirred for 5 minutes and the temperature was increased to 40–45 °C. At this stage, the polymer was slowly added to the solution, after all, the solution was maintained at approximately 40–45 °C until all of the polymer was dissolved, and then the final mixture cooled down to room temperature. HPMC solutions in water were prepared following the same steps except for the temperature (80 °C) during polymer addition. Aqueous HPC solutions were prepared at room temperature using an over-head impeller.

Table 1.2 Formulation Compositions

Name of the formulation	***Polymer type***	***Solvent used in polymer solution preparation***
Slurry-HPMC	HPMC E15	Water
MeOH-HPMC	HPMC E15	Water : methanol (1:4)
EtOH-HPMC	HPMC E15	Water : ethanol (1:4)
Ace-HPMC	HPMC E15	Water : acetone (1:4)
DCM-HPMC	HPMC E15	Dichloromethane : ethanol (1:1)
Slurry-HPC	HPC-L	Water
EtOH-HPC	HPC-L	Water : ethanol (1:4)
Ace-HPC	HPC-L	Water : acetone (1:4)

2.3.2 Precursor preparation

To create the film precursor, dry FNB powder was incorporated into the polymer solution via planetary centrifugal mixing (Thinky Model ARE-310). Process parameters were adapted from a previous work which showed that planetary mixer resulted in good mixing of powder and polymer solution regardless of powder properties [30]. However, here the mixing time had to be increased since the API needs to be dissolved, which was not the case in [30]. In addition, a defoaming step was added due to increased mixing time and since casting was to be done right after precursor preparation. Consequently, the drug powder and polymer solution were mixed for 10 min at 2000 rpm, followed by defoaming for 2 min at 2200 rpm. All the films had 10% FNB loading unless it is stated otherwise.

2.3.3 Casting and drying

Film precursor suspensions were cast onto a plastic substrate (Scotchpak TM 9744, 3M, MN, USA) with a doctor blade (Elcometer, Rochester Hills, MI) in a different range of wet thicknesses to achieve a uniform thickness from each solvent precursor using a Lab-Cast Model TC-LC Tape Caster (HED International, Ringoes, NJ). Drying of the HPMC films made with 1:4 (w:EtOH) at 50 or 40 °C created irregularities on the film surface due to the fast evaporation (Figure A.2). In order to obtain defect-free film for all the formulations, following the casting step, samples were dried in a fume hood at ambient temperature overnight. Once dry, the films were peeled from the substrate and stored in sealed plastic bags until analyzed. All the characterizations were conducted on the same day that films were dried and peeled.

2.4 Characterization

2.4.1 Solubility

The excess amount of FNB was added into 50 mL of pure solvents and their binary mixtures listed in Table 2.1 at room temperature and stirred for 24 h. Some of the suspension was extracted via a syringe, filtered (pore size of 0.2 µm) and diluted using fresh solvent/solvent mixtures. Absorbances of the solutions were measured via UV-vis spectrophotometer (Thermo Fisher Scientific Inc., MA, USA). Concentrations were calculated using respective calibration curves and solubilities were reported in Table 1.1.

2.4.2 Morphology

The films were analyzed using a digital microscope with polarized back-lighting mode (Carl Zeiss Microscopy, LLC. Germany). Each film with a 1 cm x 3 cm dimensions was fixed on a glass slide by a tape on the edges and images were taken from the top. For thin films produced here, this approach allowed for the detection of the recrystallization within and on the surface of the film.

2.4.3 Extent of recrystallization

A differential scanning calorimeter (DSC, Mettler Toledo, Inc., Columbus, OH) analysis was performed in the examination of the extent of recrystallization in the film samples loaded with FNB. Approximately 5–8 mg of sample in an aluminum standard pan was heated from 25 °C to 120 °C with a constant heating rate of 10 °C/min under a nitrogen flow and cooled down to 25 °C with the same rate. Crystallinities in the films were calculated using the melting peaks (if occurred) on the thermograms (Equation 2.2). Specific enthalpy of crystalline material in the film was calculated by calculating the area under the melting peak. Specific enthalpies of slurry films were used as 100% crystalline material in the calculations. All the samples were run triplicates.

$$Extent\ \ of\ \ recrystallization\ \% = \frac{Specific\ \ enthalpy\ \ of\ the\ \ sample\ film}{Specific\ \ enthalpy\ \ of\ the\ \ slurry\ film} \times 100 \qquad (2.2)$$

In the case of shoulder appearance on the thermograms, the curve was deconvoluted using OriginLab 2020 software [71]. Each fitted curve represents a

different form of FNB. They were used in crystallinity calculations for the corresponding form of FNB. Same slurry films were used as the reference for each form of FNB as Tipduangta et al. stated that form I and II would have similar melting enthalpies due to their similar crystal structures [72].

2.4.4 Content uniformity

In order to measure the dispersion and uniformity of drug particles in the dried film, ten circular punches, ~0.7 cm^2 area, were sampled from the films randomly [27, 30]. Such a small sample size (~0.7 cm^2), about $1/10^{th}$ of the intended dosage size (2 cm x 3 cm), was selected for improved discernment of the effect of the key factors [27, 30]. Mass and thickness of these samples were recorded. Then, they were dissolved in a 20 mL of 7.2 g/L concentration solution of sodium dodecyl sulfate (SDS) solution and stirred via magnetic bars for at least three hours. The absorbance of each solution was measured via a UV-vis spectrophotometer (Thermo Fisher Scientific Inc., MA, USA) at the maximum wavelength for FNB (290 nm) and concentrations were calculated using a pre-prepared calibration curve. Label claim% (the average drug loading with respect to label claim), and relative standard deviations (RSD, average value divided by standard deviation) for thickness, drug amount per area and drug loading% (FNB weight with respect to total weight) were calculated and reported. Acceptance value (AV) for each formulation was also calculated using Equation 2.3 [73].

$$Acceptance\ value(AV) = \left|M - LC_{avg}\%\right| + k \cdot s \tag{2.3}$$

In the above equations, $LC_{avg}\%$ is the average drug loading with respect to label claim; *s* is the standard deviation of $LC_{avg}\%$, k is the acceptability constant, 2.4. Parameter M is set as shown below.

M: Reference value;

$$98.5 \; if \; LC_{avg}\% < 98.5 \tag{2.4}$$

$$LC_{avg}\% \; if \; 98.5 < LC_{avg}\% < 101.5 \tag{2.5}$$

$$101.5 \; if \; LC_{avg}\% > 101.5 \tag{2.6}$$

2.4.5 Mechanical properties

Investigation of the mechanical properties of the dried films was done using a TA-XT Plus Texture Analyzer (Stable Microsteps, UK). From each film, 5 rectangular samples, 50 mm x 15 mm, were taken. These samples were attached between two grips and elongated at a constant rate (1 mm/s) until the sample broke. From the resultant stress-strain curve, tensile strength (TS), Young's modulus (YM), and percent elongation at break (EB%) were calculated. For each film, the average values and standard deviations were reported. Further details about mechanical properties may be found in [29, 74].

2.4.6 Dissolution under sink conditions

Measurement of the drug release profile under sink conditions was performed using previously established procedures for closed-loop flow-through cell dissolution apparatus (USP IV; Sotax, Switzerland) [27, 30, 75]. For each film, 6 circular film samples with an area of ~0.7 cm^2 were selected randomly from the film and placed between 5 g of 1 mm glass beads within the dissolution cell. A flow

rate of 16 ml/min was used for the dissolution media (175 mL of 3.6 g/L SDS solution) and the temperature was maintained constant at 37 ± 0.5 °C. The dissolution results are reported as a percentage of FNB dissolved with respect to time.

2.4.7 Dissolution under non-sink conditions

Dissolution studies for non-sink conditions were conducted in USP II (Sotax, Switzerland). The procedure was adapted from an early study on the paddle method under sink conditions [75]. Experiments were conducted at 37 °C and paddles were rotated at 50 rpm. 500 mL of 3.6 g/L SDS solution was used as dissolution media. Film samples (amount corresponds to 100 mg FNB) were introduced to dissolution vessel in a sinker to prevent any floating sample and sticking of the sample to the vessel. Samples were taken at predetermined time intervals and replaced with the same amount of fresh medium. Taken samples were filtered using a syringe filter (pore size of 0.2 µm). After adequate dilutions, absorbances of the solutions were measured using UV-vis Spectroscopy. The dissolution results are reported as the concentration of FNB dissolved (mg/L) with respect to time. The supersaturation capability was characterized by measuring the area under the curve (AUC) for all dissolution curves.

2.4.8 Stability

Films to be tested for stability were stored in a plastic bag at room temperature (20–25 °C) and humidity (30–40% RH) for 1 year. DSC measurements and dissolution tests under sink conditions were conducted according to the procedures described in Sections 2.4.3, and 2.4.6, respectively.

2.5 Results and Discussion

2.5.1 Morphology

Optical microscopy images taken through the back-lighting mode of films prepared with HPMC and HPC for various cases are presented in Figure 1.1. The DCM-HPMC film was completely clear, hence those images are not included. HPMC and HPC films prepared with acetone (Figure 1.1.a and e) contained mostly small crystal seeds but not fully-grown crystals while films made with ethanol (Figure 1.1.b, and f) showed large crystals on the film surface and also likely within the films. Even though the solubility of FNB in water-methanol (11.6 g/L) and water-ethanol (23.7 g/L) were not drastically different, EtOH-HPMC and MeOH-HPMC showed different shaped FNB crystals, needle-like and triclinic shapes, respectively (Figure 1.1.b, and c). Ace-HPMC film had larger crystals than Ace-HPC film, and EtOH-HPMC film surface was covered with crystals while EtOH-HPC was not, even though it had larger crystals within the film as compared with its HPMC counterpart. These images qualitatively revealed the extent of recrystallization, recrystallite sizes and shape differences with the solvent as well as the polymer. Considering different crystals shapes might be due to polymorphic crystal growth [72, 76], possible occurrences of FNB polymorph were assessed via DSC measurements, discussed in the next section.

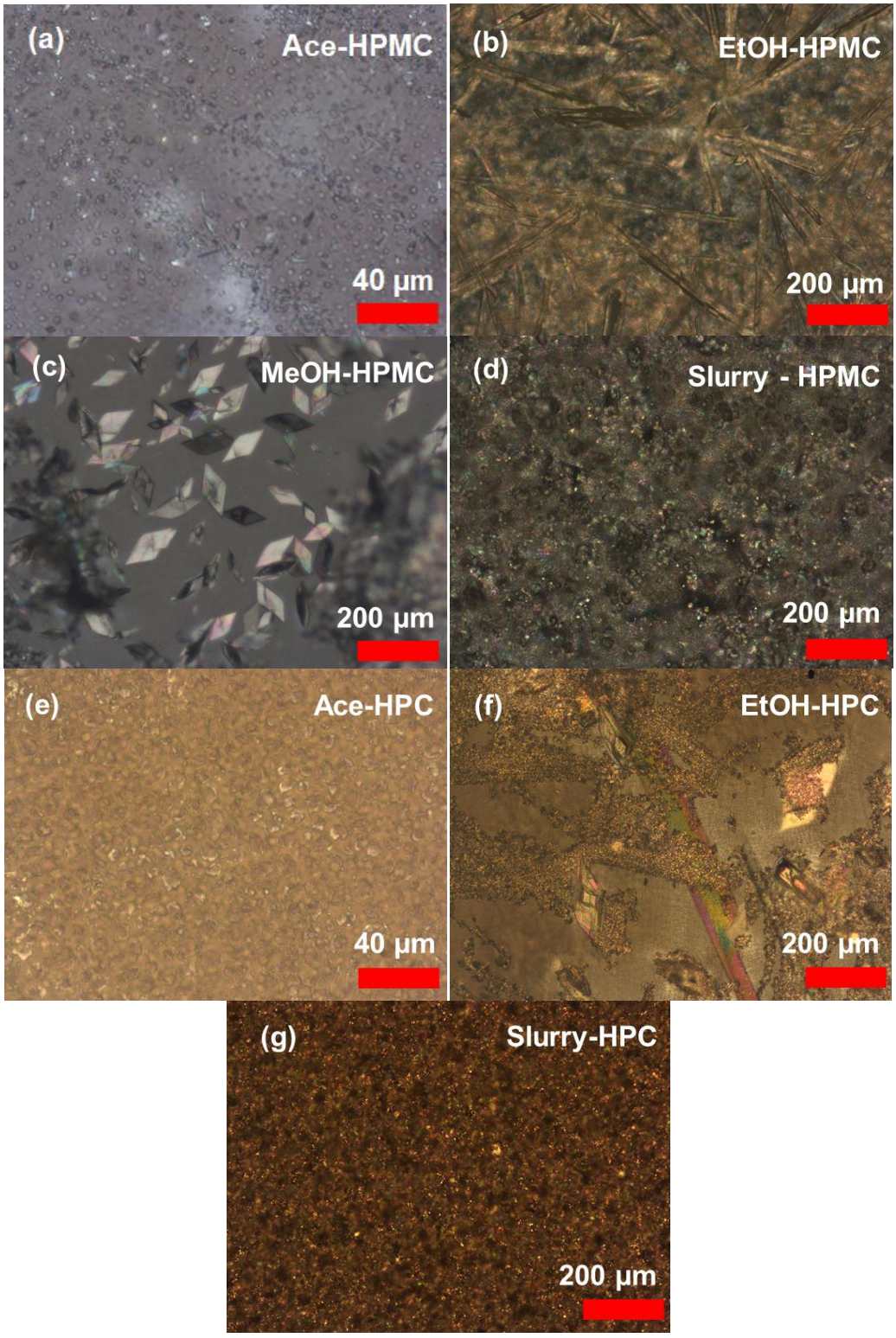

Figure 1.1 Optical images of HPMC (a-d) and HPC (e-g) films loaded with 10% fenofibrate. (a) Ace-HPMC (b) EtOH-HPMC (c) MeOH-HPMC (d) Slurry-HPMC (e) Ace-HPC (f) EtOH-HPC (g) Slurry-HPC.

Generally, it appeared that recrystallized FNB particle sizes were inversely correlated with the solubility of FNB in the corresponding solvent being of the order; DCM > Ace > EtOH > MeOH. While the images were selected to represent the whole film as a general, the observed distribution of the drug crystals was non-uniform throughout the prepared film structures.

2.5.2 Extent of recrystallization

Figure 1.2.a and b present DSC thermograms of HPMC and HPC films, respectively. In each graph, slurry films loaded with 100% crystalline FNB (form I) are used as reference for recrystallization analysis which had a melting peak at 79 °C corresponding to FNB (form I), comparable to previous reports at 80 °C [77]. DCM-HPMC and Ace-HPMC did not have a melting peak indicating the absence of crystalline FNB in the film. However, the rest of the formulations showed melting peaks indicating the occurrence of recrystallization during film drying. While EtOH-HPMC and MeOH-HPMC films had a single melting peak at 79 °C (Form I FNB, same as control), shoulder for Ace-HPC film and peak for EtOH-HPC film was observed around 74 °C and 76 °C, respectively, along with a peak at 79 °C. Heinz et al. reported the melting peak of commonly used and most stable form of fenofibrate (form I) as 80 °C and unstable form of FNB (form II) as 73 °C [77]. This observation is similar to present results (form I FNB at 79 °C and form II FNB at 74–76 °C) and confirmed that there is FNB polymorph formation in HPC films made with organic solvents.

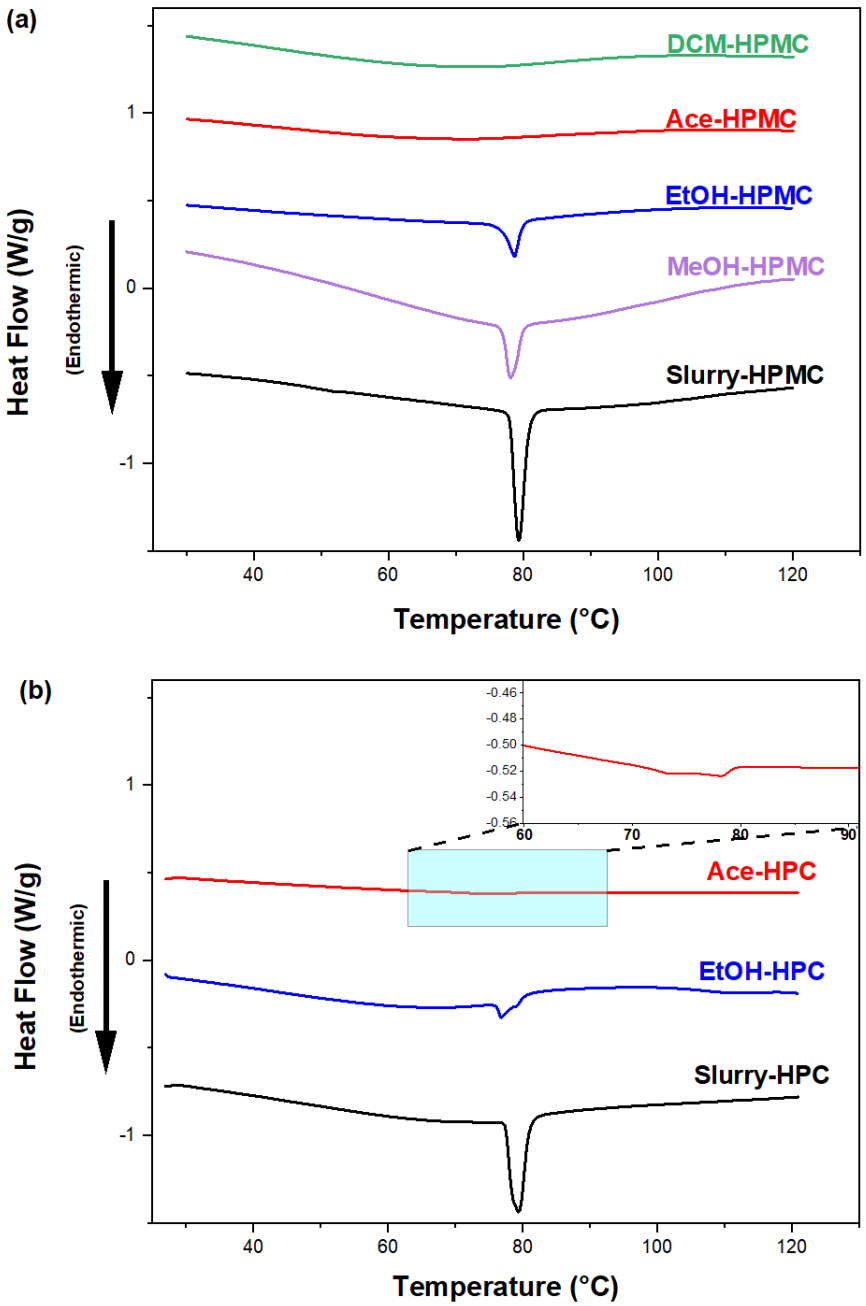

Figure 1.2 DSC thermograms of films made using different solvents; (a) HPMC films (b) HPC films.

Crystallinities for HPMC and HPC films, calculated from the melting peaks obtained via DSC measurements, Figure 1.2, were in line with optical images in Figure 1.1. EtOH films showed higher crystallinity than Ace films for both HPMC

(40.1% and not detected) and HPC (18.9% and 3.6%) films. The high values of the standard deviations in estimated crystallinities for EtOH-HPMC (± 20.8) and MeOH-HPMC (± 11.4) further confirmed non-uniform and uncontrolled recrystallization in the film while Ace-HPC (± 0.8) and EtOH-HPC (± 2.1) had lower standard deviations. As mentioned in Section 2.3.1, the polymers HPMC E15 and HPC-L have different MWs, viscosities, substituents and their degrees. A polymer with a higher MW may inhibit recrystallization better than its lower MW forms, in part due to increase in the viscosity, which can slow the drug diffusion in the solution and decrease the nucleation rate [68, 78-80]. The functional groups in the polymer can also affect the recrystallization [78, 81]. Even when the polymer concentrations were already adjusted to account for the differing viscosities, Ace-HPMC film did not have recrystallization while Ace-HPC film did. Besides, polymorphism was observed in both Ace-HPC and EtOH-HPC films. Thus, it appears that the impact from the substituents and degree of substitution (DS) of the polymers may have been more than from MW in terms of stabilizing amorphous FNB, in line with the previous observation [82].

The recrystallization of FNB in the films was examined with respect to its solubility in the corresponding solvent as well as the polymer type. These results, plotted in Figure 1.3, show a highly nonlinear effect of the FNB solubility on recrystallization for both polymer types. To the best of our knowledge, there are no reports correlating solubility with the crystallinity of freshly dried films. Mugheirbi et al. reported that increased solvent viscosity leading to a decrease in diffusivity and decreased boiling point leading to increased drying rate may both result in

decreased recrystallization [63]. However, they did not observe any correlation between the solubility of the API and crystallinity [63]. That could be because the solubility of the API in their work was in a much narrower range (1 to 6 g/L). The API-polymer interactions and polymer chain conformations in the solvent may also affect the recrystallization, but the effect of different polymer types is not easy to discern from the limited results in the present study [83, 84]. Further investigation of the relation between extent of recrystallization and solubility would be a good topic for future work.

Table 1.3 Extent of Recrystallizations in Solution Cast Films Computed from DSC Thermograms (n=3)

Formulation	***Crystallinity%***			
	Fresh Films			***1-year-old films***
	Form I	**Form II**	**Total**	**Form I**
MeOH-HPMC	48.0 ± 11.4	ND	48.0 ± 11.4	81
EtOH-HPMC	40.1 ± 20.8	ND	40.1 ± 20.8	70.5
Ace-HPMC	ND	ND	-	75
DCM-HPMC	ND	ND	-	NT
EtOH-HPC	9.9 ± 1.1	9.1 ± 1.1	18.9 ± 2.1	NT
Ace-HPC	1.1 ± 0.3	2.5 ± 0.5	3.6 ± 0.8	NT

ND: Not detected
NT: Not tested

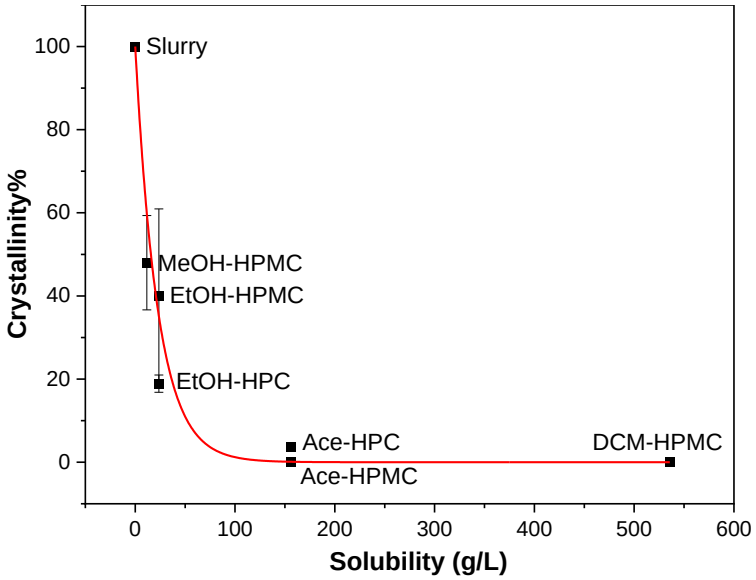

Figure 1.3 Crystallinity in freshly made 10% FNB loaded HPMC and HPC films versus solubility of FNB in the corresponding solvents. Fitted trend-line based on a power-law function.

Appendix B offers a solution for the recrystallization during the film preparation. It was demonstrated that another polymer layer on top of the drug-loaded solution cast film may prevent recrystallization during the drying process. Decreased or prevented recrystallinity helped to improve supersaturation capability even though the initial dissolution rate was decreased.

2.5.3 Content uniformity

Relative standard deviation (RSD) values of thickness, drug amount per area, and drug loading, along with label claim% (LC%) and acceptance values (AV) [73] for 10% FNB loaded solution and slurry cast films are presented in Table 1.4. The RSD values (Table 1.4) were mostly in line with the recrystallization observed, both quantitatively (Table 1.3) and qualitatively (Figure 1.1). However, despite the large variations in the recrystallization in different films, its impact on the drug amount RSDs was not as significant, since RSD was <6% in most cases. Films with high

recrystallization amount and standard deviation (EtOH-HPMC and MeOH-HPMC) had RSD >6% for drug amount per area (Table 1.4). DCM-HPMC film, in which there was no detected recrystallization, had the lowest RSD of drug per area (3.1%) among all formulations while MeOH-HPMC had the highest (7.8%) as it had the most recrystallization (Table 1.4). As compared to HPMC films, the HPC films had lower RSD values, which also corresponded to smaller re-crystallites (Ace-HPC ,Figure 1.1.e) or lower recrystallization (EtOH-HPC, Figure 1.1.f and Table 1.3) and less recrystallization variation (Table 1.3) in the HPC films. These results demonstrated that the uncontrolled recrystallization in the HPMC films affected the dosage (drug amount per area) uniformity which may be detrimental for pharmaceutical manufacturing. Non-uniform recrystallization also negatively impacted RSD of the thickness (Table 1.4). It is emphasized that while RSD of drug loading (wt%) indicated the composition uniformity, RSD of drug amount per area indicated the dosage uniformity which is affected by thickness uniformity. Fortunately, the RSD values for drug loading, which is another important measure, were <6% for all the formulations indicating that the FNB was well distributed in the precursor and maintained such uniformity after casting and drying. These findings were in line with previous results for slurry casting where using the planetary mixer and similar viscosity and drug loading range, uniformity was assured [30]. For all formulations, the films passed the acceptance value test (AV <15),Table 1.4. Even there, two cases (MeOH-HPMC and Slurry-HPC) with higher uncontrolled recrystallization had the highest AV values that are rather close to the failing level. Thus, uncontrolled recrystallization, which is highly likely for solution-

cast films, has an adverse impact on some of the film CQAs, such as the content uniformity.

Table 1.4 Drug Content Uniformity for Various 10% FNB Loaded Films

Polymer type	***Solvent***	***LC%***	***RSD of thickness***	***RSD of drug amount per area***	***RSD of drug loading***	***Acceptance value***
HPMC E15	Water	103.1	3.5	3.5	1.6	5.7
	1:4 (w:MeOH)	89.3	11.3	7.8	1.8	13.2
	1:4 (w:EtOH)	99.7	10.2	6.2	1.8	4.3
	1:4 (w:Ace)	98.3	4.2	4.8	2.3	5.5
	1:1 (DCM:EtOH)	94.5	4.3	3.1	1.6	7.7
HPC-L	Water	91.4	2.7	3.7	3	13.7
	1:4 (w:EtOH)	96.8	5.0	3.5	0.97	4
	1:4 (w:Ace)	97.1	3.2	3.8	1.6	5

2.5.4 Mechanical properties

Although there are no well-defined acceptance criteria for film mechanical properties, generally, high tensile strength (TS) and elongation at break (EB), and low Young's modulus (YM) are desired for handling purposes [85]. These three properties for HPMC and HPC films with and without FNB for various solvents were measured and presented in Figure 1.4. HPMC placebo films had a higher impact

of the solvent on Young's modulus than on tensile strength and elongation at break, whereas elongation at break was affected the most for HPC placebo films. This might be due to the combined effects of polymer solubility in these solvents and the boiling points of the solvent mixtures on the conformation of the polymer chains [63]. The addition of FNB decreased almost all film mechanical properties, in line with previous work [11, 86]. As reported before [11], an increase in elongation at the break due to APIs plasticizing effect was observed with only DCM-HPMC film having no detectable crystallinity. When recrystallization occurred, crystal FNB particles may have caused disruption sites in the film and decreased tensile strength, elongation at break and young's modulus. The crystal particles in the slurry films had a smaller size and less size variation than those for recrystallized particles in films. Further, the slurry films had more uniformly distributed FNB particles (Figure 1.1) and better thickness uniformity (Table 1.4). Consequently, slurry films had stronger (higher tensile strength) and more elastic structure than solution cast films with recrystallization. In previous work for slurry-cast films loaded with micron-sized particles also, the TS, YM and EB values were lower compared to those for films loaded with nanoparticles [27, 30]. Thus, the state of the API, including its crystal sizes and their distribution, all greatly impact the film mechanical properties.

Changing the preparation solvent between acetone, ethanol and water, HPMC and HPC films exhibited similar trends for all the mechanical properties. However, HPC films had much lower tensile strength and Young's modulus compared to HPMC counterparts showing the effect of the polymer itself.

Therefore, the selection of both the solvent and the film-forming polymer in solution casting can strongly impact film mechanical properties.

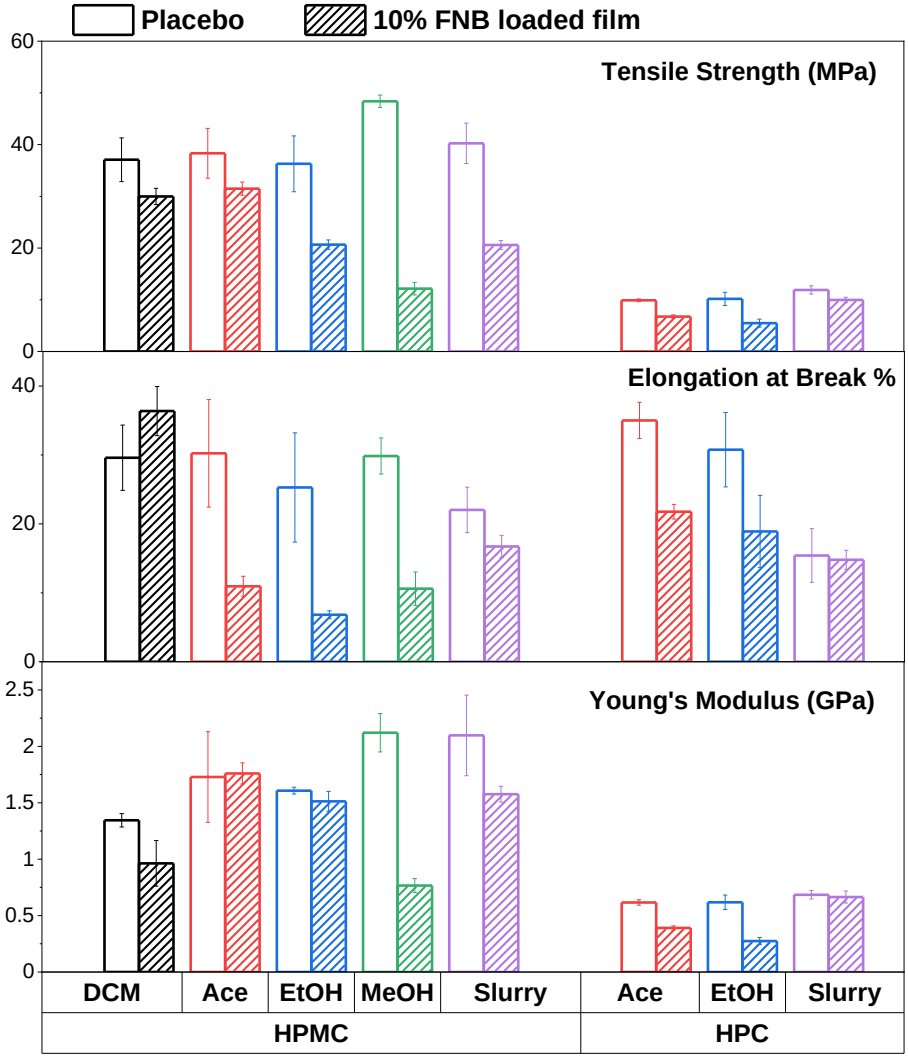

Figure 1.4 Mechanical properties of placebo and 10% FNB loaded HPMC and HPC films.

2.5.5 Dissolution under sink conditions

The dissolution profiles of HPMC and HPC films under sink conditions are presented in Figure 2.5.a and b, respectively. Generally, one would expect films having some level of amorphous content to dissolve faster unless the effect of the film matrix structure dominates. For HPMC films (Figure 2.5.a), three out of four

solution-cast films were faster than the slurry- film, which by design had 100% crystalline FNB. The exceptional case was MeOH-HPMC film, which had many large FNB crystals. The fastest dissolution was for the Ace-HPMC films, likely due to little or no recrystallization. Between DCM-HPMC and Ace-HPMC films, slower dissolution of the former may be attributed to its film matrix structure induced by different solvents i.e., lower elongation at break with similar tensile strength [11, 15, 34]. Similar observations have also been reported for different polymer and solvents used in spray-dried amorphous solid dispersions [62, 87]. For the DCM-HPMC film, its high elongation at break and tensile strength may have led to its slower dissolution as compared with the EtOH-HPMC film. For HPC films, Ace-HPC and EtOH-HPC films showed a higher dissolution rate compared to their slurry counterpart (Figure 2.5.b) while they had a similar dissolution rate despite the differences in crystallinity and polymorph formation.

HPC films were slightly faster than HPMC films, see Figure A.3, Appendix A, for better visualization. The low inherent viscosity of the HPC-L might have affected the film structure, i.e., much lower tensile strength, leading to a higher dissolution rate under sink conditions. This is in line with a previous work, which showed that the addition of HPMC into HPC film resulted in a decrease in the dissolution rate [19]. Overall, the dissolution profiles under sink conditions were affected by polymer type and the matrix structure created by the combination of the polymer, drug, and the solvent used. It is noted that most films did not attain full dissolution during the testing time of 90 minutes. Such outcomes have been observed previously for films containing microparticles, nanoparticles or

amorphous APIs [18, 19, 29-31, 88]. Besides, the amount of SDS in the buffer used here was only 3.6 g/L, which was half that of previous studies [27, 30].

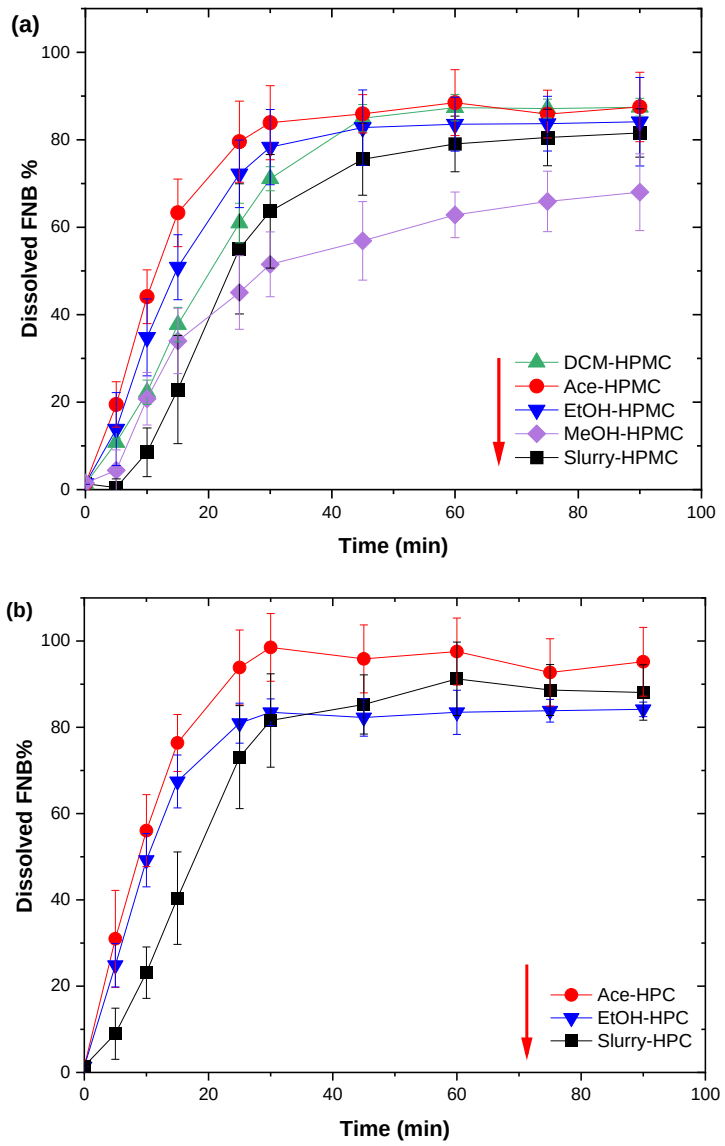

Figure 1.5 Film dissolution profiles under sink conditions, (a) HPMC-E15 (b) HPC-L (arrows indicate decreasing FNB solubility).

2.5.6 Dissolution under non-sink conditions

In order to examine the FNB supersaturation capability of the HPMC (Figure 2.6.a) and HPC (Figure 2.6.b) films during dissolution, non-sink conditions were used. Varying degrees of supersaturation levels were obtained for all the solution cast films, both in terms of the peak amount of drug dissolved and the area under the dissolution curve, AUC (Figure 2.6.a and b). Dissolution profiles of Ace-HPMC, DCM-HPMC and Ace-HPC films were compared to highlight the effect of solvent as well as polymer, see Figure A.4, Appendix A. Films made with the same solvent (acetone) reached a similar maximum FNB concentration with a similar initial dissolution rate. However, using DCM with HPMC led to a slower dissolution rate. Although these are not exhaustive results, it is likely that the effect of the solvent on the dissolution profiles might be more than the effect of polymer in some cases. Interestingly, the dissolution rate of DCM-HPMC was slightly slower than all the other solution cast films, which could be attributed to the solvent affecting the film matrix structure [11, 15, 34].

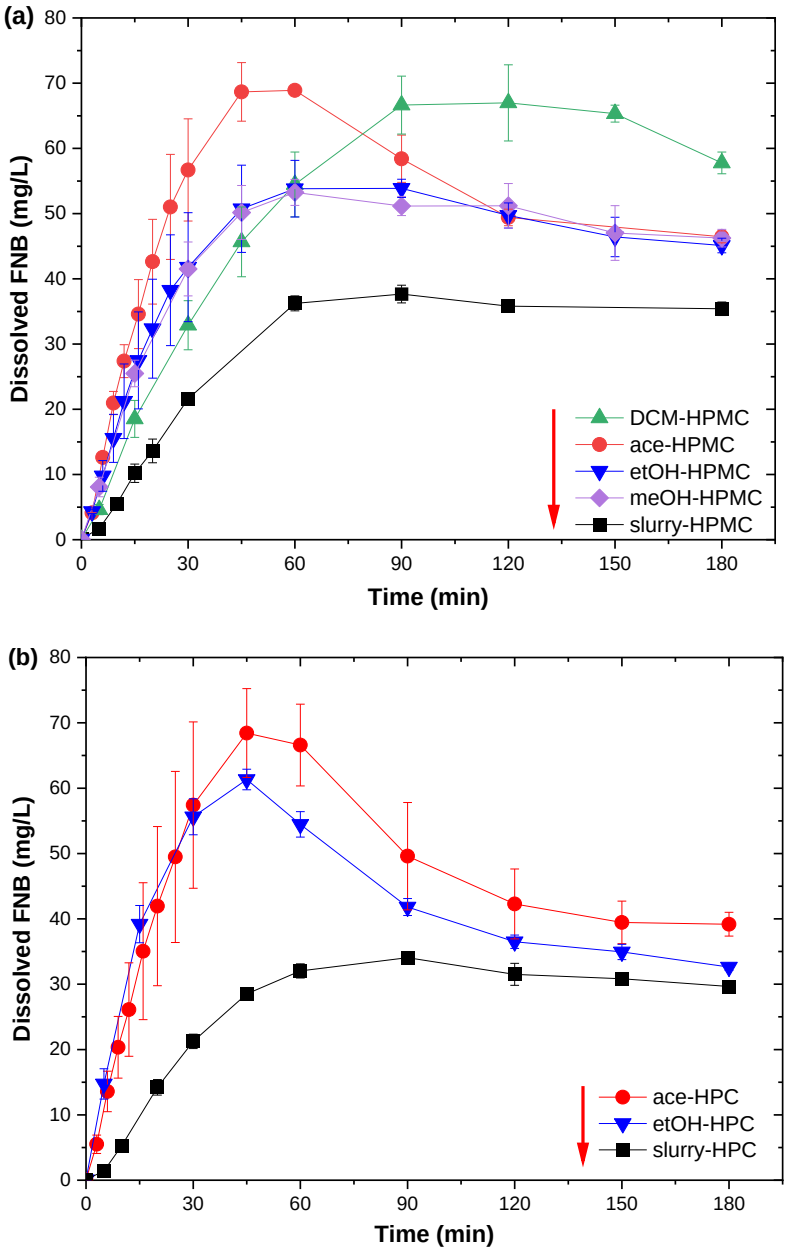

Figure 1.6 Film dissolution profiles under non-sink conditions, (a) HPMC-E15 (b) HPC-L (arrows indicate decreasing FNB solubility).

Since supersaturation capability, quantified through AUC, was expected to be dependent on the degree of recrystallization, their relationship was further analyzed, see Figure 2.7. For both the polymers, a linear trend was observed between the AUC and the degree of recrystallization, which was affected by both

the solvent and the polymer. The films that had better stabilization, indicated by lower crystallinity, reached higher AUC. In all cases, HPMC exhibited better supersaturation maintenance capability as compared to HPC. Amongst solvents, Ace performed better than EtOH. These trends demonstrated how both the polymers and solvents have an impact on the dissolution performance. However, since the form of the drug in solution cast films being unstable, the dissolution performance would continue to change with time of storage. Therefore, the storage stability of these films was examined next by evaluating the degree of recrystallization and changes in the dissolution profiles.

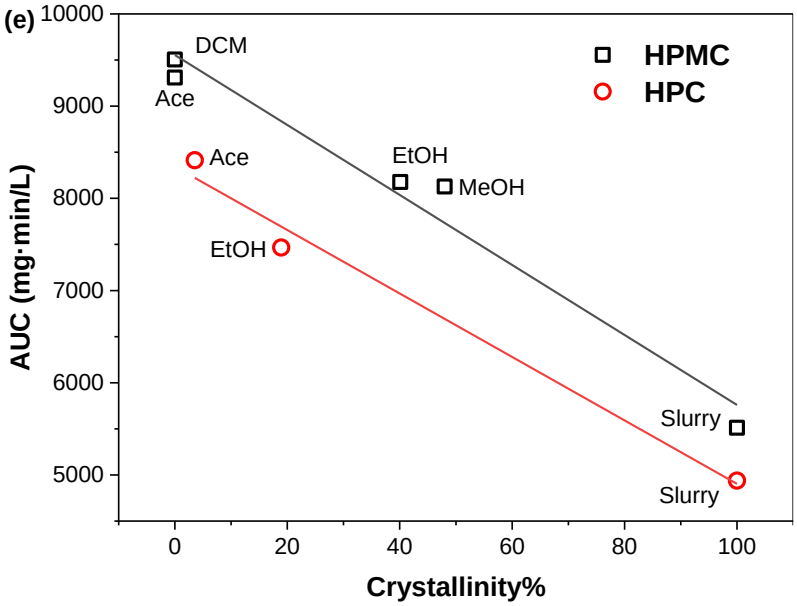

Figure 1.7 Correlation between AUC of non-sink dissolution profiles and crystallinity.

2.5.7 Stability

Selected cases of HPMC films made using three different solvents, Ace-HPMC, EtOH-HPMC and MeOH-HPMC films having varying degrees of recrystallization when fresh, were considered for testing time stability of the state of

recrystallization, and the subsequent impact on dissolution. They were stored in plastic bags at room temperature and humidity up to 1 year and tested for dissolution. Sink conditions were used for better discrimination of the effect of large recrystallized particles, as was the case for fresh films, e.g., MeOH-HPMC, discussed in Section 2.5.6.

The most interesting outcome is that the increase in the recrystallization amount after 1-year storage was inverse of initial recrystallization levels. Thus, low initial recrystallization did not guarantee better stability. In fact, Ace-HPMC having no detected recrystallization in the fresh film had the most increase in the recrystallization in a year, reaching a high level of 75%. Recrystallization increased by ~30% in EtOH-HPMC (from 40.1% to 70.5%) and by ~30% in MeOH-HPMC film (from 48% to 81%). It was interesting that although the dissolution rates of the Ace-HPMC and MeOH-HPMC films decreased after a year, EtOH-HPMC was not affected (Figure 2.8). Such an outcome could be attributed to larger error bars of the dissolution curves for stored films, indicating differing levels of recrystallization amongst various film samples, and probably no significant changes in the crystal sizes after storage. In contrast to such significant stability issues with solution-cast films, the dissolution rates of the slurry-cast films loaded with nano-sized crystalline API did not significantly change after accelerated storage testing of 6 months exposure at 40 °C and 75% RH [33]. Whereas for amorphous dispersions, dissolution profiles could change significantly even when no significant increase in the crystallinity was found for spray-dried solid dispersions after 1-month exposure at 40 °C and 75% RH [87]. Overall, uncontrolled recrystallization and apparent lack

of stability during storage may pose formidable challenges in developing more stable solution-cast film formulations without requiring extensive investigation of the complex inter-play between the drug, film-forming polymer, and solvents.

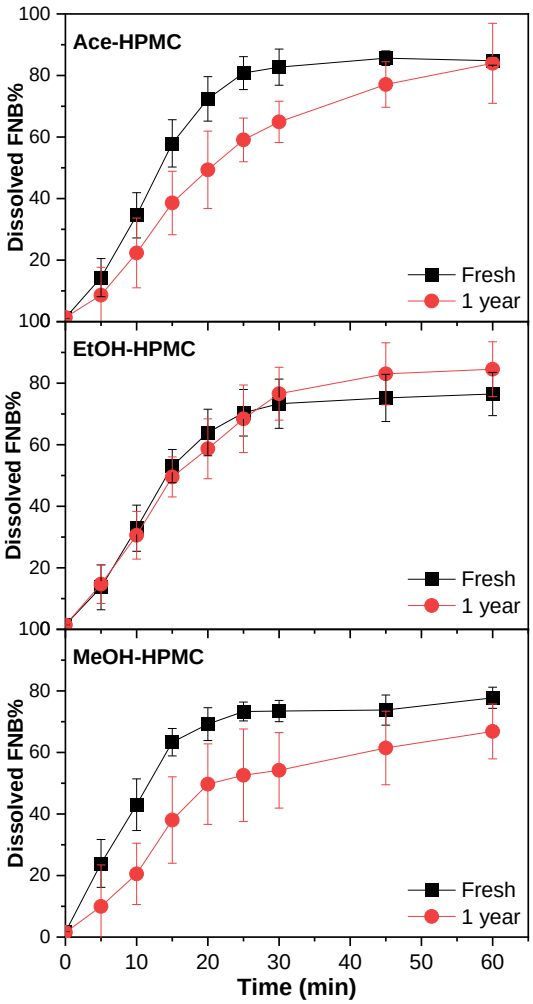

Figure 1.8 Dissolution profiles under sink conditions for fresh and 1-year-old 10% FNB loaded solution cast films; Ace-HPMC, EtOH-HPMC and MeOH-HPMC.

2.6 Conclusions

For solution casting of FNB, a poorly water-soluble drug, the choice of the polymer and the solvent system affected the film quality attributes, such as the drug recrystallization, drug content uniformity, film mechanical properties, drug

dissolution rate including supersaturation, and storage stability. In addition to the solvent affecting the film structure, it had a significant impact on FNB recrystallization, which in turn impacted many other film attributes, including the content uniformity and film mechanical properties which were found to be adversely affected by uncontrolled recrystallization leading to the occurrence of large and uneven crystals in some of the films. The most important finding was that the drug recrystallization was affected strongly by FNB solubility in the solvent, and to a lesser extent by the polymer type, which also affected the film structure and related properties. Consequently, the recrystallization of FNB also affected its dissolution rates as well as supersaturation under non-sink conditions, again largely attributed to uncontrolled crystal sizes. Quantitatively, AUC, one of the parameters defining bioavailability, was found to be linearly correlated with drug crystallinity in fresh films. It was also affected by the supersaturation maintaining capability of the polymer. The degree of FNB recrystallization in solution-cast films significantly increased after one-year storage, reaching very high levels even for the films with no initial recrystallization. These results demonstrated that for solution-cast films, uncontrolled recrystallization and poor time-stability would be unavoidable, and over time, amorphous drug content would diminish significantly.

CHAPTER 3

EFFECT OF CASTING TECHNIQUES ON CQAS OF FILMS LOADED WITH POORLY WATER-SOLUBLE DRUGS

3.1 Introduction

Recently, oral films drew the attention of many researchers owing to their favorable characteristics such as patient compliance, improved bioavailability, flexible dosing and adaptability to continuous manufacturing [1, 2, 4, 6, 8]. Having these advantages, oral films are believed to play a key role in the reduction of time and the cost of manufacturing [7]. Solventless casting, i.e., hot-melt extrusion (HME) [9-11, 13-19], and solvent casting, i.e., solution [20-26] and slurry casting [27-32, 36, 41], are commonly utilized techniques for pharmaceutical oral film manufacturing. In the literature, each technique was shown to be enhancing the bioavailability of a poorly water-soluble active pharmaceutical ingredient (API) by increasing the dissolution rate. However, it is unknown that which technique would create a better performing product under similar conditions, i.e., same API and loading, same polymer, thickness, etc. Therefore, this paper presents a comparative assessment of solvent casting techniques, i.e., solution and slurry casting, to have a better understanding of the capabilities and limitations of film manufacturing techniques.

The dissolution rate can be explained by the Noyes-Whitney equation [42] in which the solubility of the API and the total surface area are the variables. Utilizing this equation, an increase in dissolution rate can be achieved for oral films

via solution or slurry casting. In solution casting, the drug is present mostly in the amorphous state which subsequently shows an increased solubility in the media leading to an increase in dissolution rate. In slurry casting, the total surface area of the API can be increased by size reduction, i.e., micronization, nano-milling, to achieve a higher dissolution rate.

Amorphous compounds are generally claimed to be better than crystalline with size reduction in terms of dissolution enhancement owing to increased solubility of API [89, 90]. However, especially at high drug loadings, the amorphous structure has disadvantages of instability which may hinder the solubility advantage. In fact, it has been shown that most of the amorphous compounds are prone to crystallize in time [51-53]. On the other hand, crystalline API may enhance the dissolution rate by increased total surface area and ensure stability. Besides, particle size reduction below 200 nm may lead to some extend of solubility enhancement. Nonetheless, particle agglomeration needs to be prevented to maintain the increased total surface area which in turn increases the dissolution rate. It has been shown that nano-sized formulations may have similar oral or intravenous (i.v.) absorptions compared to amorphous formulations of poorly water-soluble APIs [91, 92]. Li et al. demonstrated that nanoparticles in a polymeric matrix may dissolve faster compared to amorphous solid dispersion with higher supersaturation capability [93]. Given the above, these techniques need to be closely investigated as choosing one technique over another would not be a simple process. In addition, compared to conventional dosage forms, i.e., tablets, capsules, liquids and i.v., film dosages incorporate more mechanisms to the

dissolution process due to matrix structure and available surface area of the dosage. Therefore, the objective of the present work was to systematically investigate the impact of two different casting techniques, i.e., solution and slurry casting on the critical quality attributes (CQAs) of the films.

Different approaches, i.e., solubilizing agent, salt formation, ion-pair complexes, etc., were successfully applied to eliminate the recrystallization disadvantage of solution casting and obtain crystal-free films [23, 94, 95]. However, in many other cases using the conventional solution casting method, different levels of initial crystallinity or recrystallization in time were observed in the film where solution casting was applied [21-23, 43, 44]. This recrystallization of API in the film would not only affect the dissolution rate but also impact other critical quality attributes (CQAs) of the film, i.e., content uniformity and mechanical properties. Morales et al. stated that solution casting adversely impacted the uniformity of the films at high drug loadings due to the high amount of recrystallization [21]. Cetindag et al. reported the effect of recrystallized API on the mechanical properties where larger particles led to more decrease in tensile strength compared to their placebo counterparts [96]. All these CAQs would also affect the dissolution rate adversely. It should also be noted that the observed recrystallizations were also unpredictable. On the other hand, the slurry casting method allows the preparation of films with predictable properties and is also loaded with stable API [29, 35]. Krull et al. reported that the films loaded with nano-sized API in varying drug loadings had similar redispersibility and dissolution

profiles after 6 months of storage at accelerated stability conditions (40 °C and 75% relative humidity) [35].

Considering the advantages and disadvantages of both techniques at high drug loadings, one may not predict which technique can produce films with better performance, i.e., content uniformity, mechanical properties and dissolution rate. Therefore, the aim of this study was to develop a better understanding of the advantages and disadvantages of two film manufacturing methods, i.e., solution and slurry casting techniques, over each other at high drug loadings. These two film casting techniques, solution and slurry casting, were compared using a BCS class II model drug with intermediate crystallization tendency, fenofibrate (FNB) [47], and a widely used polymer in pharmaceuticals, hydroxypropyl methylcellulose E15 (HPMC E15), as the film former [64]. Critical quality attributes of the films prepared using different preparation techniques were measured, such as the content uniformity, film mechanical properties, and dissolution profiles. These results were analyzed to assess the hypothesis that comparable or even faster dissolution rates than solution cast films can be obtained via particle engineering in the film (slurry casting) without compromising the stability of the product.

3.2 Materials

Fenofibrate (FNB, Jai Radhe Sales) was used as a model BCS Class II drug with 0.1 mg/L solubility in water [69]. Hydroxypropyl methylcellulose (HPMC; Methocel E15 Premium LV, M_w ~40 000, 12-18 *cP*; The Dow Chemical Company, Midland, MI) as a film former and glycerin (Sigma-Aldrich, Saint Louis, MO) as plasticizer

were used. Acetone (Honeywell, Burdick & Jackson, ACS/HPLC) was used as received for FNB solubilization in solution casting. Sodium dodecyl sulfate (SDS; Sigma-Aldrich, Saint Louis, MO) was used as a stabilizer for nanoparticle stabilization and surfactant for dissolution experiments. Pharmaceutical-grade hydrophilic silica (M5P, Cabot Corporation, MA) with a primary particle size of 16 nm was used as the coating material of the micronized API.

3.3 Methods

3.3.1 Preparation of micronized coated drug powders

Micronized dry coated drug powder was prepared via procedures adapted from previous works [30, 97]. Briefly, as-received fenofibrate (FNB) powder and silica were pre-mixed using Laboratory Resonant Acoustic Mixer (LabRAM; Resodyn Acoustic Mixers, Inc., Butte, MT) with a ratio of 97:3 at 61 Hz frequency and 75 G acceleration for 5 min. Then, the FNB-silica mixture was micronized and coated via a fluidized energy mill (FEM, qualification model, Sturtevant Inc., Hanover, MA) where the powder was fed into FEM with a constant 1 g/min rate at a feeding pressure of 45 psi and grinding pressure of 40 psi. The particle size of micronized coated FNB powder (MC-FNB) was measured via Rodos/Helos system (Sympatec, NJ, USA) using 1 bar dispersion pressure.

3.3.2 Preparation of drug nanosuspensions

FNB nanosuspension was prepared via wet stirred media milling (WSMM) (MicroCer, Netzsch, Exton, PA). The milling method was adapted from previous studies where further information can be found [29, 98, 99]. Briefly, sodium dodecyl

sulfate (SDS) and HPMC were added into DI water for stabilization of FNB particles in the suspension. Then, AR-FNB powder was added under a shear mixer (Fisher Scientific Laboratory Stirrer, Catalog No. 14-503, Pittsburgh, PA). The AR-FNB suspension was composed of 2.5% (wt%, w.r.t. to water) HPMC, 0.05% (wt%, w.r.t. to water) SDS and 20% (wt%, w.r.t. to water) FNB. Prepared AR-FNB suspension was milled via WSMM for 120 minutes. Collected FNB nanosuspension was stored for overnight to remove bubbles created from milling. The particle size of the FNB in the suspension was measured via a laser diffraction particle size analyzer (Coulter LS 13320, Beckman Coulter, FL, USA).

3.3.3 Preparation of films loaded with fenofibrate

Formulation names and composition of the polymer solutions that were used in different casting techniques, i.e., solution or slurry casting, are presented in Table 3.1. All polymer solutions were prepared using HPMC E15 as film former and glycerin as a plasticizer with a ratio of 3:1 (w/w). In the slurry casting method for micron-size API, the viscosity of the polymer solution cannot be too high due to a viscosity increase by the addition of powder API in the following step [30]. On the other hand, the viscosity of the polymer solution cannot be too low for the slurry casting method for nano-size API due to a viscosity decrease by the addition of nanosuspension in the following step [35]. Lower polymer concentration was needed for solution-cast films due to the increased viscosity by the organic solvent used and the limited solubility of the polymer in the organic solvent [96]. Fixing the polymer concentration according to one method would cause a disadvantage to other preparation methods leading to an unfair assessment of the preparation

methods. Therefore, optimized polymer concentrations were used for each preparation method to ensure the best conditions for each method since the aim was to compare films at their best conditions for each considered method. The compositions of polymer solutions were adapted from Zhang et al. [30], Krull et al. [35] and Cetindag et al. [96] for slurry cast films loaded with micron-sized particles, slurry cast films loaded with nano-size particles and solution-cast films, respectively (Table 3.1).

Table 3.1 Formulation Compositions of Films Prepared via Different Casting Methods

Name of the formulation	***FNB (wt%) in dry film***	***Polymer (wt%)****	***Plasticizer (wt%)****	***Water (wt%)****	***Organic solvent (wt%)****
Solution	10, 20, 30 or 40	10	3.3	17.3	69.4
Slurry - AR	10, 20, 30 or 40	12	4	84	-
Slurry - MC	10, 20, 30 or 40	12	4	84	-
Slurry - nano	10, 20, 30 or 40	17	5.7	77.3	-

* With respect to total polymer solution amount

Cetindag et al. showed that when 1:4 water:acetone (w:Ace) or 1:1 ethanol:dichloromethane (EtOH:DCM) mixtures were used to prepare solution-cast films, crystal-free films may be produced [96]. However, DCM has a safety

limitation in pharmaceutical products according to the Guidance for Industry by Food and Drug Administration [70]. Therefore, 1:4 w:Ace was chosen as the solvent mixture for the preparation of solution-cast films at high drug loadings. More details on solvent selection may be found in [96].

Polymer solutions were prepared via previously established methods [29, 96]. Briefly, the required water or solvent mixture (Table 3.1) were heated up to 30 °C while stirring and the plasticizer was added. The solutions were continued to be heated up to 80–90 °C or 40–45 °C for water or organic solvent-based solutions, respectively. Then, the polymer powder was added to the mixture slowly and the final solutions were cooled down to room temperature.

Aqueous polymer solutions were mixed with either AR-FNB or MC-FNB powder or FNB nanosuspension, to prepare the film precursor for Slurry-AR, Slurry-MC, or Slurry-nano films, respectively. Polymer solution prepared with 1:4 (w:Ace) mixture was mixed with AR-FNB powder to prepare the film precursor for Solution films. Polymer solutions were mixed with FNB at different ratios to obtain 10, 20, 30, or 40% (wt%) drug loading in the dry film using a planetary centrifugal mixer (Thinky Model ARE-310). Mixing was performed for either 2 min or 10 min at 2000 rpm for slurry or solution cast film precursors, respectively and followed by defoaming for 2 min at 2200 rpm.

Each precursor was cast onto a plastic substrate (Scotchpak TM 9744, 3M, MN, USA) with a doctor blade (Elcometer, Rochester Hills, MI) using a Lab-Cast Model TC-LC Tape Caster (HED International, Ringoes, NJ). Wet film thickness for each formulation was adjusted to obtain 100 µm dry film thickness. Slurry-cast

films were dried at 50 °C for 1 h while solution-cast films were dried at room temperature overnight. Following the drying, films were peeled and stored in plastic bags until further analysis. More details on the selection of process parameters for mixing or drying can be found in [30, 96].

3.3.4 Crystallinity of fenofibrate in the film

The films were analyzed using a digital microscope with polarized back-lighting mode (Carl Zeiss Microscopy, LLC. Germany). Each film with 1 cm x 3 cm dimensions was fixed on a glass slide by tape on the edges and images were taken from the top. For thin films produced here, this approach allowed for the detection of the recrystallization within and on the surface of the film.

The crystallinity of fenofibrate in the film was analyzed using a differential scanning calorimeter (DSC, Mettler Toledo, Inc., Columbus, OH). An aluminum standard pan loaded with ~8 mg of the film was heated from 25 °C to 120 °C at a constant heating rate of 10 °C/min under a nitrogen flow and cooled down to 25 °C at the same rate. The FNB in the Slurry-AR films was assumed to be fully crystalline. Specific enthalpies (area under melting peaks, if occurred) were used to calculate the percentage of crystallinity in the solution-cast films using the thermograms (Equation (2.7)).

$$Extent\ of\ \ recrystallization\ \% = \frac{Specific\ enthalpy\ of\ the\ sample\ film}{Specific\ enthalpy\ of\ the\ slurry\ film} \times 100 \qquad (2.7)$$

3.3.5 Redispersion of particles from dried films

The drug particles were re-dispersed from dried films and size distribution was analyzed to assess the particle size maintenance in the film structure. The procedure was modified from earlier works [27, 30]. Briefly, 2 or 3 (depending on drug loading) circular punches of 0.72 cm^2 in the area were vortexed in 10 ml deionized water at 1500 rpm for 2 min. The size of drug particles in the suspension was measured via a laser diffraction particle size analyzer (Coulter LS 13320, Beckman Coulter, FL, USA).

3.3.6 Content uniformity

The uniformity of the dried films was analyzed in terms of content, i.e., drug loading and drug amount per area, and thickness via relative standard deviations. For each formulation randomly selected ten circular punches, ~0.7 cm^2 area, were dissolved in 7.2 g/L sodium dodecyl sulfate (SDS) solution following mass and thickness measurements. Either 20, 30, 50, or 100 mL of 7.2 g/L SDS solution were used depending on the theoretical drug loading, i.e., 10%, 20%, 30%, or 40% drug loading, respectively. It should be noted that the small sample size used for the uniformity testing, which was about $1/10^{th}$ of the intended dosage size (2 cm x 3 cm), was for better discrimination between samples [27, 30]. The absorbance of each solution was measured via a UV-vis spectrophotometer (Thermo Fisher Scientific Inc., MA, USA) at the maximum wavelength for FNB (290 nm) and concentrations were calculated using a pre-prepared calibration curve. Label claim% (the average drug loading with respect to label claim), and relative standard deviations (RSD, average value divided by standard deviation) for drug

amount per area and drug loading% (FNB weight with respect to total weight) were calculated and reported. The acceptance value (AV) for each formulation was also calculated Equation (2.8) [73].

$$Acceptance\ value(AV) = \left|M - LC_{avg}\%\right| + k \cdot s \qquad (2.8)$$

In the above equations, $LC_{avg}\%$ is the average drug loading with respect to label claim; *s* is the standard deviation of $LC_{avg}\%$, k is the acceptability constant, 2.4. Parameter M is set as shown below.

M: Reference value, 98.5 if $LC_{avg}\% < 98.5$

$LC_{avg}\%$ if $98.5 < LC_{avg}\% < 101.5$

101.5 if $LC_{avg}\% > 101.5$

3.3.7 Mechanical properties

The mechanical properties of the films were analyzed via tensile test using a TA-XT Plus Texture Analyzer (Stable Microsteps, UK). Results were analyzed in terms of the tensile strength (TS), Young's modulus (YM), and percent elongation at break (EB%). Briefly, five film samples, 50 mm in length and 15 mm in width were cut for each formulation. Each sample was elongated between two parallel grips along the length of the film until failure. The elongation was performed at a constant rate (1 mm/s). YM, TS and EB were calculated from the stress-strain curve recorded during the tensile test and the average values along with standard deviations were reported. Further details about mechanical properties may be found in [29, 74].

3.3.8 Dissolution under sink conditions

The dissolution profiles were tested under sink conditions using previously established procedures for closed-loop flow-through cell dissolution apparatus (USP IV; Sotax, Switzerland) [27, 30, 75]. From each formulation, 6 circular film samples in an area of ~0.71 cm^2 were punched randomly and placed between 5 g of 1 mm glass beads within the dissolution cell. 3.6 g/L SDS solution with a flow rate of 16 ml/min was used as the dissolution medium at 37 ± 0.5 °C. Fixed dissolution media volumes (175 mL, 300 mL 460 mL and 600 mL) were used for each drug loading (10%, 20%, 30% and 40%) ensuring similar sink conditions. The dissolution profiles were plotted as the percentage of FNB dissolved with respect to time.

As the statistical analyses on dissolution profiles of films, bootstrap similarity (f_2) analyses were conducted due to high variation, seen as larger standard deviations, in the dissolution profiles [100, 101].

3.4 Results and Discussion

3.4.1 Crystallinity of fenofibrate in the film

Figure 3.1 presents the optical microscopy images taken using polarized light for the films prepared with the solution casting method for various drug loadings. Films at 10% drug loading contained crystal seeds and small crystals on a few occasions while films with higher drug loadings qualitatively indicated the increased recrystallization. At 40% drug loading, drug recrystallization was also observed in layers as indicated by arrows in Figure 3.1.d. It should be noted that the observed drug crystals were non-uniformly distributed along the film surface and the most

representative images were selected for each film at 20, 30 and 40% drug loadings (Figure 3.1.b-d) while the image at 10% drug loading was selected as an example of recrystallization occurrences (Figure 3.1.a).

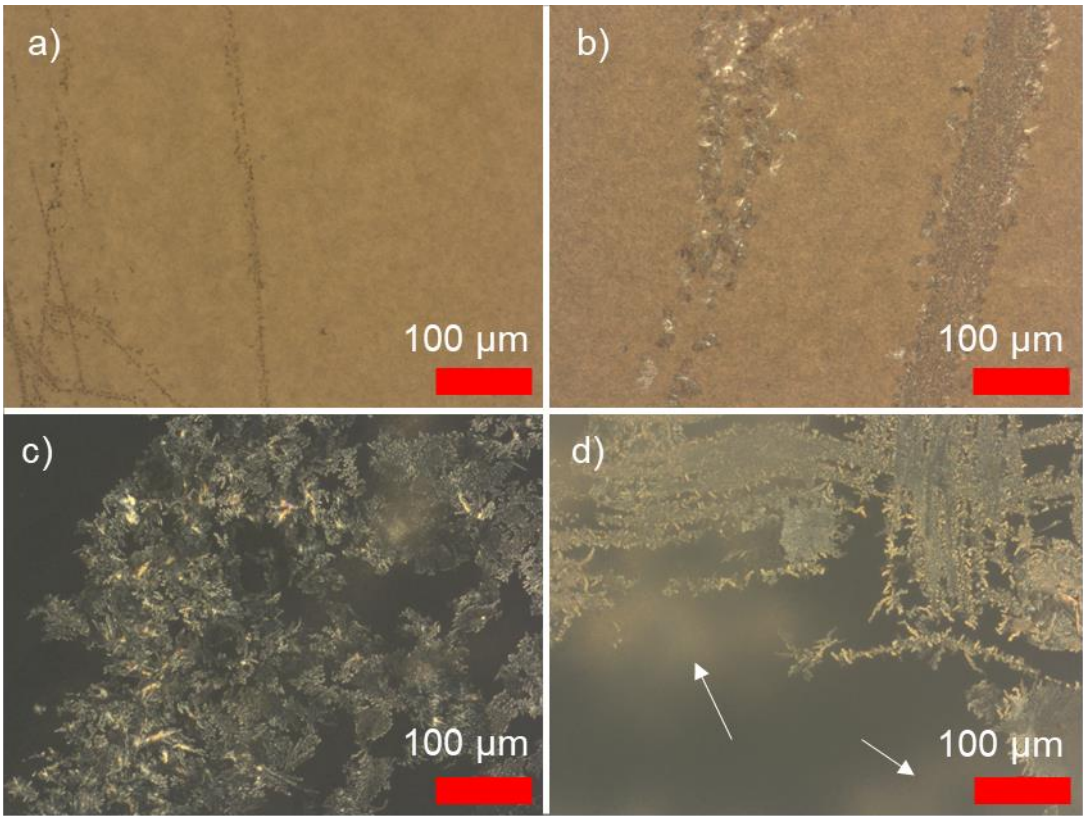

Figure 3.1 Optical images of Solution films loaded with a) 10% b) 20% c) 30% and d) 40% FNB.

DSC analyses were conducted to assess any possible polymorph formation of FNB since different crystallite shapes may be observed due to polymorphism [72, 76], Figure 3.2.a presents DSC thermograms of films with varying drug loadings. A single melting peak at 79 °C corresponding to FNB (form I) was observed for films with a drug loading of 20-40%, comparable to previous reports at 80 °C [77] showing no polymorph occurrence.

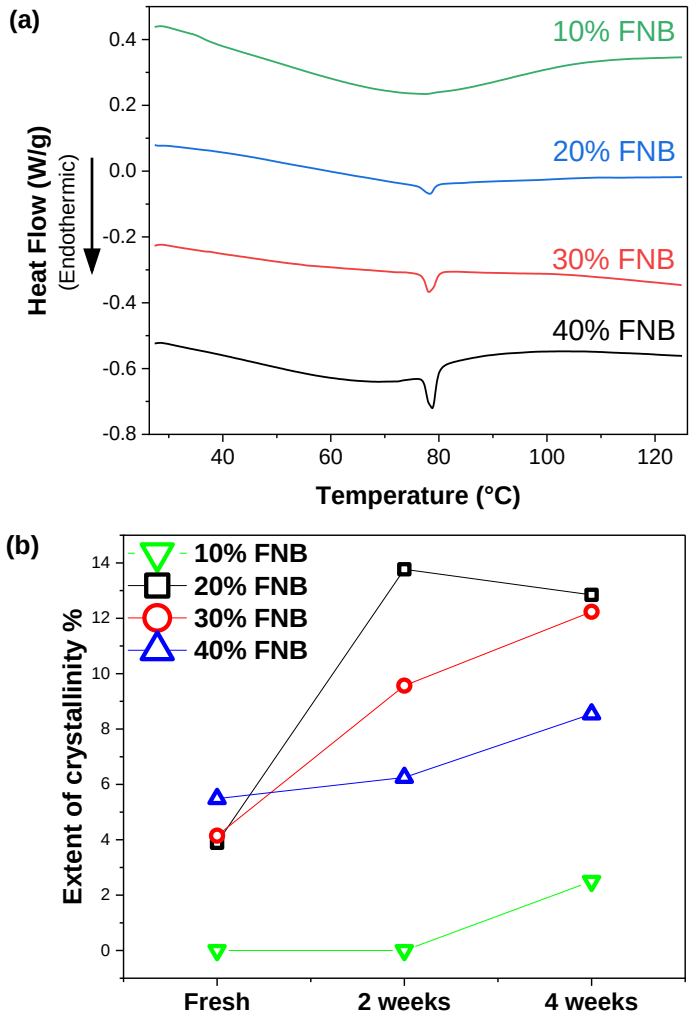

Figure 3.2 a) DSC thermograms of Solution cast films with varying drug loadings b) Extent of recrystallizations in solution cast films computed from thermograms.

The percentage of crystallinities for Solution films with varying drug loadings (10-40%), calculated from the melting peaks obtained via DSC measurements (Figure 3.2.b) were in line with optical images in Figure 3.1. Figure 3.2.b compares the crystallinity of FNB in the films with various drug loadings and aging times. As drug loading increased, the crystallinity of FNB in the fresh films slightly increased. After storage of the films (at room temperature and humidity), the increase in crystallinity was more prominent for lower drug loadings (20 and 30% drug

loading). Cetindag et al. also revealed that low initial crystallinity may not result in better stability which is in line with the present findings.

3.4.2 Redispersion of particles from dried films

The particle sizes of as received (AR) and micronized-coated (MC) FNB powders and the nanosuspension before mixing with polymer solution were reported in Table 3.3. The preservation of particle sizes during preparation and drying was anticipated for Slurry formulations while the AR-FNB powder was dissolved for Solution formulation and expected to remain in the dry film.

Table 3.2 Formulation Names, Processing Conditions and Particle Sizes of FNB before Mixing with Polymer Solution

Formulation	Drug form	d_{10} (µm) ± SD	d_{50} (µm) ± SD	d_{90} (µm) ± SD
Solution Slurry - AR	As received powder	2.10 ± 0.02	6.18 ± 0.07	13.27 ± 0.12
Slurry - MC	Micronized coated powder	0.68 ± 0.02	2.77 ± 0.1	5.32 ± 0.08
Slurry - nano	Wet milled suspension	0.103 ± 0.001	0.159 ± 0.001	0.241 ± 0.001

SD: Standard deviation

The particle size maintenance and recovery of FNB particles from dried Slurry films were analyzed through the redispersion test. The redispersibility of recrystallized FNB in the Solution films and/or recrystallization in the test medium (DI water) was also analyzed using the same conditions as was for Slurry films.

Figure 3 presents the particle size distributions (PSDs) of redispersed particles from Solution, Slurry-AR, Slurry-MC and Slurry-nano at varying drug loadings, 10–40%. PSDs belonging to Slurry films at each drug loading were unimodal where AR particles had the broadest PSD. However, PSDs for Solution films were very broad and multi-modal indicating the great variance in the recrystallization of FNB either in the film or after contact with the test medium (DI water).

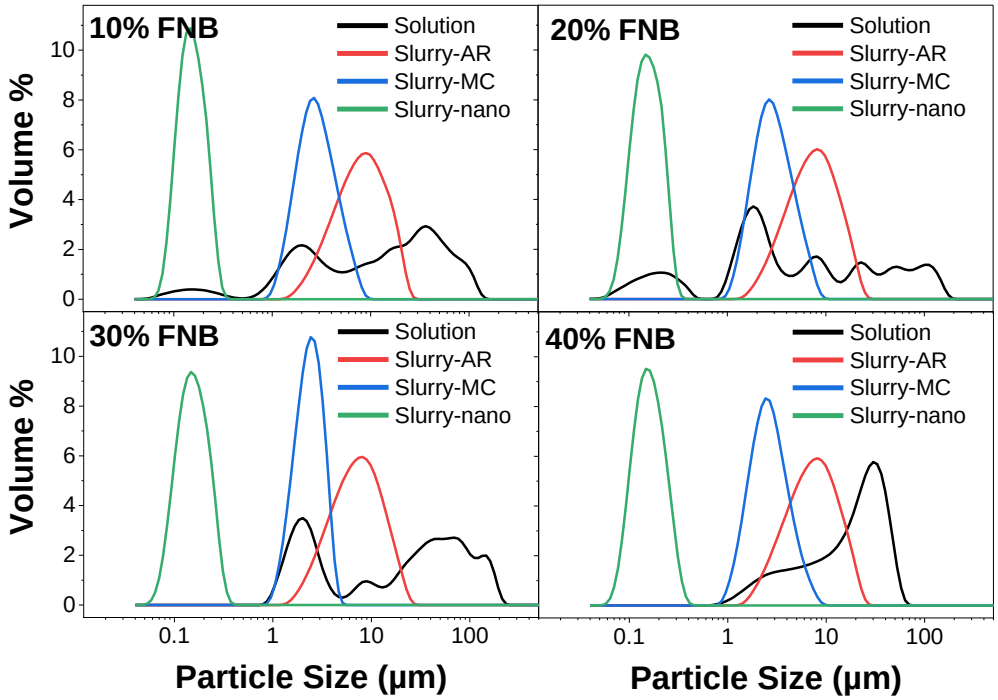

Figure 3.3 Particle size distribution of re-dispersed particles from dry films with varying drug loadings and different preparation methods.

As explained in the previous section, Solution film at 10% drug loading did not show any crystallinity according to DSC results (Figure 3.2) and optical imaging (Figure 3.1) revealed that there were only crystals or very small. However, the redispersion test showed a very broad PSD varying from 40 nm to 160 μm suggesting the recrystallization in the test medium. Similar behaviors were

observed for Solution films at 20 and 30% drug loadings while only a bi-modal and relatively narrower distribution was observed for 40% drug loading. This may be due to the presence of already recrystallized FNB in higher amounts compared to lower drug loadings. Therefore, low initial crystallinity may not mean better stability.

Table 3.3 presents the particle sizes of each formulation along with calculated standard deviations and relative standard deviations (RSDs). Comparison between the particle sizes after redispersion (Table 3.3) and the primary particle sizes (before mixing with the polymer solution, Table 3.2), showed that Slurry-MC and Slurry-nano films were able to redisperse from the film while preserving their particle sizes. However, there was a slight increase in the redispersed particle size of Slurry-AR film compared to its primary particle size. Nonetheless, repeatable sizes with low RSDs were obtained for all Slurry films while Solution films, especially at 10% drug loading, resulted in high RSD values further confirming the unpredictability of the recrystallization process.

At high loadings of micron-size APIs, particle agglomeration may be promoted due to close proximity of the drug particles, especially for films (thickness of 100 µm).

Table 3.3 Particle Size Distribution of Re-Dispersed Particles from Dry Films

Formulation	Drug loading%		$d_{4,3}$ (µm)	d_{10} (µm)	d_{50} (µm)	d_{90} (µm)
Solution	10%	AVG	13.885	0.300	3.827	35.975
		SD	0.771	0.274	4.883	3.698
		RSD	5.551	91.452	127.599	10.280
	20%	AVG	20.290	0.242	3.367	71.935
		SD	1.937	0.015	0.099	8.111
		RSD	9.549	6.149	2.940	11.275
	30%	AVG	42.100	1.685	24.680	116.850
		SD	1.994	0.020	2.008	6.293
		RSD	4.736	1.175	8.137	5.386
	40%	AVG	21.840	3.179	20.850	42.685
		SD	0.226	0.082	0.368	0.191
		RSD	1.036	2.580	1.764	0.447
Slurry-AR	10%	AVG	10.030	3.650	8.652	18.835
		SD	0.467	0.090	0.287	1.223
		RSD	4.653	2.461	3.318	6.495
	20%	AVG	8.812	3.404	7.766	15.945
		SD	0.016	0.001	0.010	0.021
		RSD	0.185	0.042	0.127	0.133
	30%	AVG	8.450	3.255	7.418	15.310
		SD	0.070	0.030	0.069	0.092
		RSD	0.829	0.907	0.936	0.599
	40%	AVG	8.615	3.302	7.603	15.570
		SD	0.064	0.008	0.025	0.170
		RSD	0.739	0.236	0.335	1.090
		SD	0.001	0.001	0.002	0.000
		RSD	0.697	0.990	1.096	0.000

AVG: Average, **SD:** Standard deviation, **RSD:** Relative standard deviation

Table 3.3 (Continued) Particle Size Distribution of Re-Dispersed Particles from Dry Films

Formulation	Drug loading%		$d_{4,3}$ (µm)	d_{10} (µm)	d_{50} (µm)	d_{90} (µm)
Slurry-MC	10%	AVG	3.324	1.670	2.943	5.576
		SD	0.055	0.005	0.016	0.151
		RSD	1.652	0.270	0.539	2.713
	20%	AVG	3.320	1.702	2.963	5.507
		SD	0.007	0.001	0.003	0.016
		RSD	0.201	0.034	0.101	0.299
	30%	AVG	2.533	1.549	2.456	3.641
		SD	0.005	0.002	0.003	0.010
		RSD	0.178	0.129	0.122	0.275
	40%	AVG	3.020	1.548	2.685	4.962
		SD	0.024	0.005	0.008	0.048
		RSD	0.801	0.342	0.298	0.968
Slurry-nano	10%	AVG	0.165	0.104	0.157	0.238
		SD	0.000	0.001	0.001	0.001
		RSD	0.000	0.553	0.367	0.243
	20%	AVG	0.166	0.101	0.158	0.243
		SD	0.001	0.001	0.002	0.000
		RSD	0.697	0.990	1.096	0.000
	30%	AVG	0.169	0.101	0.161	0.248
		SD	0.001	0.001	0.001	0.001
		RSD	0.342	0.570	0.358	0.232
	40%	AVG	0.173	0.108	0.165	0.250
		SD	0.002	0.005	0.001	0.014
		RSD	1.206	4.264	0.606	5.543

AVG: Average, **SD:** Standard deviation, **RSD:** Relative standard deviation

3.4.3 Content uniformity

Relative standard deviation (RSD) values of drug amount per area, and drug loading, along with label claim% (LC%) and acceptance values (AV) [73] for solution and slurry cast films with varying drug loadings (10%, 20%, 30% and 40%) are presented in Table 3.4. All the prepared films, via solution or slurry casting, had good content uniformity (RSD <6% and AV < 15). Previously, it was shown that higher viscosity increased the uniformity of films loaded with nanoparticles and good content uniformity could be achieved at drug loadings 10-50% which was in line with the present results [35, 74]. Zhang et al. demonstrated that usage of planetary mixer with sufficient viscosity would result in good uniformity for the films loaded with micron-sized particles at 20% drug loading [30]. Unlike slurry casting, particle size, shape and amount are unpredictable in solution casting. Therefore, recrystallization may lead to non-uniformity as was described by earlier studies [96]. One may expect less uniformity in the films prepared by solution casting method at high drug loadings (>10%) due to more recrystallization. However, the present results further showed that optimized mixing of the drug and the polymer solution at sufficient viscosity would result in good content uniformity at FNB loading between 10% and 40% for films loaded with crystalline FNB particles or amorphous FNB. Also, it should be noted that a small sample size (~1/10th of intended dosage form) was used in content uniformity testing to better discriminate the differences between formulations. Yet, good content uniformity was assured for all four techniques by optimized preparation parameters for each film preparation technique.

Table 3.4 Relative Standard Deviation (RSD) Values of Drug Per Area and Acceptance Values (AV) of Films Loaded with FNB

	Drug loading%	***LC %***	***R.S.D. of drug amount per area***	***R.S.D. of drug loading***	***Acceptance value***
Solution	10	99.6	2.1	1.7	4.2
	20	96.3	4.0	1.4	5.3
	30	101.7	0.8	1.6	4.2
	40	99.8	3.6	1.0	2.4
Slurry-AR	10	93.3	1.6	1.8	9.2
	20	92.2	3.5	3.3	13.6
	30	91.9	2.2	1.1	9.0
	40	98.3	2.0	0.8	2.2
Slurry-MC	10	92.8	4.9	2.3	10.8
	20	98.0	2.1	1.1	3.0
	30	100.0	1.4	1.2	2.9
	40	98.0	2.1	0.4	1.4
Slurry-nano	10	98.2	1.8	0.8	2.3
	20	99.8	0.9	0.8	1.9
	30	99.2	3.0	0.8	1.9
	40	98.7	1.6	0.8	1.9

3.4.4 Mechanical properties

Each preparation method at varying drug loadings was compared in terms of the tensile strength (TS) and elongation at break (EB), and low Young's modulus (YM) (Figure 3.4). Solution and Slurry-nano films had higher tensile strength compared to Slurry-AR and Slurry-MC films. As it was stated in the literature, larger particles

may lead to more disruption on the matrix leading to weaker films [30, 96]. An increase in the drug loading affected the Slurry-AR and Solution films the most. Again, it may be due to larger particle effect on the matrix, i.e., as received (d_{90} of ~13 µm) and recrystallized FNB particles for Slurry-AR and Solution films, respectively. Increased drug loading decreased the elongation at break of Slurry-MC and Slurry-nano films while did not affect the Slurry-AR films. It may be due to the better orientation of smaller particles. Increased drug loading slightly increased the elongation at break of Solution films due to more solubilized FNB in the matrix which was in line with previous studies [11, 96]. The flexibility (YM) of the Slurry-MC films was improved as drug loading increased while an opposite trend was observed for Slurry-AR films and the flexibility of Slurry-nano films was not affected by drug loading (Figure 3.4). The flexibility of Solution films was not affected for 20-40% drug loading while it was higher for 10% drug loading.

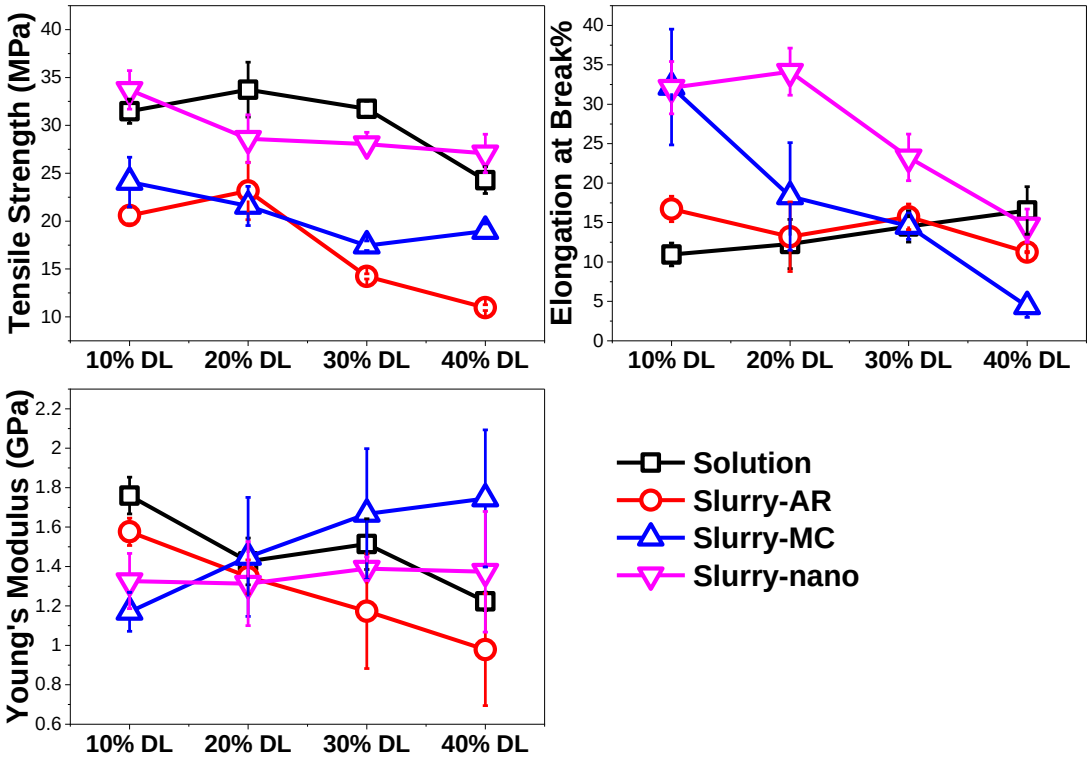

Figure 3.4 Mechanical properties of films prepared with different methods and having varying drug loads.

Considering all these changes, mechanical properties depended highly on drug loading and the effect of drug load may not be similar for different preparation techniques. For example, Slurry-MC at 10% drug loading was the least flexible film while it was the most flexible at 40% drug loading. Thus, the state of the API, particle size and amount, all impact the film mechanical properties and needed to be considered for the investigation of preparation techniques.

3.4.5 Dissolution under sink conditions

Dissolution profiles of dried films loaded with FNB were analyzed under sink conditions (Figure 3.5). It was observed that the dissolution rates were depended on the drug loading. At each drug loading, Slurry-AR films were the slowest while

they had similar dissolution profiles with Slurry-nano films at 30 and 40% drug loadings. Surprisingly, the Slurry-nano film was one of the slowest films at 40% drug loading while it film was the fastest among all the films prepared including Solution at 10% drug loading. At 20% drug loading, Solution, Slurry-MC and Slurry-nano films exhibited similar but enhanced dissolution rates compared to Slurry-AR films. At 30% drug loading Slurry-MC film was the fastest among all while Solution film got to similar dissolution rate as Slurry-MC at 40% drug loading.

Ultimately, different trends were observed between films prepared using different methods at fixed drug loadings. This was risen due to the unique impact behaviors of drug loading when the particle size and solid-state varied. Considering the good redispersibility for all Slurry formulations (Table 3.3 and Figure 3.3), the dissolution rate was expected to be correlated with the particle size. However, depending on the drug loading smaller particles (for example Slurry-nano at 40% drug loading) did not result in a faster dissolution rate.

Krull et al. showed that increasing drug loading led to decreasing dissolution rates for the films loaded with nanoparticles [35]. However, it was noted that the thickness and sink condition variation might have affected this trend. Present results demonstrated that increasing drug loading did not significantly affect the dissolution rate of films loaded with nanoparticles at the fixed thickness and sink conditions (Figure 3.5.b). Further, increased drug loading enhanced the dissolution rate of Slurry-MC film the most. It may be due to one of the inherent parameters affecting the dissolution, mechanical properties.

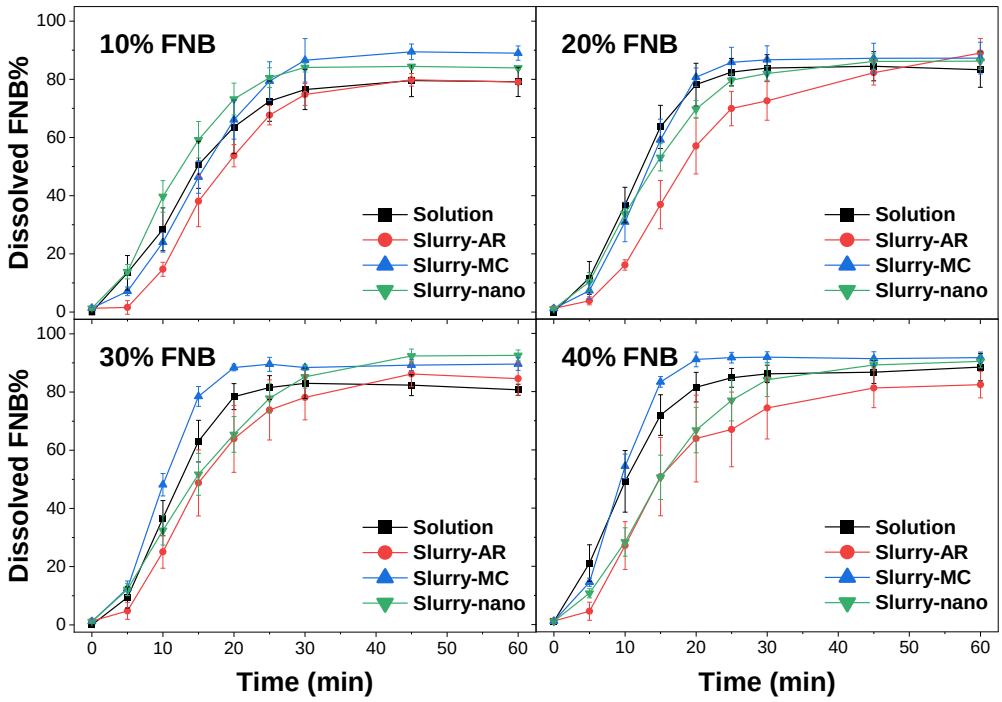

Figure 3.5 Dissolution profiles of films prepared with different methods loaded with varying preparation methods at fixed drug loadings, 10 – 40 wt%.

As it was discussed in the previous section (3.4.4), Slurry-MC films had lower TS compared to Slurry-nano and Solution films which theoretically had the most dissolution enhancement potential. Besides, EB of Slurry-MC films was lower than Slurry-nano for drug loadings higher than 10% which was the only case Slurry-nano film was faster than all formulations. Lower TS and elongation at break may have led to faster disintegration and resulting in faster dissolution despite the particle size or solid-state differences. Similarly, Zhang et al. stated that films loaded with MC-API may provide similar dissolution profiles at around 20% drug loading compared to nano-API loaded films by discussing the results from the literature [27, 30].

Again, an increasing trend was observed for Solution and Slurry-AR films (Figure 3.5.b). Even though there were recrystallizations in Solution films, an enhancement in the dissolution rate was observed due to largely amorphous content in the film.

The bootstrap similarity analyses for dissolution profiles of films under sink conditions are presented in Table C.1, Appendix C. Slurry-MC and Slurry-nano films at 20% drug loading were found to be similar. Slurry-MC and Solution films at 10% drug loading; Solution and Slurry-nano at 20% drug loading; Slurry-AR and Slurry-nano at 40% drug loading were found to be very close to the similarity limit while a similarity was not confirmed for the rest of the combinations at fixed drug loadings.

Overall, due to greater dissolution enhancement with increasing drug loading, Slurry-MC films performed similarly to Solution films and better than Slurry-nano and Slurry-AR films at 40% drug loading.

3.5 Conclusions

A comparative assessment of solution and slurry casting methods, which were used to improve bioavailability, was demonstrated considering the quality attributes of the films, i.e., content uniformity, redispersion, recrystallization, mechanical properties, and dissolution.

Initial crystallinity was observed for the Solution films at drug loadings higher than 10% and continued to recrystallize in time demonstrating the instability of Solution films. Redispersion results of Solution films showed that initial crystallinity

may not be the only issue, API may continue to recrystallize in the body while all Slurry films showed repeatable unimodal particle size distributions. It was shown that the solid-state of API and/or particle size affected the mechanical properties of the films which are very important from many aspects, i.e., patient compliance, handling and effect of other quality attributes (disintegration, dissolution). Even with the optimized formulations for each technique, the results showed that similar or even better dissolution rates can be obtained by films loaded with crystalline FNB over mostly amorphous FNB at high drug loadings.

Considering the present findings along with the common knowledge regarding the tremendous effort required for formulation optimization in solution casting, it can be concluded that Slurry-MC films may be a better option among all the techniques considered at high drug loadings.

CHAPTER 4

EFFECT OF PARTICLE SIZE AND DRUG LOADING OF API ON CRITICAL QUALITY ATTRIBUTES OF THE FILM

4.1 Introduction

Under the recent developments, 90% of new chemical entities (NCE) are poorly water-soluble, either in Biopharmaceutics Classification System (BCS) class II or IV [102-104]. Because of the large number of poorly water-soluble drugs, there is a need for the development of a bioavailability enhancement step. The bioavailability of BCS Class II active pharmaceutical ingredients (APIs) may be improved using many different approaches: amorphous solid dispersions, particle size reduction, polymorph, salt formation, lipid-based systems, cocrystals, etc. [29, 30, 105-110]. Enhancement of dissolution rate by particle size reduction is one of the most frequently used techniques amongst others. The increased total surface area via particle size reduction leads to an enhancement in the dissolution rate of API suspensions or powders as explained by the Noyes-Whitney equation [42]. Besides, the solubility of API may also be increased according to Freundlich–Ostwald equation with reduced particle size to nanometer level (< 200 nm) which in turn will enhance the dissolution rate [111, 112]. It should be noted that these particle size-dissolution rate relationships mostly valid for free forms such as suspension and powder. However, in a film dosage, API is embedded into a matrix where other mechanisms, i.e., disintegration, swelling, chain relaxation, and drug diffusion, play a role in the overall dissolution along with the dissolution of the

particle itself. Therefore, this paper is seeking an answer to the question of “How the change in particle size and number of particles in the film matrix affect the product performance, i.e., dissolution rate?”.

Hot-melt extrusion (HME) [11, 15, 18], solution [21-23], and slurry casting [27-32] are commonly used film manufacturing techniques that can be utilized for bioavailability enhancement. Adopting HME and solution casting methods, amorphous API in the film can be achieved facilitating higher solubility. However, re-crystallization is a major challenge in both techniques [21-23, 43, 44, 96]. Amorphous API tends to recrystallize in time due to its unstable nature [20, 50, 52, 53]. The recrystallization may occur right after preparation or in the longer-term. Therefore, the formulation development requires an intensive optimization step to prevent the recrystallization in fresh product and extend the stable period. It also should be noted that when API starts to recrystallize in the product, neither extend of the recrystallization nor the recrystallized particle size can be controlled [21, 96, 113]. This uncontrolled change in the solid-state of API leads to unpredictable product performance [21, 96]. On the other hand, slurry casting is a more predictable process due to the solid-state stability of crystalline API. In addition, Krull et al. proved the robustness of the slurry casting technique by adopting the same formulation and processing parameters to produce 5 different API loaded wrinkle-free films with good content uniformity [27]. Considering these, dissolution rate enhancement via slurry casting might be a more reliable and desirable technique compared to solution casting despite the limited solubility of crystalline API. Micronization and nano-milling steps can be added to the oral film

manufacturing process to compensate for the solubility limitation. Many studies show that particle size reduction would increase the dissolution rate of the film while assuring good content uniformity, stability, and acceptable mechanical properties [29, 30, 32].

Many researchers confirmed that particle size reduction increases the dissolution rate of a drug suspension [114-118]. Nevertheless, due to the increased number of particles and high surface energy, particle size reduction increases agglomeration in turn affecting the dissolution rate. Thus, there is intensive research on the stabilization of drug suspensions [107, 119-122]. Also, to avoid the stability issue, a solid dosage form can be prepared by drying the drug suspensions (e.g., freeze-drying, spray-drying, fluid bed coating, nanoextrusion, incorporating suspension into the film, etc.) [107, 123, 124]. However, formulation and process parameters need to be adjusted to prevent agglomeration and obtaining good redispersibility [125]. The redispersibility of the drug is a critical parameter since it would define the available surface area for dissolution, in turn mitigating or maintaining the dissolution and solubility advantages of particle size reduction.

It was demonstrated that the embedded nanoparticles in the film could be redispersed while preserving their primary particle sizes (before adding them into the film) [27, 35]. Zhang et al. examined the redispersion of micron-sized particles which were incorporated into films as powders [30]. Particle size reduction of API powder was found to be promoting agglomeration in the film despite the high polymer content. However, it was shown that the dispersion of API in the film can

be significantly improved via dry coating achieving primary particle size after the redispersion [30]. Interestingly, despite the good redispersibility in both nano-sized and micronized coated API loaded films, it was found that these two films would have comparable dissolution rates [27, 30].

Along with the effect of dissolution rate, the size of the embedded particles in the film may also affect the mechanical properties of polymeric composites. It was shown that a reduction in particle size increases the tensile strength of the composites [126-129]. The addition of nanoparticles into the films is used for reinforcement when desired. However, a moderate tensile strength is preferred for oral films due to the need for quick disintegration, patience compliance, and handling [1, 85].

Considering two similar oral film formulations from the literature, nano-size API loaded film had higher tensile strength compared to films with micro-size [27, 30]. This difference in mechanical properties led to similar dissolution rates despite the total surface area differences. Therefore, the particle size should not be evaluated only in terms of available surface area, but also mechanical properties need to be considered to adjust the dissolution rate.

The aforementioned results indicate that when a matrix is in question, the effect of API particle size on the dissolution rate of the particles itself and the structure of the dosage form might be contrary. Even with a good particle redispersibility, it may not result in fast dissolution due to the confounding effect of particle size on the film structure. Thus, this paper systematically examines the

effect of particle size and drug loading on the quality attributes of the film, i.e., mechanical properties, dissolution profiles.

The purpose of this work was to examine the effect of the particle size and loading on the dissolution rate of poorly water-soluble active pharmaceutical ingredients (APIs) loaded oral films. The effect of particle size in the film was examined using five different particle sizes of a model poorly water-soluble API, fenofibrate (FNB). Besides, four different drug loading, 2.5, 10, 25, and 40%, were analyzed. Product performance was evaluated in terms of content uniformity, redispersion, mechanical properties, and dissolution profiles to assess the hypothesis that smaller API particles would increase the dissolution of API due to increased surface area while the film matrix gets tougher in turn might be slowing down the dissolution from film dosage.

4.2 Materials

Fenofibrate (FNB, Jai Radhe Sales) as a model BCS Class II drugs, low molecular weight hydroxypropyl methylcellulose (HPMC; Methocel E15 Premium LV, The Dow Chemical Company, Midland, MI) as a film former and glycerin (Sigma-Aldrich, Saint Louis, MO) as plasticizer, sodium dodecyl sulfate (SDS; Sigma-Aldrich, Saint Louis, MO) as stabilizer were used.

4.3 Methods

4.3.1 Preparation of pre-milled drug powder

Pre-milling of fenofibrate (FNB) powder, Micronized FNB (M-FNB), was prepared using fluidized energy mill (FEM, qualification model, Sturtevant Inc., Hanover, MA). The procedure was adapted from previous works [30, 97]. Briefly, as-received (AR) FNB fed with a constant 1 g/min rate into FEM using a feeding pressure of 45 psi and grinding pressure of 40 psi. The sample was collected from the filter at the end of the line and used for further preparations.

4.3.2 Preparation of drug suspensions

Five different drug suspensions having FNB in different particle sizes were prepared for analysis; one with AR-FNB, another with M-FNB, three further milled AR-FNB suspensions via wet stirred media milling (WSMM) (MicroCer, Netzsch, Exton, PA). As-received (AR) and micronized fenofibrate (M-FNB) suspensions were prepared using previously established methods [29, 99]. For drug particle stabilization purposes, SDS (surfactant) and HPMC-E15 (polymer) were used in the suspension. Briefly, 0.1g of SDS, 5 g of HPMC, and 40 g of FNB were added into 200 mL of DI water in corresponding order while it was stirred using a shear mixer (Fisher Scientific Laboratory Stirrer, Catalog No. 14-503, Pittsburgh, PA). The resulted suspensions were consisted of 2.5% (w/w) (wrt to water) HPMC, 0.05% (w/w) (wrt to water) SDS and 20% (w/w) (wrt to water) FNB. For further particle reduction, three separately prepared AR-FNB suspensions were milled via WSMM for 5, 15, or 120 minutes [29, 98, 99]. The milling method was adapted from previous studies where further information can be found [29, 98, 99].

4.3.3 Preparation of polymer solution and precursors

An aqueous polymer solution was prepared according to Dow and previously established protocols [29, 30, 67]. A polymer solution consists of 12% HPMC and 4% glycerin was selected considering previous works [29, 30]. Briefly, DI water was heated up to 35-40 °C while stirring, glycerin was added. When the solution reached 80-90 °C, HPMC powder was added slowly and allowed to disperse well. Then, the solution was left to cool down to room temperature while mixing.

Polymer solution and FNB suspensions were mixed at different ratios to get 2.5, 10, 25, and 40% drug loading in the dry film. Mixing was carried out for 2 min at 2000 rpm following by a defoaming step for 30 s at 2200 rpm in a planetary centrifugal mixer (Thinky ARE- 310, Laguna Hills, CA, USA). Prepared suspensions were called precursors throughout the manuscript.

4.3.4 Casting & drying

Film precursors suspensions were automatically cast onto a plastic substrate (Scotchpak TM 9744, 3M, MN, USA) using Lab-Cast Tape Caster (Model TC-LC, HED International, Ringoes, NJ). Wet film thicknesses were adjusted by changing the opening of the doctor blade (Elcometer, Rochester Hills, MI) to achieve 100 µm dry film thickness from each precursor. Following the casting step, samples were dried at 50 °C for 1 h. Once dried, the films were peeled from the substrate and stored in sealed plastic bags until characterization. The compositions of dry films are shown in Table 4.1.

Table 4.1 Formulation Compositions of the Dry Films

Drug loading / Components	2.5%	10%	25%	40%
HPMC E15 (wt%)	73.2%	68%	57%	46%
Glycerin (wt%)	24.3%	22%	18%	14%
FNB (wt%)	2.5%	10%	25%	40%
SDS (wt%)	0.006%	0.025%	0.063%	0.100%

4.4 Characterization

4.4.1 The particle size of FNB in suspension and after redispersed from dry films

The redispersibility of FNB from the film was examined in terms of particle size distribution. The method was adopted from earlier works where more details can be found [27, 30]. Briefly, randomly taken circular punches (0.72 cm^2) were added into a vial filled with 10 ml deionized water. Then, it was vortexed at 1500 rpm for 2-5 min to dissolve the polymer. A laser diffraction particle size analyzer (Coulter LS 13320, Beckman Coulter, FL, USA) was used to measure the particle size of FNB in the prepared suspension.

4.4.2 Content Uniformity

The mass and thickness of randomly selected ten circular punches (0.71 cm^2) were recorded for each film sample. Then, each punch was dissolved in 20 - 100 mL 7.2 g/L sodium dodecyl sulfate (SDS) solution. The volume of SDS was selected depending on the drug loading to ensure sink conditions. Absorbances of each solution were measured using a UV-vis spectrophotometer (Thermo Fisher

Scientific Inc., MA, USA). Drug amount per area (mg/cm^2), drug loading for each sample was calculated and relative standard deviations (RSD) of thickness, drug loading, and drug amount per area were reported for uniformity assessment. Also, label claim% and acceptance values were calculated. Equation (3.1) was used to calculate AV [73].

$$Acceptance\ value(AV) = \left|M - LC_{avg}\%\right| + k \cdot s \qquad (3.1)$$

In the above equations, $LC_{avg}\%$, s, and k are the average drug loading with respect to label claim, standard deviation of $LC_{avg}\%$, and the acceptability constant, 2.4, respectively. The "M" Parameter is chosen according to the below disequilibriums.

M: Reference value, 98.5 if $LC_{avg}\% < 98.5$

$LC_{avg}\%$ if $98.5 < LC_{avg}\% < 101.5$

101.5 if $LC_{avg}\% > 101.5$

While RSDs give insight about the variation along the film values explain to what degree the drug amount per area or drug loading varies along the film. Acceptance value (AV) is defined by United States Pharmacopedia [73] as an indicator taking into account the closeness to the label claim, as well as the drug content uniformity. This method offers a more complete picture of a film's quality.

4.4.3 Morphology

The cross-section of the films loaded with the drug was examined via field emission scanning electron microscopy (SEM) (JSM-7900F, JEOL USA, Inc. MA). Film samples were cut into small pieces and fixed onto double-sided carbon tape where

the cross-section of the films facing upwards. The samples were coated with gold via a sputter coater (EMS 150T ES, Quorum Technologies Ltd., Laughton, East Sussex, England) to prevent the charging of the sample due to the high polymer content. Images were taken as representative of the sample.

4.4.4 Mechanical properties

Mechanical properties of the films were investigated using a TA-XT Plus Texture Analyzer (Stable Microsteps, UK). Film samples having dimensions of 50 mm x 15 mm were analyzed via tensile test where the film was elongated until failure. More details can be found in [29, 74]. Tensile strength (TS), Young's modulus (YM), and percent elongation at break (EB %) were reported for an average of 5 samples from each formulation.

4.4.5 Dissolution profiles

Dissolution profiles of the film samples were analyzed using a flow-through cell dissolution apparatus (USP IV; Sotax, Switzerland) under sink conditions. Dissolution medium of 3.6 g/L SDS solution was circulated at a flow rate of 16 mL/min and a constant temperature of 37 ± 0.5 °C. A dissolution medium of 100 – 600 mL was used ensuring similar sink conditions for each formulation with varying drug loading. During the dissolution, timely UV measurements were taken automatically. Results for each formulation were reported as percent dissolved API of an average of randomly selected 6 circular punches (0.71 cm^2). More details can be found in [75].

4.4.6 Curve fitting and analysis of dissolution curves

Dissolution curves of each formulation were compared between each other using bootstrap similarity (f_2) analysis due to the high standard deviation for some of the samples [100, 101]. In addition to the statistical analysis, area under the curve (AUC) was calculated and dissolution curve were fitted to five different commonly adopted models. The fitting of dissolution curve were performed up to 60% dissolved FNB. The fitting of each formulation was analyzed in terms of the dissolution rates and dissolution mechanisms.

Zero-order model [130]:

$$\frac{M_t}{M_\infty} = k \cdot t \tag{3.2}$$

First-Order model [130, 131]:

$$\frac{M_t}{M_\infty} = 100 \cdot (1 - e^{k \cdot t}) \tag{3.3}$$

Higuchi model [132]:

$$\frac{M_t}{M_\infty} = k \cdot t^{0.5} \tag{3.4}$$

Korsmeyer – Peppas model [133, 134]:

$$\frac{M_t}{M_\infty} = k \cdot t^n \tag{3.5}$$

Hixson – Crowell model [135]:

$$\frac{M_t}{M_\infty} = 100 \cdot \left[1 - (1 - k \cdot t)^3\right] \tag{3.6}$$

In above equations, M_t/M_∞ is the percent drug dissolved, *k* is a constant representing dissolution rate, *t* is time and *n* is release exponent where applicable.

4.5 Results and Discussion

4.5.1 Particle size of FNB in suspension and after redispersed from dry films

Particle sizes of unprocessed and dry milled FNB powders were also measured in a dispersive system, Rodos/Helos system (Sympatec, NJ, USA). The unprocessed FNB particles had d_{10}, d_{50} and d_{90} of 2.23 ± 0.12 µm, 8.86 ± 0.05 µm, 14.82 ± 0.06 µm, respectively while dry milled FNB powder had 1.23 ± 0.06 µm, 4.35 ± 0.07 µm, 8.70 ± 0.11 µm. The particle sizes of FNB in the primary suspensions before mixing with polymer solution were measured via the light scattering method. The particle sizes of prepared FNB suspensions are presented in Table 4.2 with respective milling conditions. The round-up d_{50} values were given as the formulation names.

The particle sizes of unprocessed and dry milled FNB powders were smaller than their suspensions. The difference in particle size of the dry and liquid state was more pronounced for unprocessed FNB. Observed particle size increase in the suspension was due to the instability of too large particles and good dispersibility during powder particle size measurement.

Table 4.2 Formulation Names, Processing Conditions and Particle Sizes of FNB Suspensions

Formulation	Processing of FNB	d_{10} (µm) ± SD	d_{50} (µm) ± SD	d_{90} (µm) ± SD
15 µm	Unprocessed	5.839 ± 0.078	15.16 ± 0.049	29.29 ± 0.057
5.5 µm	Dry milling	2.295 ± 0.002	5.477 ± 0.003	11.66 ± 0.078
700 nm	Wet milling for 5 min	0.242 ± 0.012	0.701 ± 0.133	2.891 ± 0.158
400 nm	Wet milling for 15 min	0.191 ± 0.004	0.361 ± 0.003	1.546 ± 0.008
160 nm	Wet milling for 2 h	0.103 ± 0.002	0.16 ± 0.001	0.246 ± 0.005

SD: Standard deviation

The particle size of redispersed FNB from dried films with varying embedded particle size and drug loading were reported in Figure 4.1. Films loaded with particles smaller than 1 µm showed good redispersion at varying drug loadings. The redispersed particle size was smaller than the primary particle sizes of the suspensions for 15 and 5.5 µm formulations except for 2.5% drug loading. However, when the size of redispersed particles was compared with the particle size of powders, some level of agglomeration was observed (Figure 4.1). These results were in line with the previous observations where nanoparticles were found to have good redispersibility and micro-size particles showed agglomeration which was prevented with the extra step of dry coating [30, 35].

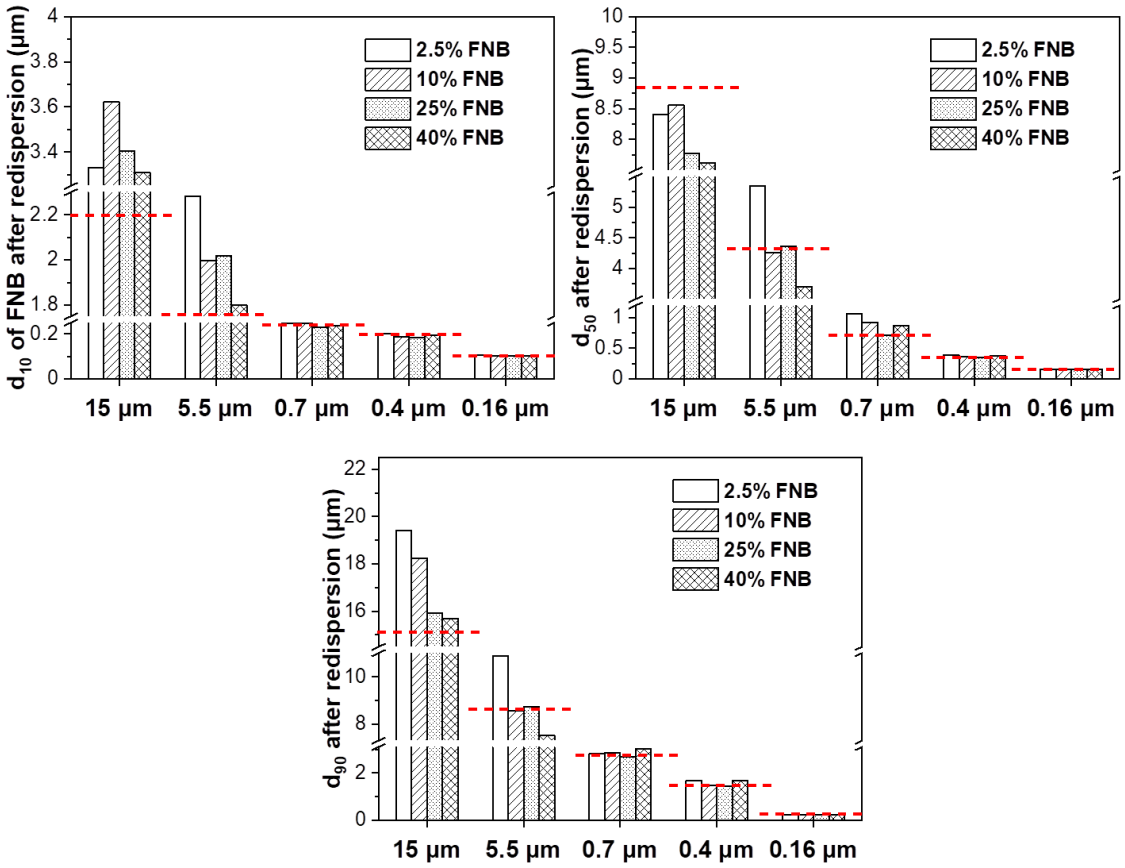

Figure 4.1 Particle sizes of redispersed FNB from films, i.e., d_{10}, d_{50}, and d_{90}. Dashed lines indicate the primary particle size.

The redispersion results for micro-sized particles, i.e., 15 µm and 5.5 µm showed that mixing of the suspension with the polymer solution would help drug dispersion in the film allowing the redispersion size of FNB similar to powder.

Considering all the size measurements, particles were tended to agglomerate more at lower drug loadings, i.e., 2.5% (wt%). Poorer redispersibility at low drug loadings may be the result of the high amount of polymer. While agglomeration was observed for some of the formulations, it was demonstrated that the particle size reduction helped to obtain good redispersibility regardless of drug loading at a range of 2.5 – 40% (wt%).

4.5.2 Content uniformity

Table 4.3 presents the uniformity of each formulation in terms of percent label claim%, acceptance values (AV), and relative standard deviation (RSD) values for thickness, drug amount per area, and drug loading. Regardless of particle size and drug loading, good uniformity (RSD < 6%) was achieved with some exceptions. When it is considered that the sampling size for the content uniformity test was about 1/10th of actual dosage, it could be fairly said that all films had good content uniformity. Also, acceptance values (AV) were in the acceptable range (<15) concluding the acceptable variation and LC%. It was previously shown that mixing with a planetary mixer would result in good content uniformity even with particles having poor redispersibility [30]. The results demonstrated that the FNB particles were well dispersed in the precursor and maintained after drying regardless of drug loading (2.5 – 40% (wt%)) and particle size (0.16 – 15 µm).

Table 4.3 Relative Standard Deviation (RSD) Values of Drug Per Area and Acceptance Values (AV)

Particle size (μm)	Drug Loading%	RSD of thickness	RSD of drug amount per area	RSD of drug loading	LC%	Acceptance value
15	2.5	7.7	8.1	1.6	108.4	11
15	10	3.0	1.6	1.0	103.5	4.4
15	25	3.5	3.6	2.1	103.2	6.8
15	40	5.4	7.2	1.0	104.2	5.3
5.5	2.5	3.1	2.3	0.9	88.1	12.3
5.5	10	1.8	1.9	0.8	100.1	2
5.5	25	5.9	7.1	1.2	101.5	3
5.5	40	5.8	5.6	1.3	101.6	3.2
0.7	2.5	5.0	4.1	0.9	113.3	14.2
0.7	10	5.6	5.7	1.0	101.0	2.4
0.7	25	4.0	5.8	2.1	98.7	5
0.7	40	6.9	6.7	1.2	98.7	3
0.4	2.5	5.7	5.9	0.9	104.9	5.7
0.4	10	3.6	3.4	0.7	104.8	4.9
0.4	25	6.9	6.4	1.9	101.7	4.8
0.4	40	5.1	4.9	0.6	101.8	1.7
0.16	2.5	4.5	2.9	0.7	101.9	2.2
0.16	10	4.7	4.9	0.7	101.9	2.1
0.16	25	7.6	4.4	1.2	105.7	7.2
0.16	40	5.4	6.0	0.6	104.0	4.1

4.5.3 Morphology

Cross-sectional SEM images of films prepared with varying particle size (160 nm, 400 nm, 700 nm, and 16 µm) at the highest drug loading and varying drug loading (10%, 25%, and 40%) at 160 nm particle size are presented in Figure 4.2.

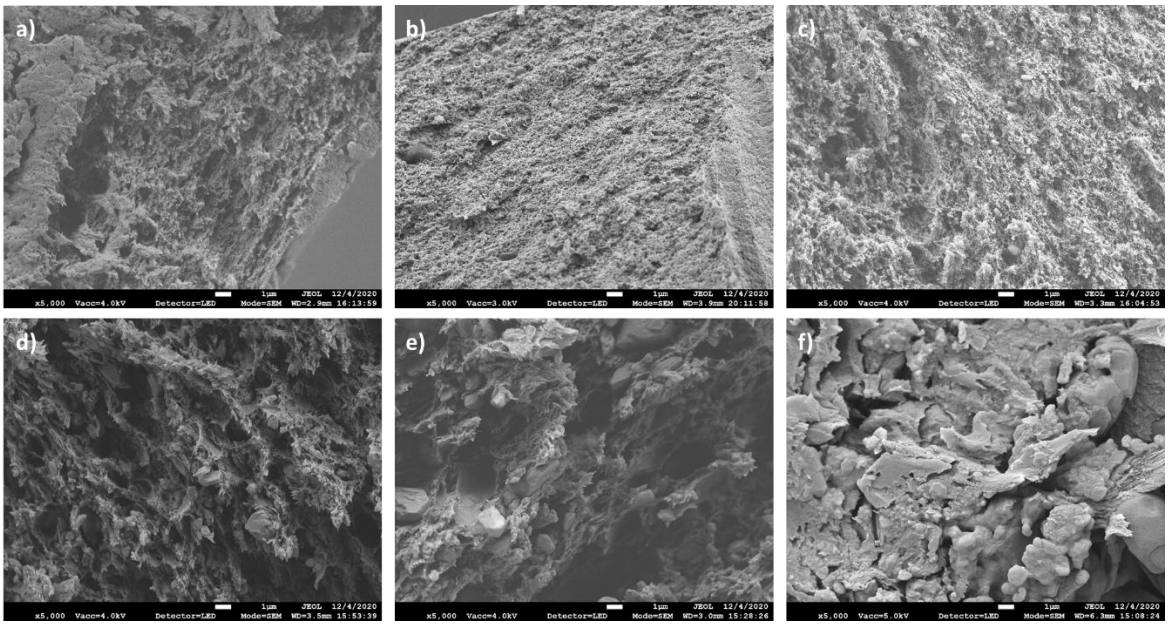

Figure 4.2 SEM images of cross-sectional area of films loaded with particles with a) 10% of 160 nm FNB b) 25% of 160 nm FNB c) 40% of 160 nm FNB d) 40% of 400 nm FNB e) 40% of 700 nm FNB f) 40% of 15 µm FNB

The films loaded with FNB in 160 nm had a closed, and uniformly distributed porous structure (Figure 4.2.a-c). There was not a significant change in the structure of the films loaded with 160 nm FNB, as drug loading varied. However, as the particle size increased pores of the film matrix were enlarged and uniformity was decreased (Figure 4.2.c-f). More uniform distribution of pores/weaker points creates tougher structures leading hard to break while non-uniform structures are easier to fail.

4.5.4 Mechanical properties

Even though there are no well-established criteria for mechanical properties of oral films, moderate tensile strength (TS) and elongation at break (EB) and low Young's modulus (YM) are desired in strip-films [85]. Mechanical properties of oral films should be strong enough for processing and handling while they should be soft enough not to disturb the mouth and disintegrated quickly.

Figure 4.3 shows the mechanical properties of films loaded with FNB in varying sizes and loading. As particle size decreased TS and YM generally increased for higher drug loadings (25% and 40%) (Figure 5.3.a and b). At low drug loadings, the effect of particle size was not significant on TS and YM. As drug loading increased, TS was decreased especially for the films loaded with large particles i.e., 5.5 µm and 15 µm. It may be due to a particle size threshold for uniform distribution along the film. The thickness of the dried film was fixed to 100 µm for all formulations. Considering thickness and the larger particle sizes, the number of particles on the thickness direction would be in the order of 1 magnitude. Therefore, there may not be much room for particles to be uniformly dispersed in the thickness direction. Thus, defective parts were formed which would allow easier tensile fail, i.e., lower tensile strength. It was also observed via SEM imaging that larger particles created less uniform pores along the cross-section of the film (Figure 4.2).

EB was not significantly affected by particle size except for 2.5% (Figure 4.3.c). However, it was significantly reduced with increased drug loading going towards a brittle structure (Figure 4.3.c). EB variation by particle size was high for

2.5% FNB loaded films mostly due to less uniformity of the low number of particles in the matrix.

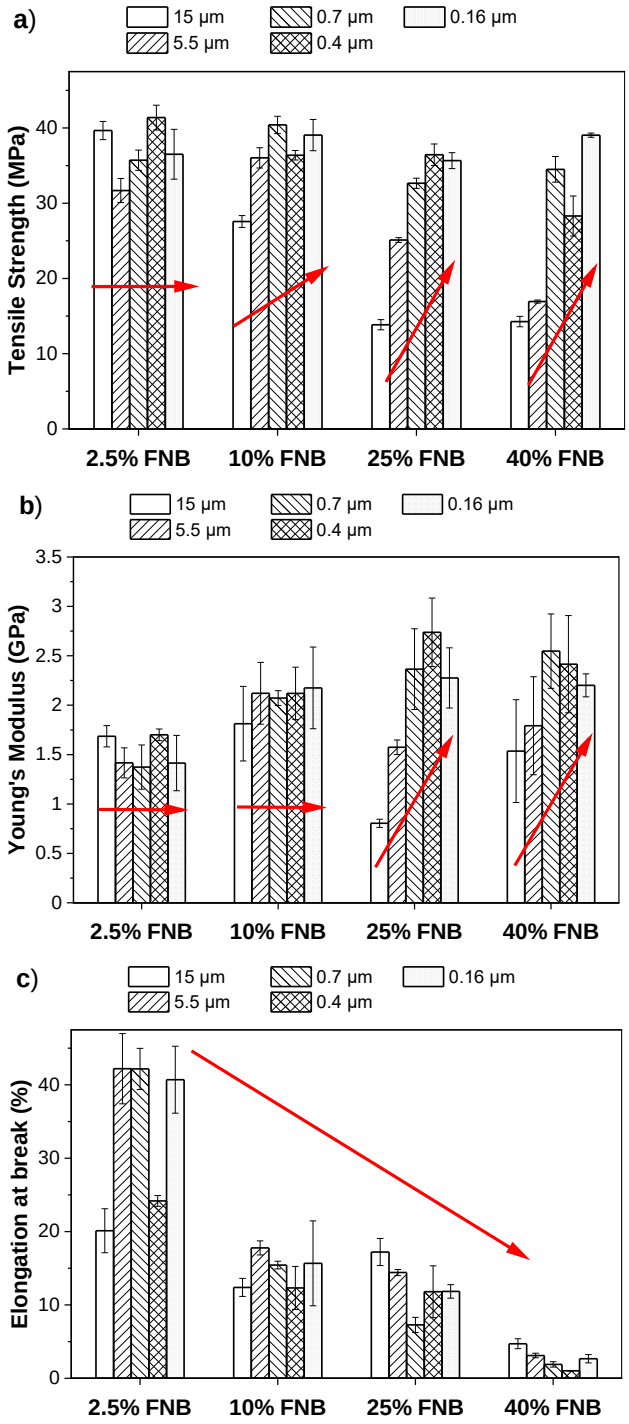

Figure 4.3 Mechanical properties of films loaded with FNB in varying sizes and drug loadings a) Tensile strength b) Young's Modulus c) Elongation at break. Arrows show the direction of change.

The aforementioned observations about the effect of the particle size and drug loading on the mechanical properties were in line with the literature [136-138]. Mysiukiewicz et al. explained that the hindering of the chain movements by the particles or stretching was the reason for the reduction in EB and TS when particle loading increased from no loading through 20 wt% [136]. As described, both particle size and drug loading were found to be significantly important parameters affecting the mechanical properties of the films.

4.5.5 Dissolution profiles

The dissolution profiles of FNB suspensions having varying particle sizes are presented in Figure 4.4. Figure 4.5 presents the dissolution profiles of films loaded with varying particle sizes and loadings.

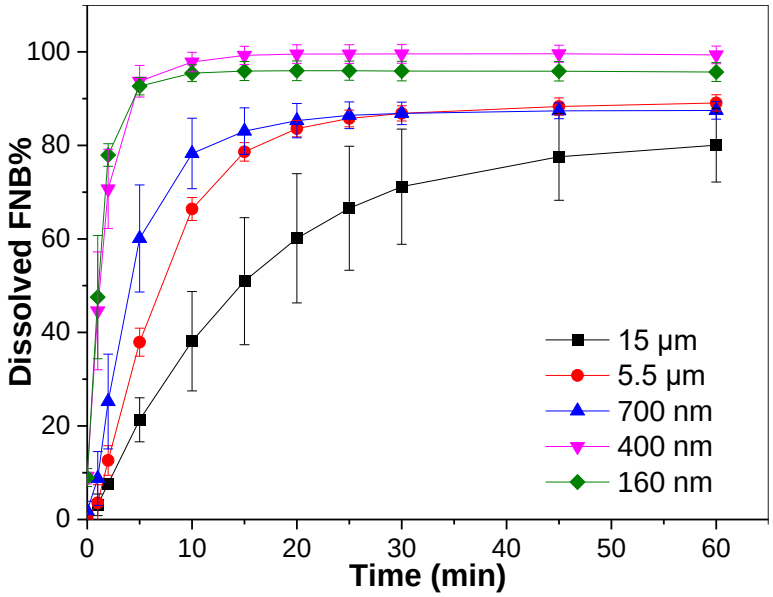

Figure 4.4 Dissolution profiles of suspensions containing drug particles with varying sizes.

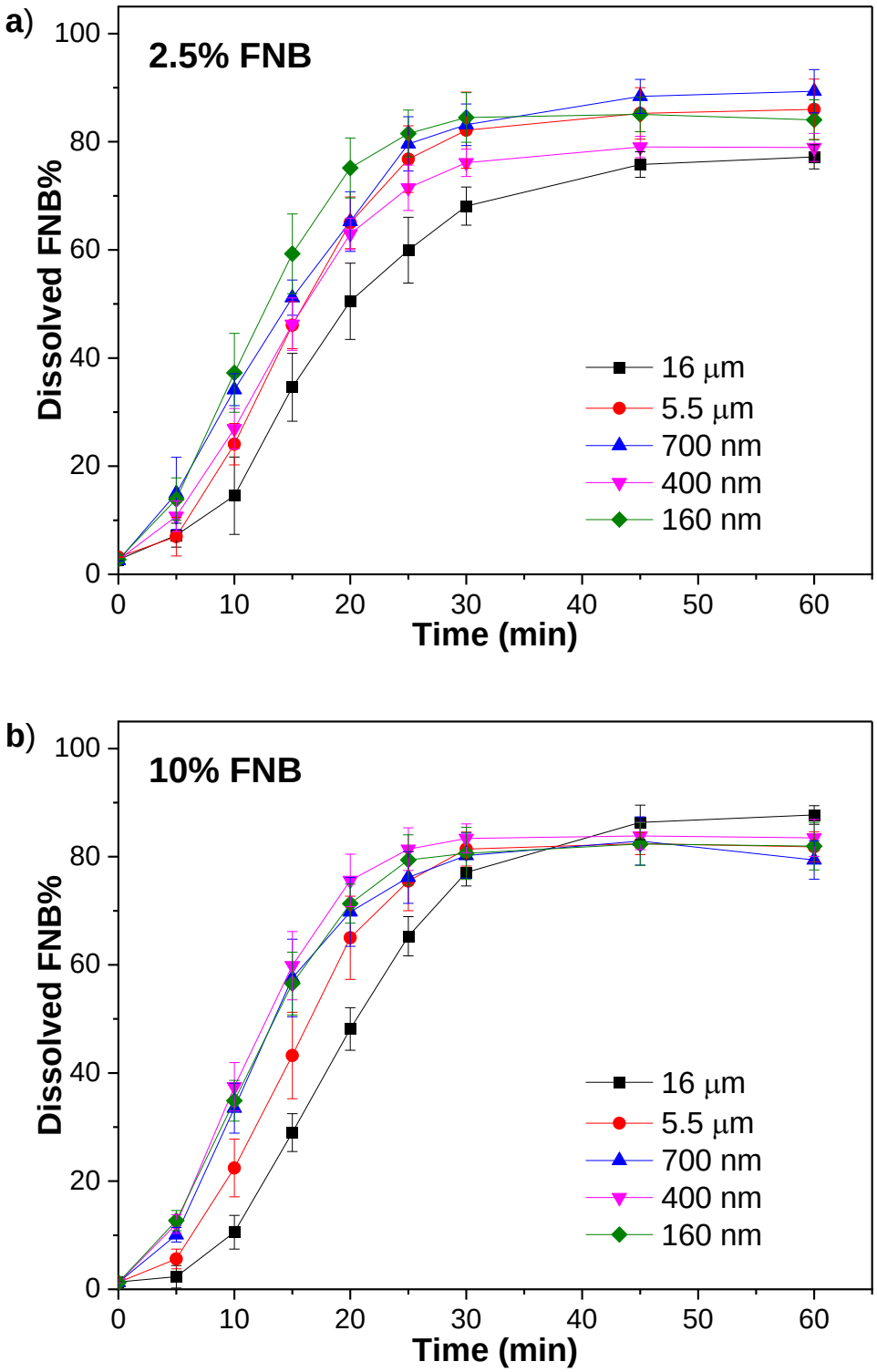

Figure 4.5 Dissolution profiles of the films loaded with FNB in varying sizes with a) 2.5% b) 10% c) 25% and d) 40% drug loading.

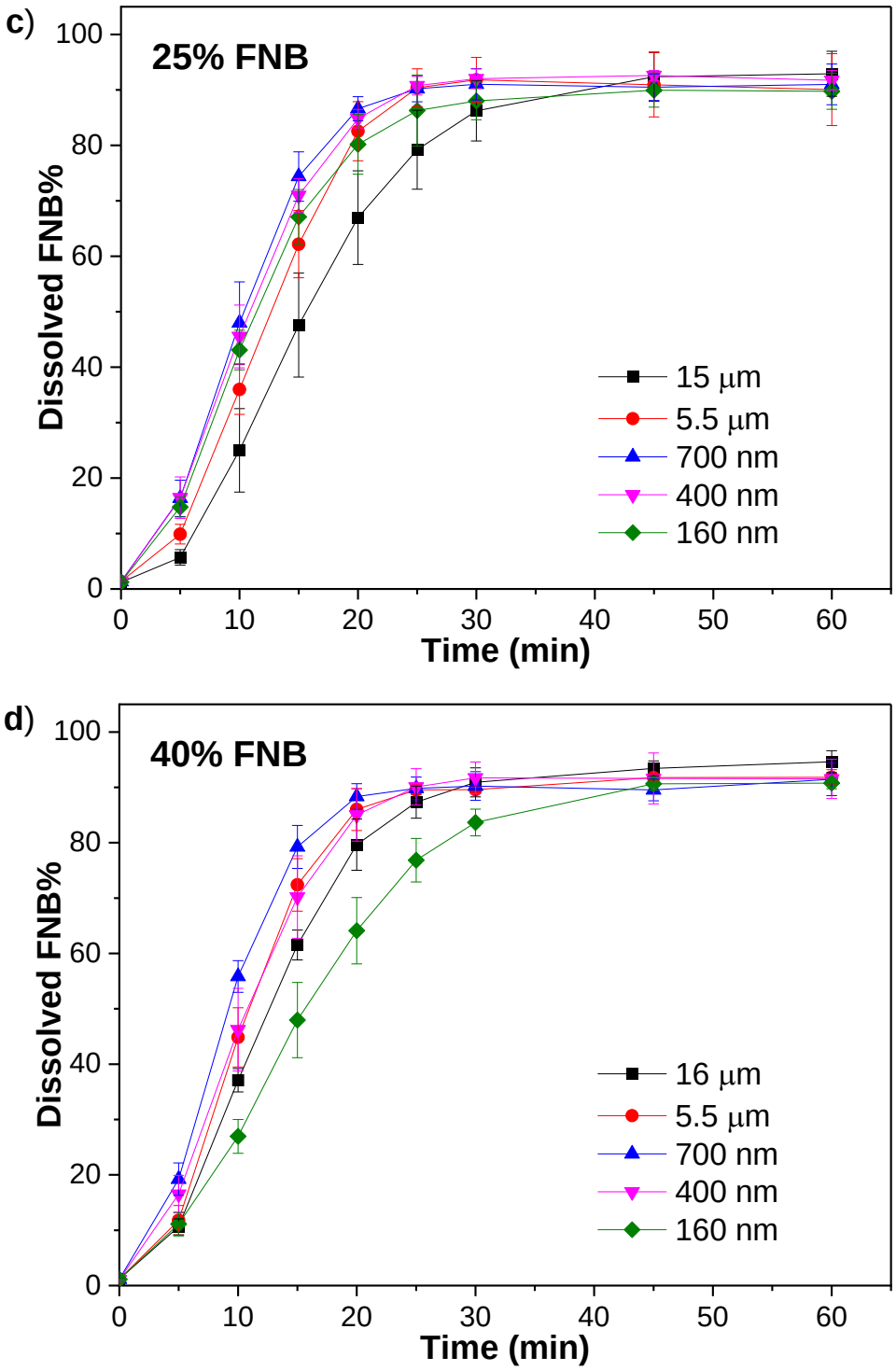

Figure 4.5 (Continued) Dissolution profiles of the films loaded with FNB in varying sizes with a) 2.5% b) 10% c) 25% and d) 40% drug loading.

As expected, the dissolution rate in suspensions was increased with decreased particle size owing to an increased total surface area [42] (Figure 4.4). The same trend was observed for the dissolution of 2.5% FNB loaded films (Figure 4.4.a). At 10% FNB loading, dissolution rate was increased as particle size was decreasing down to 700 nm and films loaded with FNB ≤ 700 nm had similar dissolution profiles (Figure 4.4.b). As drug loading increased, the increasing trend was reversed for FNB < 700 nm. Interestingly, at the highest tested drug loading (40 wt%), an increase in the dissolution rate was observed down to d_{50} of 700 nm particle size, while smaller particles than this size resulted in a slower dissolution rate (Figure 4.4.d) as opposed to general particle size behavior in suspension. More importantly, dissolution of the films loaded with the smallest FNB particles (d_{50} of 160 nm) was the slowest at the highest drug loading. These may be explained by the mechanical properties. The mechanical properties of the films at 2.5% drug loading were not affected by particle size significantly. Therefore, one could expect to observe an increased dissolution rate by increased total surface area. At 10% drug loading, only tensile strength was slightly affected by particle size. At 25 and 40% drug loadings, tensile strength was increased significantly as particle size decreased. Besides, at higher drug loadings, elongation at break was lower. These changes in the mechanical properties could affect the dissolution rate adversely.

The results for statistical similarity analysis on dissolution profiles can be found in Table D.2. Some of the films were found to be similar considering the

bootstrap similarity factor and they were considered when the above comments were made.

Table 4.4 presents the fitting parameters and R^2 values for the five different models (Zero-order, First-order, Higuchi, Korsmeyer–Peppas, and Hixson–Crowell) and area under the curve (AUC) results for each formulation. When R^2 of each fitting was considered, Korsmeyer–Peppas model was found to be the best fitting among the other models for all the formulations. The release exponent (*n*) in the Korsmeyer-Peppas model was found to be higher than 1 (in the range of 1.01 – 1.89) suggesting Super Case II transport for all the formulations. Super Case II transport corresponds to a combination of several mechanisms during dissolution, such as polymer swelling, chain relaxation, and drug diffusion [139]. Therefore, it could be stated that the mechanical properties would easily play a role in the dissolution.

The dissolution curves were fitted again where *n* was fixed to the average of all *n* values (1.4) to fairly compare dissolution rate constants (*k*) amongst all the formulations (Table 4.4). Again, R^2 of each fitting was found to be higher than 0.99 with some exceptions. In addition, the area under the curve (AUC) was calculated for all the formulations to analyze the dissolution profiles (Table 4.4).

Table 4.4 Fitting Parameters of Dissolution Models Used for Dissolution Profiles of FNB Loaded Films with Varying Drug Loading and Particle Size

Models:	Zero Order		First Order		Higuchi		Hixson-Crowell	
Particle size (μm) — DL%	k (%/min)	R^2	k (min^{-1})	R^2	k (%/$min^{1/2}$)	R^2	k (min^{-1})	R^2
15 — 2.5	2.32	0.948	0.03	0.888	9.35	0.714	0.04	0.700
15 — 10	2.16	0.870	0.03	0.803	8.16	0.603	0.04	0.908
15 — 25	2.99	0.936	0.04	0.873	10.23	0.689	0.05	0.797
15 — 40	3.73	0.932	0.05	0.870	11.37	0.687	0.06	0.803
5.5 — 2.5	2.92	0.931	0.04	0.867	10.04	0.684	0.05	0.795
5.5 — 10	2.80	0.920	0.03	0.859	9.56	0.666	0.05	0.832
5.5 — 25	3.65	0.920	0.05	0.856	11.08	0.668	0.06	0.839
5.5 — 40	4.23	0.921	0.05	0.857	12.01	0.672	0.07	0.835
0.7 — 2.5	3.41	0.990	0.05	0.962	11.75	0.840	0.05	0.401
0.7 — 10	3.52	0.952	0.05	0.892	11.49	0.717	0.06	0.739
0.7 — 25	4.50	0.945	0.06	0.890	12.37	0.708	0.08	0.787
0.7 — 40	4.96	0.934	0.06	0.873	13.04	0.694	0.08	0.825
0.4 — 2.5	2.99	0.967	0.04	0.917	10.34	0.744	0.05	0.682
0.4 — 10	3.79	0.966	0.05	0.910	12.05	0.742	0.06	0.705
0.4 — 25	4.40	0.961	0.06	0.905	12.63	0.734	0.07	0.741
0.4 — 40	4.46	0.972	0.06	0.920	12.88	0.758	0.07	0.690
0.16 — 2.5	3.83	0.982	0.05	0.934	12.30	0.782	0.06	0.602
0.16 — 10	3.53	0.963	0.04	0.910	11.21	0.735	0.06	0.722
0.16 — 25	4.20	0.969	0.05	0.915	12.56	0.750	0.07	0.703
0.16 — 40	3.09	0.974	0.04	0.923	10.71	0.756	0.05	0.674

Table 4.4 (Continued) Fitting Parameters of Dissolution Models Used for Dissolution Profiles of FNB Loaded Films with Varying Drug Loading and Particle Size

Models:	**Korsmeyer-Peppas (n varies)**			**Korsmeyer-Peppas (n=1.4)**		**Area Under curve**
Particle size (μm) — DL%	**k ($\%/min^n$)**	**n**	**R^2**	**k ($\%/min^{1.4}$)**	**R^2**	**AUC (%·min)**
15 — 2.5	0.77	1.37	0.984	0.71	0.984	3259.0
15 — 10	0.16	1.89	0.994	0.63	0.963	3755.3
15 — 25	0.75	1.52	0.995	1.04	0.992	4521.6
15 — 40	1.02	1.53	0.994	1.42	0.990	4546.1
5.5 — 2.5	0.71	1.53	0.992	1.01	0.989	3547.4
5.5 — 10	0.56	1.61	0.994	0.98	0.987	4336.1
5.5 — 25	0.80	1.62	0.995	1.39	0.987	4596.0
5.5 — 40	1.04	1.61	0.995	1.71	0.987	4132.6
0.7 — 2.5	3.30	1.01	0.990	1.19	0.943	4080.2
0.7 — 10	1.25	1.41	0.993	1.27	0.993	4483.8
0.7 — 25	1.57	1.48	0.996	1.86	0.995	3641.3
0.7 — 40	1.50	1.56	0.997	2.13	0.993	3945.5
0.4 — 2.5	1.31	1.31	0.994	1.03	0.992	4405.3
0.4 — 10	1.65	1.34	0.996	1.40	0.995	4085.0
0.4 — 25	1.82	1.39	0.997	1.76	0.997	4052.7
0.4 — 40	2.23	1.30	0.997	1.78	0.995	4349.9
0.16 — 2.5	2.33	1.20	0.995	1.41	0.985	3858.9
0.16 — 10	1.44	1.36	0.996	1.30	0.996	3857.3
0.16 — 25	1.96	1.33	0.997	1.63	0.996	4553.3
0.16 — 40	1.44	1.29	0.997	1.06	0.994	4037.2

The dissolution rate constants (*k*) obtained from Korsmeyer–Peppas model and AUC were plotted with respect to the available total surface area of FNB in the film, separately. The total surface area of FNB was calculated using the measured $d_{4,3}$ after redispersion and with the assumption of spherical particles. Both dissolution profile analysis parameters, i.e., *k* and AUC, were found to have similar trends. Therefore, only AUC versus surface area was shown here for the sake of brevity (Figure 4.6). Total surface area dependence on *k* can be found in Appendix D (Figure D.1).

AUC change with respect to the total surface area was found to be more drastic with varying drug loading (Figure 4.6.b) than the particle size (Figure 4.6.a). It may be due to a more pronounced adverse effect on structure (i.e., tensile strength) with varying particle size than it was for drug loading change. Therefore, the expected surface area effect on the dissolution could be observed better with varying drug loading without the hindrance of mechanical properties.

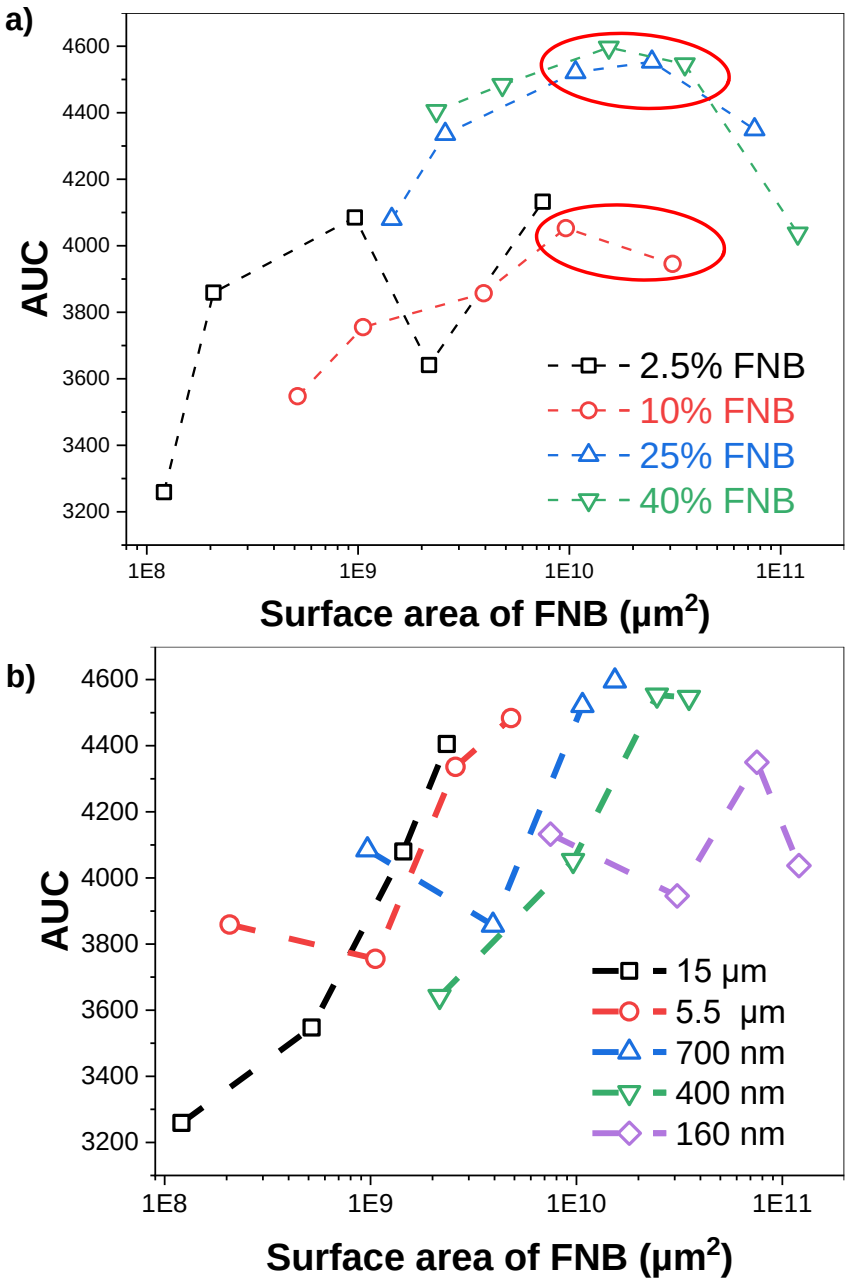

Figure 4.6 Dissolution analysis with respect to total surface area of FNB a) drug loading and b) particle size grouping.

4.6 Conclusions

As one of the most important steps in the pharmaceutical industry, the dissolution rate enhancement technique of particle size reduction was examined on oral films. Films were produced with acceptable uniformity regardless of the particle size and drug loading. It was shown that particle size and number significantly affected the polymer structure, mechanical properties, and in turn dissolution rate. Larger particles and the higher number of particles led to physically weaker films while smaller particles led to especially at high drug loadings. There was a combined effect of particle size and drug loading on dissolution rate with the confounding effect of mechanical properties. Particles in the polymer matrix may lead to slower dissolution above a certain surface area threshold due to adversely affected mechanical properties. The results demonstrated that nano-sized particles do not necessarily mean to outperform micro-sized particles in a matrix.

CHAPTER 5

EFFECT OF PROCESS PARAMETERS ON THE FILMS LOADED WITH POORLY WATER-SOLUBLE DRUG: DRYING

5.1 Introduction

In addition to the optimization of the formulation in dosage, design researchers followed various strategies to overcome the challenges encountered in every preparation step due to the different structure and solubility characteristics of materials. Drying is one the most important steps in film manufacturing due to its effects on film texture (i.e., skin, bubble formation), mechanical properties, thickness, and content uniformity of the film (i.e., agglomeration of drug particles). Depending on the needs, both the selection of the drying technique and the pace of drying should be introduced in the process development. In addition to that, drying is the step where residual solvent content is finalized. There are restrictions about the residual solvents for health effect concerns. Even though a non-hazardous solvent (water) is used in the formulation instead of organic solvents, for mechanical stability and texture purposes drying is still lies in the center of design parameters. To control the drying process, Critical Process Parameters (CPPs), *types of drying modes, air flow rate, temperature, humidity, drying (residence) time,* needs to be optimized specifically.

There are various studies on polymeric film drying which with many different purposes i.e., packaging [140-142], support material [143], edible films [144], coating [145], orodispersible films (ODFs) with or without drug [40, 74, 146-153].

Even though there is an extensive research on drying of polymeric films in the literature, it should also be emphasized that current literature is also lacking in terms of systematic investigations on the processing parameters of the oral film manufacturing.

For the drying of oral films, from ambient temperature to 60˚C and from 6 h to 48 h, different drying parameters are investigated Most of the drying processes are performed in the oven, leading high drying time. Susarla et al. introduced forced convection drying for the oral films [74]. Effect of the air temperature and the air velocity were systematically investigated on the oral films loaded with poorly water-soluble API using two different precursor viscosities. They optimized drying temperature range and air velocity to be suitable for drying API loaded films. Preis et al. studied the impact of drying conditions on the disintegration of the films [152]. In their study, films are dried at the ambient temperature, 40˚C, 60˚C and 80˚C for 48 h. Depending on the polymer type, different effects of drying temperature on the disintegration time were analyzed. An important observation in this study is, while disintegration time has increased with increasing drying temperature in the films made of polyacrylic acid (PAA) and methylcellulose (MC), temperature increment did not change any of the disintegration characteristics in the films made of hydroxypropyl methylcellulose (HPMC) and hydroxypropyl cellulose (HPC). Velaga et al. studied the drying kinetics of polymeric films with plasticizer using a convection oven and thermo-gravimetric analysis (TGA) as a metric [146]. They divided the drying into three phases, increasing temperature, constant temperature, and diffusion. On a side note, it is important to emphasize that the

thickness of the film may affect the drying kinetics and the thickness cannot be controlled in TGA. Even though they concluded that TGA can be used an easy metric to design drying conditions for thin films, the study clearly shows that there are differences in the fitted parameters which can lead to mistakes in the design.

Thabet et al. compared batch and continuous casting and drying processes [147]. From this study, it is clearly seen that while there is a lot of research about optimization of the formulation and process parameters, the design of the manufacturing devices plays an important role and needs to be paid attention by the regulating authorities. Therefore, to gain insight into drying mechanisms, identify and predict failure modes, and create a design space of drying process for production of high quality particle-loaded films, three drying modes and CPPs were analyzed. Polymer solution and drug loaded precursors were used to investigate the drying kinetics through conduction, convection and infrared heating as well as the final product quality of drug loaded films.

5.2 Materials

Griseofulvin (GF; Sigma–Aldrich, Saint Louis, MO) and fenofibrate (FNB, Jai Radhe Sales) as model BCS Class II drugs, pharmaceutical grade amorphous hydrophilic silica (M5P, Cabot Corporation, MA) with a primary particle size of 16 nm as the coating material of the drug particles, hydroxypropyl methylcellulose (HPMC; Methocel E15 Premium LV, The Dow Chemical Company, Midland, MI) as film former and glycerin (Sigma-Aldrich, Saint Louis, MO) as plasticizer were used.

5.3 Methods

5.3.1 Preparation of micronized-coated drug

Simultaneous micronization and dry coating technique used in this study were modified from a previous work [97]. As received griseofulvin powder and M5P silica was pre-mixed with a ratio of 97:3 using Laboratory Resonant Acoustic Mixer (LabRAM; Resodyn Acoustic Mixers, Inc., Butte, MT). LabRAM is operated at a frequency of 61 Hz and with 75 G acceleration for 5 min. This pre-mixture was fed with a constant 1 g/min rate into fluidized energy mill (FEM, qualification model, Sturtevant Inc., Hanover, MA) for simultaneous coating and micronization of GF. Feeding pressure was 65 psi while grinding pressure was 60 psi throughout the process. The particle size of micronized-coated GF (MC-GF) was tested using Rodos/Helos system (Sympatec, NJ, USA). The micronized coated particles had a d50 of 5.64 µm.

5.3.2 Preparation of precursor

An aqueous polymer solution with a composition of 14% HPMC E15 and 4% glycerin was prepared by first adding glycerin into the water at 35-40˚C. After the reached solution temperature of 90˚C, HPMC powder was added slowly with continuous stirring. Following HPMC addition, the solution cooled down slowly to room temperature. Polymer solution and MC-GF or MC-FNB were mixed using Thinky ARE-310 planetary centrifugal mixer (Thinky, Laguna Hills, CA, USA) with a ratio of 48:1. They were mixed at 2000 rpm for 2 min, defoamed at 2200 rpm for 30 s. The theoretical final composition of the precursor (wet %) and the film (dry %) are shown in Table 5.1.

Table 5.1 Composition of Wet and Dry Films

Ingredients	*Type*	*Wet %*	*Dry %*
Polymer	HPMC E15	13.7%	69.8%
Plasticizer	Glycerin	3.9%	19.9%
API	Griseofulvin or Fenofibrate	2.0%	10.0%
Coating agent	Silica (M5P)	0.1%	0.31
	Water	80.3%	-

5.3.3 Drying of films

The custom-made drying chamber used in this study (Figure 5.1) was designed to have conduction, convection and infrared heating modes. Conduction was supplied using a heating pad underneath a steel plate and convection was supplied using a hot air fan (HG 2510 ESD, Steinel). The temperature in the chamber was recorded using two mounted thermocouples before and after the film via a thermocouple recorder (Easy View 15 Thermometer Datalogger, Extech Instruments). The air velocity was measured right above the film using a hot wire thermo-anemometer (407123, Extech Instruments).

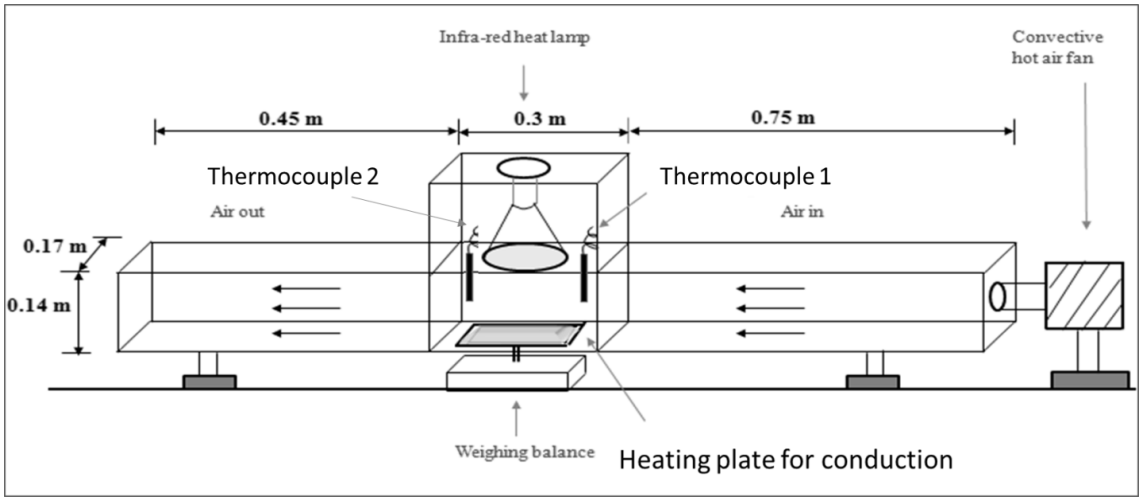

Figure 5.1 Schematic of drying setup.

Table 5.2 Experimental Conditions in the Drying Chamber

Run #	T_{plate} (°C)	T_{air} (°C)	Air Velocity (m/s)	Infrared lamp power level	T_{dew} (°C)
1	40	40	0.2	-	11
2	40	40	1	-	11
3	55	55	0.6	-	11
4	70	70	0.2	-	11
5	70	70	1	-	11
6	40	40	0.2	-	0
7	40	40	0.2	-	5
8	40	40	0.2	-	8
9	-	-	-	1	11
10	-	-	-	2	11
11	-	-	-	3	11
12	-	40	0.4	1	11
13	-	40	0.4	2	11
14	-	40	0.4	3	11

The conditions for each drying run shown in Table 5.2 was set and let it reach steady-state before the film was placed into the setup. Films were cast on a

polyester substrate (9744 Release Liner, 3M Scotchpak) using a doctor blade with a 0.5 mm aperture thickness. Then the film was cut into 8 cm x 12 cm (W x L) size and placed into drying chamber. During the drying, the weight of the film was recorded every 2 s and the film surface temperature was measured manually and recorded every minute using an IR thermometer (Sper Scientific, 800107). The experiment for each run was repeated for 3 times at each condition. All the mass data recorded during the experiments were converted to moisture ratio (MR) using Equation 5.1 to make a fair comparison between different conditions.

$$MR = \frac{m_t - m_s}{m_0 - m_s} = \frac{X_t}{X_0} \tag{5.1}$$

where m_t is mass at time "*t*", m_s is solid mass and m_0 is the mass when time is zero. All the data was smoothed using 1st order Savitzky-Golay filtering with 11 points step to eliminate the variation caused by the effect of flow on the weighing.

The thickness of the films was measured using a digital micrometer with an accuracy of 0.001 mm. Thickness was measured at five different locations across the film and used for calculating the average and relative standard deviation.

5.3.4 Thermo-gravimetric analysis (TGA) and Differential scanning calorimetry (DSC)

Thermo-gravimetric analysis (TGA) were conducted to measure the final moisture in the films using a TGA/DSC1/SF Stare system (Mettler Toledo, Inc., Columbus, OH, USA). A small sample of a film (~5.0 mg) was placed in a ceramic crucible,

heated from 25˚C to 250˚C in a nitrogen atmosphere at a constant heating rate of 10˚C/min.

A differential scanning calorimeter (DSC, Mettler Toledo, Inc., Columbus, OH) analysis is also performed in the examination of the melting point of aforementioned film samples loaded with drug. In DSC, approximately 5-8 mg of sample in an aluminum standard pan was heated from 25°C to 200 °C with constant heating rate of 10 °C/min under a nitrogen flow and cooled down to 25 °C with the same rate.

5.3.5 Mechanical properties

Investigation of the mechanical properties of the dried films was done using a TA-XT Plus Texture Analyzer (Stable Microsteps, UK). From each film, 5 rectangular samples, 50 mm x 15 mm, were taken. These samples were attached between two grips and elongated at a constant rate (1 mm/s) until the sample broke. From the resultant stress-strain curve, tensile strength (TS), Young's modulus (YM), and percent elongation at break (EB%) were calculated. For each film, the average values and standard deviations were reported. Further details about mechanical properties may be found in [29, 74].

5.4 Results and Discussion

5.4.1 Drying kinetics: process parameters

Drying kinetics of MC-GF loaded films were analyzed where conduction and convection were applied. Figure 5.2 shows the effect of temperature and air velocity on the drying rate of films with 0.3 mm and 0.5 mm wet film thicknesses.

Drying times were varied from 5 min to 20 min depending on the drying condition and film thickness. Drying curves clearly showed that increasing temperature and air velocity increased the rate of drying due to increased driving force. Furthermore, comparing two different film thickness drying rates, the effect of the air velocity was found to be more pronounced in thinner films (0.3 mm).

Drying curves fitted by Page model (Equation 5.2) for quantitative analysis [154]. Moisture ratio (MR) was explained with respect to time using this semi-empirical model where Fitting parameter, *k*, corresponds to the drying constant (min^{-n}).

$$MR = \exp\left(-k \cdot t^{n}\right) \tag{5.2}$$

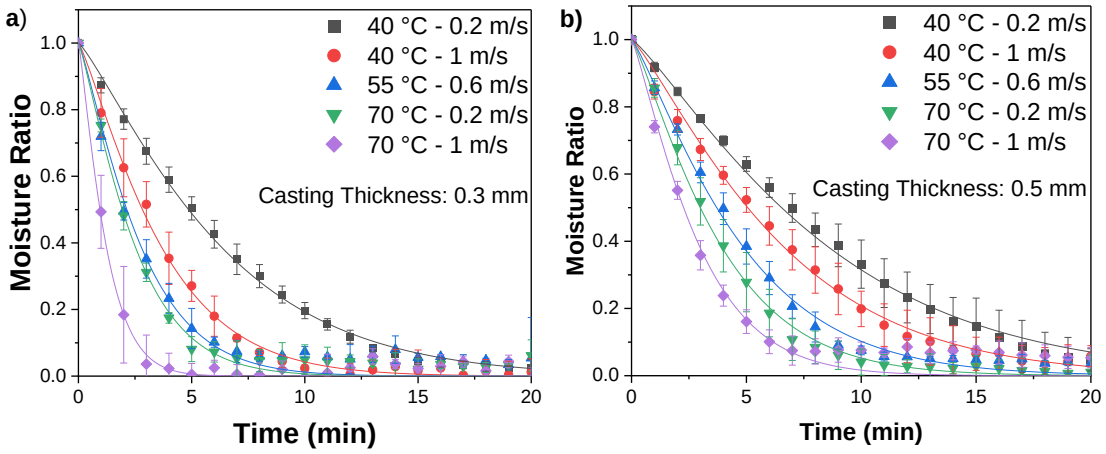

Figure 5.2 Drying curves at different temperatures and air velocity with a casting thickness of a) 0.3 mm b) 0.5mm. Symbols represent experimental data points while lines are the fitted modified model.

Fitting of curves according to Page model (Equation 5.2), yielded R^2 of 0.99 for each case with exceptions (Table 5.3). In these fitted models, *n* varied from 0.88 to 1.32 with an average of 1.2 ± 0.2. The drying constant *k* varied along with

n preventing a direct comparison for drying curves in terms of drying rate. Therefore, each curve was fitted with a modified version of the Page model (Equation 5.2) where *n* was fixed to its averaged value 1.2. Table 5.3 shows the fitting parameters for both equations at varying conditions.

The drying constant, *k,* from the modified model was considered as the drying rate analyzed for varying conditions, i.e., temperature, air velocity, and wet film thickness. When conductive and convective heating was applied, the increase in drying rate with increased air velocity was 91% and 134% for 0.3 mm thick films while it was 36% and 40% for 0.5 mm thick films (Table 5.3). Similarly, the increase in drying rate by increased temperature was more pronounced in 0.3 mm thick films than 0.5 mm thick films, i.e., 201% / 269% and 155% / 162%, respectively. This may be due to the increased diffusion layer of 0.5 mm thick films leading to the limiting parameter for the evaporation.

Table 5.3 Fitting Parameters for Drying Curves of Films Dried with Conduction and Convection Heating

Fitting Equations:		$MR = \exp\left(-k \cdot t^{n}\right)$			$MR = \exp\left(-k \cdot t^{1.2}\right)$	
Wet film Thickness	**Drying conditions**	***k***	***n***	***R²***	***k***	***R²***
0.3 mm	40 °C-0.2 m/s	0.099	1.22	0.9979	0.104	0.9979
	40 °C-1 m/s	0.192	1.22	0.9964	0.199	0.9965
	55 °C-0.6 m/s	0.383	0.92	0.9784	0.278	0.9707
	70 °C-0.2 m/s	0.313	1.20	0.9852	0.313	0.9859
	70 °C-1 m/s	0.703	1.31	0.9877	0.734	0.9879
0.5 mm	40 °C-0.2 m/s	0.057	1.31	0.9985	0.073	0.9966
	40 °C-1 m/s	0.114	1.13	0.9918	0.099	0.9913
	55 °C-0.6 m/s	0.133	1.24	0.9888	0.144	0.9890
	70 °C-0.2 m/s	0.155	1.32	0.9974	0.186	0.9962
	70 °C-1 m/s	0.378	0.88	0.9589	0.259	0.9524

Infrared (IR) drying kinetics were analyzed with and without forced convection in the drying setup (Figure 5.3). The addition of air flow into the system with an IR lamp accelerated the drying of the films. The increment in the drying rate was more pronounced for the lowest IR lamp power setting, compared to second and third settings.

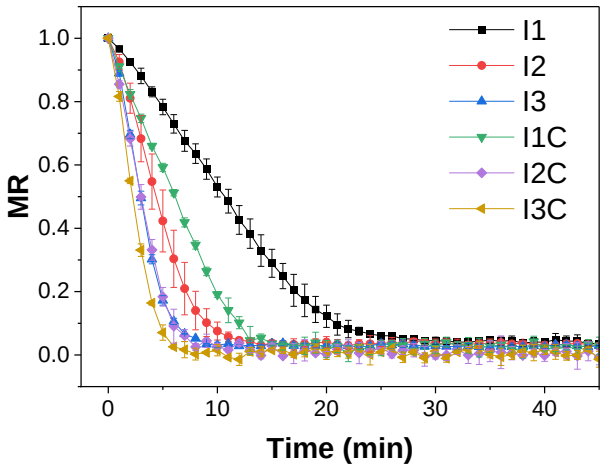

Figure 5.3 Drying curves under varying infrared lamp power and forced convection presence.

Another parameter affecting the drying rate is humidity. Since the saturation level of the air depends on both temperature and relative humidity, the dew point was calculated and kept constant during the experiments. The effect of all the other parameters was analyzed with a dew point of 11 °C. The effect of the humidity on the polymeric film without drug was analyzed using four different dew points at 40 °C – 0.2 m/s. Parallel to the expectations, decreasing dew points caused an increment in drying rates except for the dew point of 8 °C which is similar to the curve at the dew point of 11 °C (Figure 5.4). Since a lower dew point means that air contains less moisture, the difference in water content between film and air has increased. The standard deviation of the MR curves was reduced as the dew point

decreased at 40 °C – 0.2 m/s meaning drying at lower dew points is more predictable Figure 5.4.

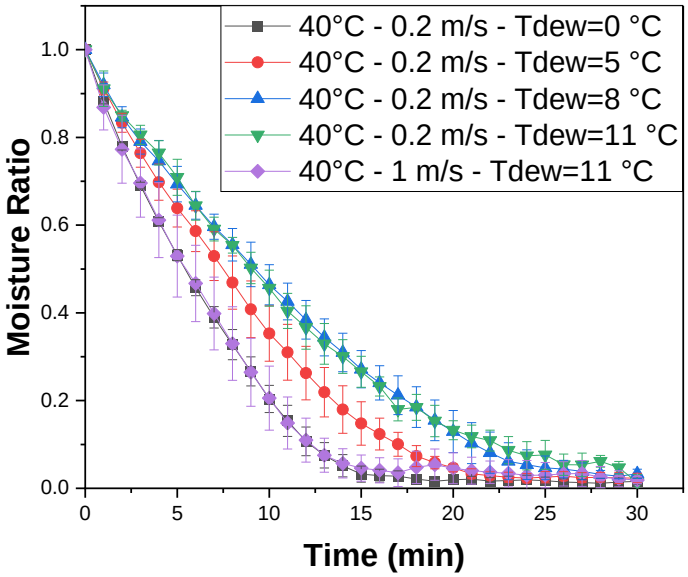

Figure 5.4 Drying curves of films dried at 40 °C and varying dew points.

In addition to process parameters, the effect of the presence of the drug was analyzed in terms of drying rates of cast films at the intermediate drying conditions, 55 °C, and 0.6 m/s, where conduction and convection were applied. Particles in sizes ranging from nano to micrometer as well as an amorphous drug were incorporated films were analyzed (Figure 5.5). Introducing the drug to the film did not affect the drying kinetics at moderate drying conditions regardless of the solid state of the drug, drug type, and size. Susarla et al. stated that there was no difference in the drying rates of the films with and without nano-sized drug particles when 40 - 60 °C was used as operating temperature and 0.5 – 1.5 m/s as operating air velocity [74]. Present findings also well align with previous studies and also confirms that even larger particles or amorphous drug did not affect the drying rate.

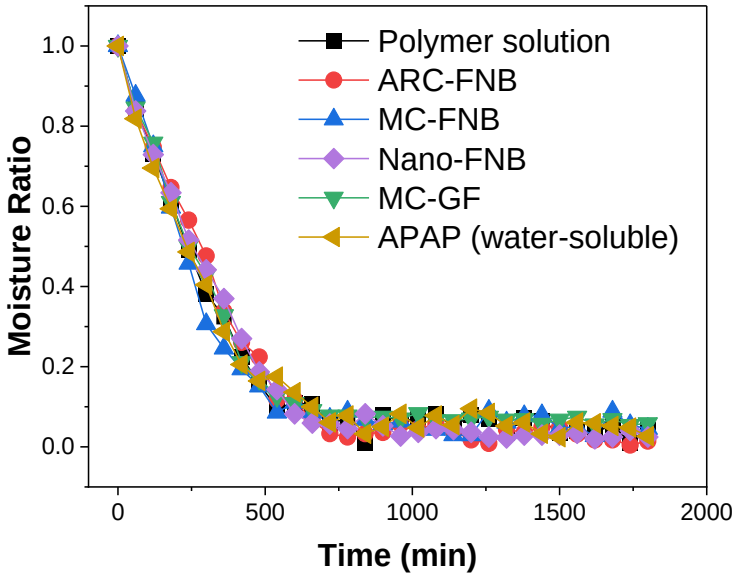

Figure 5.5 Drying curves of films loaded with different drugs.

5.4.2 Characterization of the films

Drying kinetics of the films were analyzed where drying time was fixed for all drying conditions at the same thickness. However, drying the films more than is needed may lead to brittle films and decomposition of the drug along with unnecessary process implementation. Therefore, for characterization purposes of micronized-coated fenofibrate (FNB) loaded films, drying times were adjusted for each selected drying condition. As a control, one film was dried at room temperature overnight (~12h). The highest drying condition (70 °C and 1 m/s) and intermediate condition (55 °C and 0.6 m/s) for conduction and convection drying were chosen for further analysis. In addition, the second lamp power with and without forced convection and the first (lowest) setting with convection was chosen. Because the lowest condition (I1) was significantly slower than the rest of the IR drying conditions and at the highest setting with and without convection did not enhance the drying rate significantly (Figure 5.3).

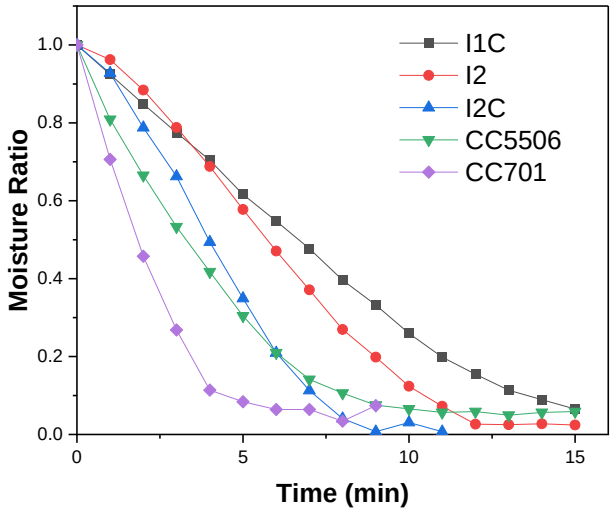

Figure 5.6 Drying curves of films loaded with 10% MC-FNB at varying drying conditions.

5.4.3 Thermal analysis of films loaded with drug

The final moisture content of the films defines the dryness of the film and has great importance since it would affect the stability, handling, mechanical properties, and peelability of the film. The moisture content of the films was calculated from TGA thermograms by taking the weight loss% until the first plateau on the thermogram which also corresponds to about 100 °C (boiling point of water). The moisture content of the dried films was found to be 2-3 wt% which led to peelable films.

The films were also analyzed via DSC to confirm the preserved crystallinity of the drug during the drying (Figure 5.7). The melting temperature of FNB in the film dried at room temperature as the control was 80 °C which was comparable to previous reports [77]. Unfortunately, the second IR lamp setting with and without forced convection and conduction-convection at 70 °C, 1 m/s induced the melting of the drug leading to no melting point on the thermogram. IR lamp might have increased the temperature on the film surface too fast causing the drug to melt.

The melting point of a compound starts before the melting point and continues after that. Therefore, FNB can start melting at 70 °C where conduction-convection was applied. However, complete melting was not expected. Considering the exposure time and the airflow, it may be stated that the drying temperature should be ~20 °C lower than the melting point of the drug.

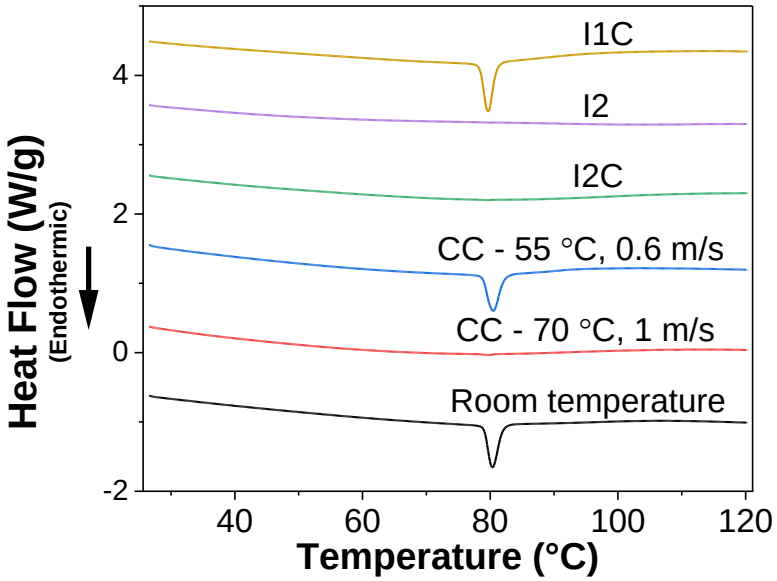

Figure 5.7 DSC thermograms of films dried at varying conditions.

The surface temperatures during the drying of the films at I2, I2C, and 70 °C, 1 m/s reached 60, 55, and 60 °C. On the other hand, it was only 45, and 50 °C for the drying conditions that protected drug crystallinity (I1C and 55 °C, 0.6 m/s, respectively). These indicated that the surface temperature of the film during the drying process should be closely monitored and kept well below the melting point of the drug (~30 °C).

5.4.4 Mechanical analysis of films loaded with drug

Films without crystallinity loss after the drying were further analyzed in terms of mechanical properties. Figure 5.8 presents the tensile strength (TS), elongation at break (EB), and Young's modulus (YM) of three films that preserved their crystallinities. While YM and EB did not vary among the different drying conditions, films dried at the lowest IR lamp setting with airflow had slightly lower TS compared to the other two. Similarly, Susarla et al. did not find a significant change in mechanical properties at the range of 40 - 60 °C and 0.5 – 1.5 m/s, temperature, and air velocity, respectively, for the films dried with conduction and convection heating [74]. I1C film was slightly compared to others suggesting that IR lamp drying can also produce good quality films faster and without damaging the drug.

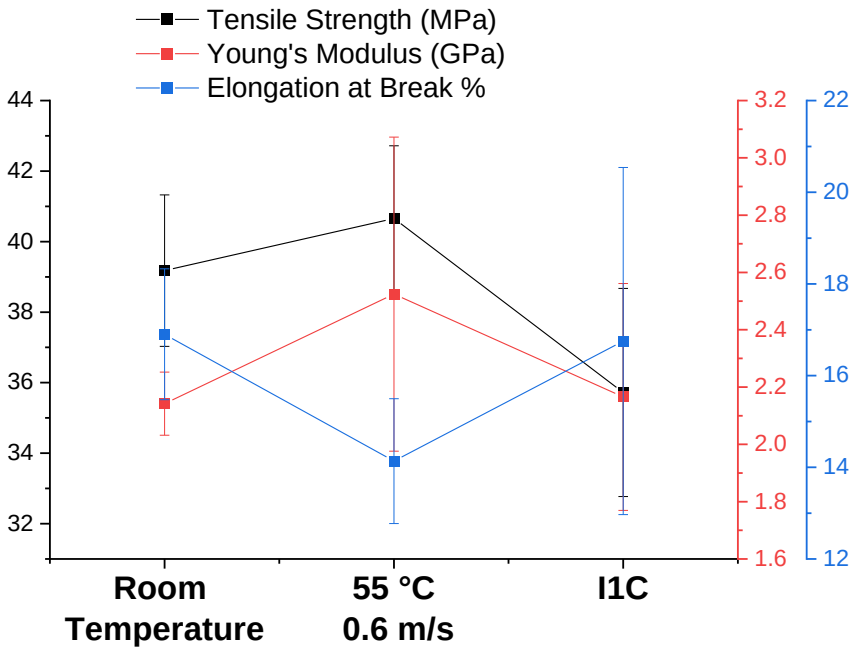

Figure 5.8 Mechanical properties of dried films at varying conditions.

5.5 Conclusions

The effect of process and formulation parameters i.e., temperature, air velocity, humidity, thickness, and the addition of drug particles in a dryer with combined conduction, convection infrared heating modes were presented. Drying times of the films varied from 5 to 30 min depending on the drying mode and strength. The effect of critical process parameters (CPPs) on the kinetics was verified while it was demonstrated that film thickness affected the extent of CPPs effect on the drying.

For the selected cases, film quality attributes, i.e., final moisture content, the crystallinity of drug, mechanical properties, were investigated. Good quality, peelable films with similar mechanical properties were produced with conduction-convection and infrared-convection systems. High temperature, air velocity, and infrared lamp power led melting of the drug in the film. Depending on the melting point of the drug, the maximum limit of CPPs should be considered. The results clearly showed that other control parameters such as film surface temperature should be introduced for process design in addition to drying rate.

CHAPTER 6

IN-LINE THICKNESS ANALYSIS VIA NEAR-IR SPECTROSCOPY ON STRIP FILMS LOADED WITH SURFACE-MODIFIED POORLY WATER-SOLUBLE DRUG

6.1 Introduction

Oral films have drawn the attention of many researchers in past few years owing to their favorable characteristics such as patient compliance, improved bioavailability, flexible dosing, and adaptability to continuous manufacturing [1, 2, 4, 6, 8]. Having these advantages, oral films are believed to play a key role in the reduction of time and the cost of manufacturing [7].

There are many studies related to the effect of material attributes and process parameters on the critical quality attributes (CQAs) of the films [24, 33-36]. Yet, a general framework towards design space and control systems is missing for film manufacturing to assure good product quality. Product quality is of importance in every different type of manufacturing, but it is critically important in the pharmaceutical industry where products must meet the CQAs needs. The CQAs can be monitored in real-time using Process Analytical Technology (PAT) allowing instant recognition of a manufacturing fault [155, 156]. However, a PAT system capable of this level of dynamic monitoring has yet to be integrated into the manufacturing of orally disintegrating films (ODFs). This paper investigates in-line Near-Infrared Spectroscopy (NIRS) analysis as PAT integration for the films loaded with poorly water-soluble active pharmaceutical ingredients (APIs) by examining formulation parameters with the goal of controlling film thickness. The

main goal is to identify the effect of particle engineering, which is a crucial addition to the formulation for improved bioavailability, with in-line chemometric analysis.

NIRS and Raman Spectroscopy are the most reported PAT analyzers [156]. They are used for different purposes, i.e., detecting granule size, water content, drug amount, and thickness detection in many different processes i.e., fluid bed drying, tablet coating, hot-melt extrusion, film manufacturing [157-159]. Off-line spectroscopic measurements have been examined to show the applicability of these tools towards the implementation of PAT to films [160-162]. In these studies, NIRS was used to determine drug content in the film with a good correlation between spectra and assay values. There are also instances of in-line studies on drug-loaded films where only the drug content was analyzed either with NIRS or Raman Spectroscopy [163-165]. Hammes et al. integrated in-line Reflectance NIRS at the end of the drying line to analyze the drug content [163]. NIR spectra were analyzed using Partial Least Squares (PLS) regression, to correlate the spectra with drug amount in the film. Considering a narrow range of drug amounts, i.e., 2.2 – 2.6 mg per dosage, were used, the applicability of their correlations may be limited. Zhang et al. used Raman Spectroscopy to determine the drug content through both in-line and off-line analysis [164]. Key factors such as the effect of the belt speed, the probe location in the drying line, and the thickness of the film were considered. Correlations between spectra and the drug amount measurements exhibited low variation (R^2>0.99) and high prediction (RMSEC< 0.6%) with both in-line and off-line cases. On the other hand, it was underlined that

varying process conditions i.e., belt speed, probe location, affected the calibration models [164].

PAT tools have been used for monitoring micron-size [160, 162], or nano [164], or amorphous [161-163, 165] APIs in the films. Finer particles such as nano-sized or amorphous dispersions are expected to increase the dissolution rate of the API [42] and are commonly used in film manufacturing [9, 18, 24, 28-32, 35, 96]. An interesting recent technique to improve the dissolution is the dry coating of the API [30, 97]. The dry coating has been shown to be effective in preventing aggregates and promotes excellent API dispersion in the films [97]. In the present work, the use of a spectroscopic method was considered to examine films loaded with micronized and/or dry coated API particles. Unfortunately, the effect of dry coating on the ability to obtain reliable NIR spectra and on the accuracy of the subsequent chemometric analysis is unknown. In addition, the particle size, as well as agglomerate sizes, may affect the NIRS analysis by changing the absorbance [166, 167]. However, neither the effect of the particle size of the API nor the presence of a coating agent on the chemometric analysis has been studied for films. Such monitoring would provide significant insight for the development of the film manufacturing and monitoring processes.

Another important film CQA besides the drug loading is thickness as it can affect other CQAs such as mechanical properties, dissolution rate, and drug dosage. Thickness can also be affected by critical material attributes (CMAs) [34] and critical process parameters (CPPs). Therefore, it is also useful to examine NIR spectroscopy to assess the thickness of the film loaded with the poorly water-

soluble drug along with the effects of particle size and dry coating. Consequently, a NIRS probe was used for in-line thickness detection. In addition, for improving the sampling of the film in motion, a moving apparatus was developed for automatically obtaining spectra from various parts of the film. Hydroxypropyl methylcellulose E15 as the film-forming polymer, glycerin as a plasticizer, fenofibrate (FNB) as a model poorly water-soluble API, and hydrophilic silica as coating agent were used. Two micron-sized FNB powders in different particle sizes and their coated counterparts were incorporated into the films for further analysis. Principal component analysis (PCA) was performed on NIR spectra to gain insight into the samples. Further, correlations between NIR spectra and thickness of the films were developed using partial least squares (PLS) regression along with complimentary characterization techniques, i.e., surface and cross-sectional morphology redispersed particle sizes and thickness and content uniformity. These results were analyzed to assess the robustness of thickness monitoring via NIRS in presence of coating agents and/or APIs with different particle sizes.

6.2 Materials

A model BCS Class II drug, Fenofibrate (FNB, Jai Radhe Sales), pharmaceutical-grade amorphous hydrophilic silica (M5P, Cabot Corporation, MA) with a primary particle size of 16 nm as the coating material of the drug particles, hydroxypropyl methylcellulose (HPMC; Methocel E15 Premium LV, The Dow Chemical Company, Midland, MI) and glycerin (Sigma-Aldrich, Saint Louis, MO) were used in film preparation.

6.3 Methods

6.3.1 Preparation of coated and uncoated micronized drug powders

Micronized and/or dry coated drug powders were prepared via procedures adapted from previous works [30, 97]. Laboratory Resonant Acoustic Mixer (LabRAM; Resodyn Acoustic Mixers, Inc., Butte, MT) were used to mix as-received fenofibrate (FNB) powder and silica with a ratio of 97:3 at 61 Hz frequency and 75 G acceleration for 5 min. This mixture was called as-receive coated fenofibrate (ARC-FNB). Micronized coated FNB (MC-FNB) was prepared with a simultaneous micronization and coating technique via fluidized energy mill (FEM, qualification model, Sturtevant Inc., Hanover, MA). Briefly, ARC-FNB fed with a constant 1 g/min rate into FEM with a feeding pressure of 45 psi and grinding pressure of 40 psi. The uncoated-micronized FNB was produced under the same conditions except for silica addition. The particle sizes of all powders, i.e., as-received, as-received coated, uncoated-micronized, and coated-micronized, were tested using Rodos/Helos system (Sympatec, NJ, USA) using 1 bar dispersion pressure.

6.3.2 Preparation of films loaded with drug

An aqueous polymer solution was prepared according to Dow and previously established protocols [29, 30, 67]. A polymer solution consists of 12% HPMC and 4% glycerin was selected considering previous works [29, 30]. Briefly, DI water was heated up to 35-40 °C while stirring, glycerin was added. When the solution reached 80 °C, HPMC powder was added slowly and allowed to disperse well. Then, the solution was left to cool down to room temperature while mixing. Polymer solution and FNB powders were mixed for 2 min at 2000 rpm and defoamed for 30

s at 2200 rpm using a planetary centrifugal mixer (Thinky ARE- 310, Laguna Hills, CA, USA). If the suspension still had bubbles, it was left overnight. The compositions of films and given abbreviated names are shown in Table 6.1.

Table 6.1 Compositions of Films Loaded with Drug

Formulation name	***FNB modification***	***HPMC in polymer solution (wt%)***	***Glycerin in polymer solution (wt%)***	***Polymer solution to powder ratio***	***Target drug loading in dry film (wt%)***	***Coating agent in the dry film (wt%)***
AR	As-received	12	4	14.6	30	NA
ARC	A-received coated	12	4	13.9	30	0.9
MUC	Micronized uncoated	12	4	14.6	30	NA
MC	Micronized coated	12	4	13.9	30	0.9

The suspensions were cast onto a moving substrate (Scotchpak™ 9744, 3M, MN, USA) using a doctor blade (Elcometer, Rochester Hills, MI) with different opening thicknesses ranging from 0.2 to 0.9 mm with an interval of 0.1 mm. Films were dried in a Lab-Cast Model TC-LC Tape Caster (HED International, Ringoes, NJ) at 50 °C. Films for both calibration and prediction sets were prepared with the same method.

6.3.3 Uniformity of the films loaded with drug

The uniformity of the films was assessed via relative standard deviations (RSD) of thickness, drug loading, and drug amount per area. The method was adapted from

previously established procedures [29, 30]. Ten circular punches with ~0.7 cm^2 of area, were taken from each film randomly. The mass and thickness of each sample were recorded. Then, samples were dissolved in a 7.2 g/L sodium dodecyl sulfate (SDS) solution on magnetic stirrers. The volume of SDS was adjusted depending on the theoretical drug amount of the film ensuring sink conditions, from 20 mL to 50 mL. Drug amount per area (mg/cm^2) and drug loading for each sample were calculated from absorbances measured via a UV-vis spectrophotometer (Thermo Fisher Scientific Inc., MA, USA) at the wavelength corresponding to FNB, 290 nm [29, 30]. Then, the reported RSDs for thickness, drug loading, and drug amount per area were calculated average and standard deviations of ten samples.

6.3.4 Re-dispersion of drug particles from the dried films

The drug particles were re-dispersed from dried films and size distribution was analyzed to assess the particle size maintenance in the film structure. The procedure was modified from earlier works [27, 30]. Briefly, 3 circular punches of 0.72 cm^2 in the area were vortexed in 10 ml deionized water at 1500 rpm for 2 min. The size of drug particles in the suspension was measured via a laser diffraction particle size analyzer (Coulter LS 13320, Beckman Coulter, FL, USA).

6.3.5 Imaging of dried films loaded with drug

The surface morphology of the films loaded with the drug was examined via field emission scanning electron microscopy (SEM) (JSM-7900F, JEOL USA, Inc. MA). The samples were pre-coated with gold via a sputter coater (EMS 150T ES, Quorum Technologies Ltd., Laughton, East Sussex, England) to prevent the charging of the sample due to the high polymer content.

The cross-section of films loaded with the drug was analyzed using an optical microscope with polarization mode (Carl Zeiss Microscopy, LLC. Germany). Film samples were cut into thin pieces and fixed onto a glass slide with the help of double-sided tape. Images were taken as representative of the sample.

6.3.6 In-line Near-IR (NIR) Spectroscopy data acquisition and analysis

A micro Near-IR probe (JDSU Inc., now Viavi Solutions, San Jose, CA) was used for diffuse reflectance spectra acquisition over 908–1670 nm spectral range. One spectrum was an average of 100 scans. The NIR probe is fixed onto a moving apparatus which allows taking data from two sides and the middle of the film (Figure 6.1). The distance between the NIR probe and the substrate was 3 mm which was found to be the optimum distance based on preliminary work. The apparatus with the NIR probe was placed into an HED drying chamber for in-line measurements (Figure 6.1). The films with varying thicknesses were prepared as explained in Section 2.2.2. The thickness of films varied by changing the opening height of the doctor blade. The measurements were taken from each dried film towards the end of the line while the film was moving at 0.16 or 0.08 cm/s speed and the temperature inside the chamber was 50 °C. The setup for spectral acquisition is demonstrated in Figure 6.1.

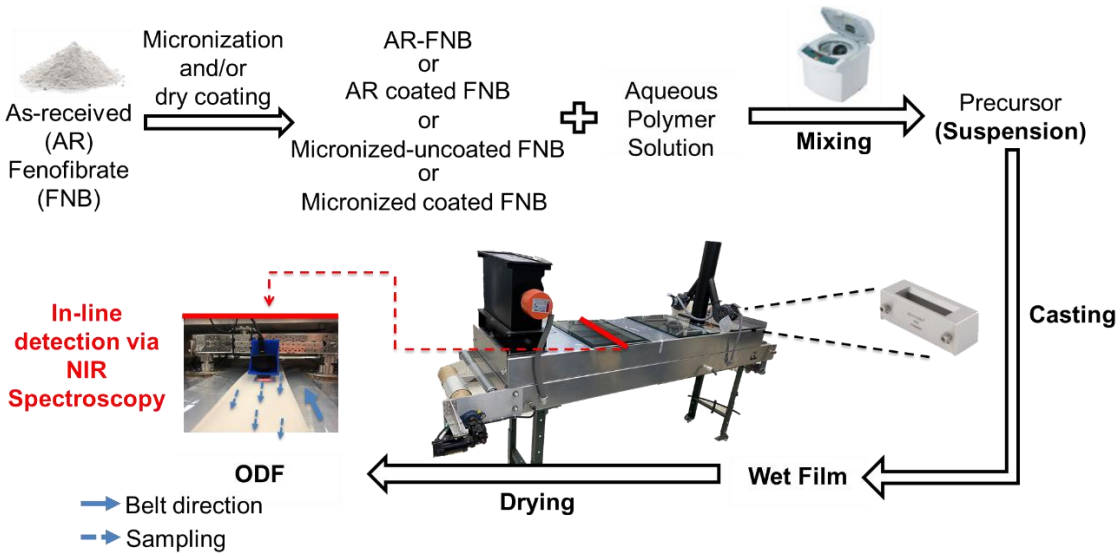

Figure 6.1 Schematic for manufacturing and detection steps.

After NIR spectra were taken, the thickness of the films was measured using a digital micrometer with an accuracy of 0.001 mm at 20 different locations across the film and the average was taken to use as a reference for model development. NIR spectra were collected from each FNB powder, i.e., AR-FNB, ARC-FNB, MUC-FNB, MC-FNB. Powders were filled into a glass petri dish where the surface was leveled. The probe was located 3 mm above the sample. 50 spectra were recorded for each powder type.

NIR spectra were analyzed using The Unscrambler X 10.5.1 software. Different pre-processing methods i.e., SNV, 2nd order Savitzky-Golay smoothing, 1st order derivatives, baseline correction, and their combinations were applied to NIR spectra.

Initially, Principal Component Analysis (PCA) was conducted as a qualitative analysis of NIR spectra belonging to films with different thicknesses to analyze the possible effects on the data. Partial Least Square (PLS) regression

was used to create a model correlating the NIR spectra to the thickness of the films loaded with FNB. NIR spectra were used as predictors and thicknesses obtained using a micrometer were used as responses. A total of 10 spectra were taken for each sample, i.e., each thickness, to use in the calibration model. Cross-validation was implemented using the leave-one-out method. For the prediction, 5 more spectra were taken from the films with the same thicknesses as in the model and with 2 different thicknesses in addition to the ones used in the calibration model.

PCA and PLS analysis were conducted on NIR spectra belonging to films loaded with 30 wt% AR-FNB to assess the most suitable pre-processing method. The 1st derivative as the pre-processing method and spectral range of 1304 – 1651 nm were selected for PCA and PLS analysis after evaluating the results in terms of RMSEC (2.47), RMSECV (2.59), bias (0.015), R2 (0.9924) (Table E.1) and PCA scores (Figure E.1). The 1st derivative was used as the pre-processing method for all the other formulations as well.

A calibration model was created separately for each formulation containing one type FNB (AR or ARC or MUC or MC). In addition, two calibration models were developed combining data belonging to films loaded with the same particle sizes (AR-ARC and MUC-MC). Another calibration model was developed combining all the data for films containing AR or ARC or MUC or MC-FNB. The films containing coated and uncoated particles or all the films were used to create one calibration model to examine the possibility of the number of calibrations needed.

The quality of the calibration models was assessed in terms of root mean square error of calibration (RMSEC), root mean square error of cross-validation

(RMSECV), root mean square error of prediction (RMSEP), bias, and R2. In addition, the optimum number of PLS factors were chosen considering the aforementioned figures of merit.

6.4 Results and Discussion

6.4.1 Uniformity of films loaded with drug

Different film thicknesses may be required for specific application sites and varying the dosage. A robust manufacturing system should be producing films in a range of thicknesses with good uniformity. The uniformity in the thickness would affect many quality attributes of the film from dosage to mechanical properties and dissolution. Therefore, the thickness is one of the most important parameters to be controlled to ensure an acceptable product. The uniformity of the films was assessed using relative standard deviations (RSD) for thickness, drug amount per area, and drug loading obtained with off-line tests (Figures 6.2.a, b, and c, respectively).

As it was reported previously, mixing with a planetary mixer and sufficient viscosity would lead to good content uniformity regardless of the drug modification [24]. RSDs indicated good thickness and content uniformity (<6%) with a few exceptions (Figure 6.2). The films that did not meet the uniformity criteria were either loaded with AR-FNB or were the thinnest films. It should be noted that the sample size (~0.7 cm^2) used for the content uniformity test was about $1/10^{th}$ of the intended dosage size (2 cm x 3 cm) for better discriminating analysis [24, 37]. Therefore, more variation in the content could be expected for thinner films due to the even lower drug amount in the sampling. RSDs of dry film thickness for the

samples loaded with AR and ARC were slightly higher than MUC and MC (Figure 6.2.a). The reduction of particle size may be helping to obtain better-organized particles leading to a more uniform thickness. Since heterogeneity of the samples adversely affects the measurements, uniformity of the samples and sampling are highly important for the calibration model in multivariate analysis of spectra [38-40]. Therefore, improved thickness and content uniformity via dry coating would help to develop better correlations between spectra and the quality attribute in question (thickness, drug loading, etc.).

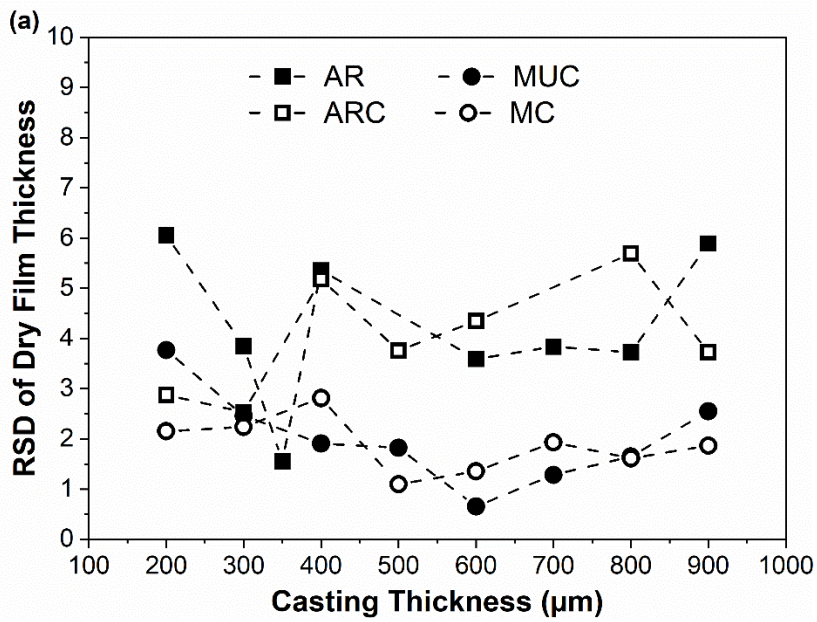

Figure 6.2 Relative standard deviation (RSD) values of a) film thickness and b) drug amount per area c) drug loading%.

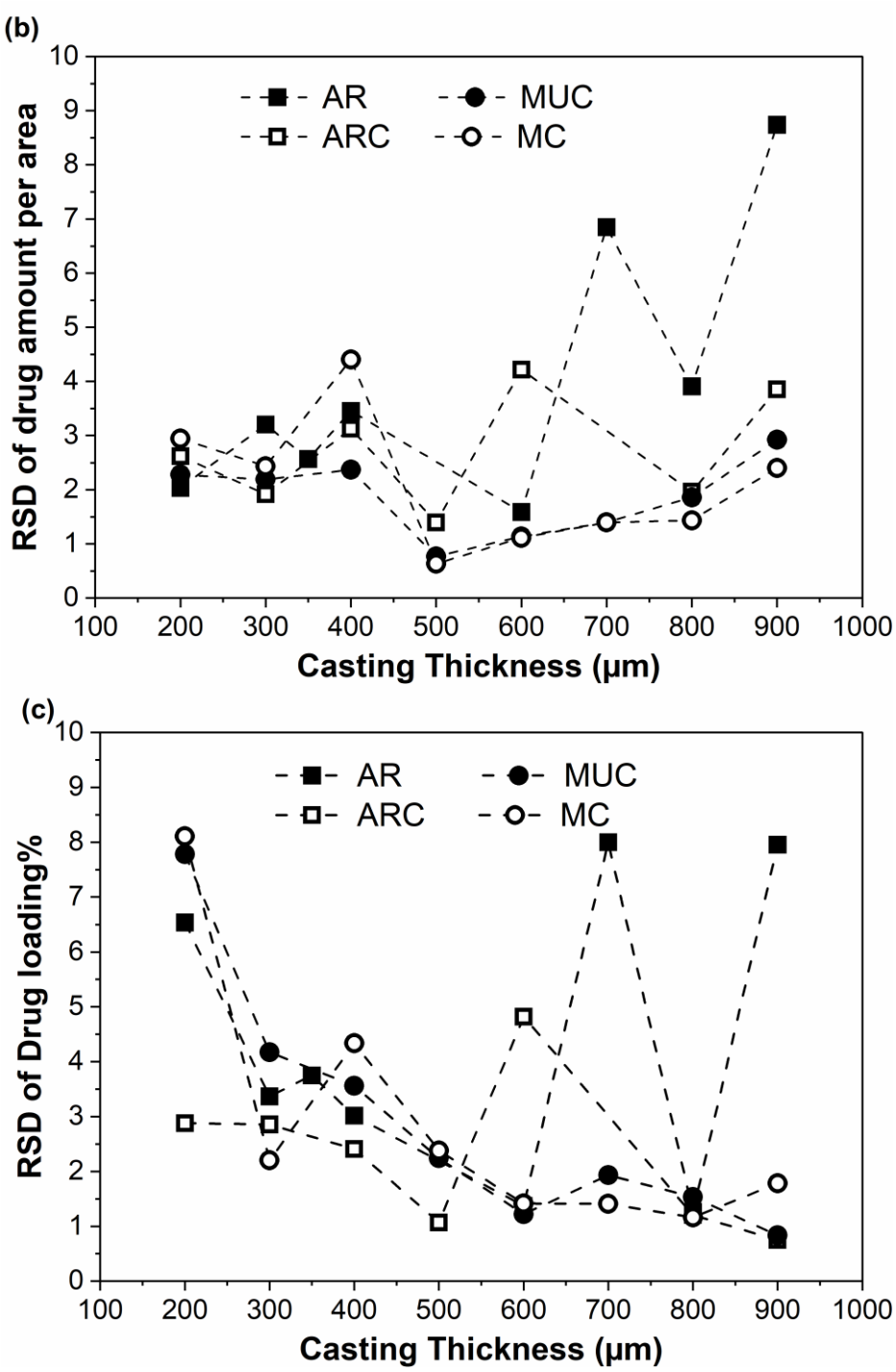

Figure 6.2 (Continued) Relative standard deviation (RSD) values of a) film thickness and b) drug amount per area c) drug loading%.

6.4.2 The particle size of drug powders and after re-dispersion of drug particles from the dried films

Particle sizes of drug powders and re-dispersed drugs from the dried films are reported in Table 6.2 as d_{10}, $d_{50,}$ and d_{90}. In all cases, there was a slight increase in particle sizes of re-dispersed FNB particles compared to powder due to an aqueous environment. Re-dispersed MUC-FNB particles showed more increase in particle size compared to others. The particle size of powder MUC-FNB was also higher compared to MC-FNB powder indicating agglomeration without coating. Only film sample with no particle size, i.e., d_{50} and d_{90}, change between powder and re-dispersed particles was the film containing MC-FNB.

Table 6.2 Particle Size Distribution of Dry Powders and Re-Dispersed Particles from Dry Films

Drug	d_{10} *(µm)* ± SD		d_{50} *(µm)* ± SD		d_{90} *(µm)* ± SD	
	Dry Powder	***Re-dispersion***	***Dry Powder***	***Re-dispersion***	***Dry Powder***	***Re-dispersion***
AR	2.12 ± 0.25	3.26 ± 0.03	6.00 ± 0.19	7.42 ± 0.07	13.39 ± 0.22	15.31 ± 0.09
ARC	2.18 ± 0.04	3.34 ± 0.01	5.88 ± 0.09	7.68 ± 0.01	12.56 ± 0.38	15.86 ± 0.09
MUC	0.67 ± 0.03	1.83 ± 0.02	2.71 ± 0.03	3.52 ± 0.13	5.38 ± 0.58	7.38 ± 0.57
MC	0.54 ± 0.04	1.44 ± 0.02	2.24 ± 0.24	2.49 ± 0.08	4.05 ± 0.40	4.14 ± 0.43

SD: Standard deviation

It has been shown that dry-coating of the drug using hydrophilic silica reduces the agglomeration in powder drug [97, 168]. Zhang et al showed that dry-coating of micronized drug particles prevents the agglomeration both in powder

and the film allowing preparing physically stable product [30]. The current findings were also in line with previous literature confirming drug agglomeration reduction via dry coating.

6.4.3 Imaging of dried films loaded with drug

The surface morphology of the films was analyzed via SEM imaging (Figure 6.3). Particle size reduction and/or coating of API particles led to qualitatively more uniform surface morphology and less surface roughness due to better distribution of the particles. It was shown that the coating of the API allows better distribution of the particles along with the film which is in line with present results [30].

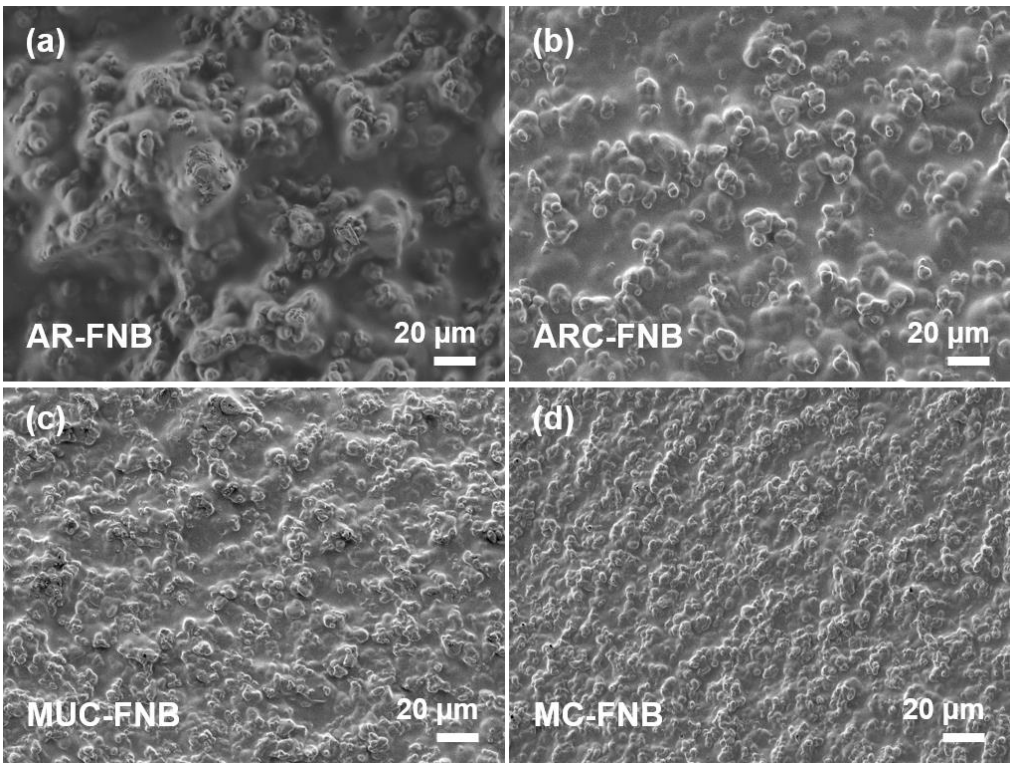

Figure 6.3 SEM images of top surfaces of films loaded with 30% a) AR-FNB b) ARC-FNB c) MUC-FNB and d) MC-FNB.

Film cross-sections were analyzed using optical microscopy with polarized light (Figure 6.4). The bottom of the film was smoother than the top due to

confinement via substrate under the film. Centkowska et al. showed using AFM measurements that the bottom of the film loaded with micro-sized API was smoother (maximum roughness of 0.14 µm) than the surface (maximum roughness of 5 µm) [169]. Cross-sectional images further showed that particle size reduction and/or coating of API particles reduced the surface roughness and increased uniformity of particle distribution close to the film surface.

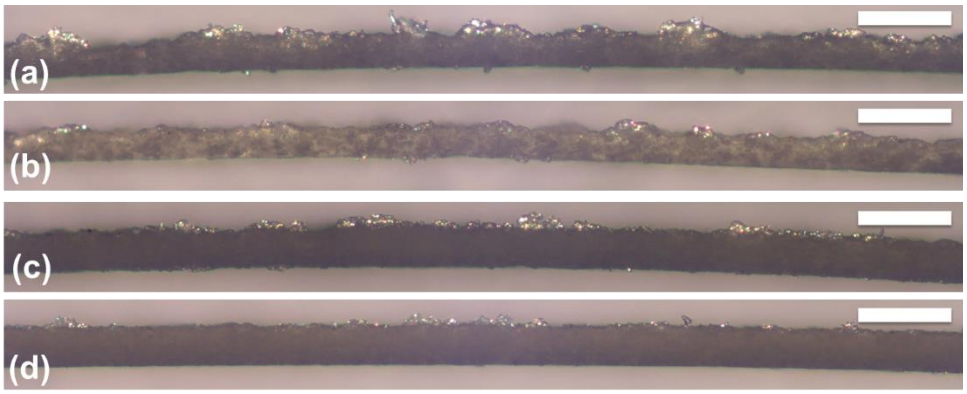

Figure 6.4 Cross-sectional optical images of films loaded with 30% a) AR-FNB b) ARC-FNB c) MUC-FNB and d) MC-FNB (scale bars represents 100 µm) (top surface of the film faces upwards).

6.4.4 Spectroscopic measurements and Multivariate data analysis

The films loaded with either AR, ARC, MUC, or MC-FNB where the average thicknesses varied from 23 to 124 µm were analyzed using in-line NIR Spectroscopy. The NIR spectra were acquired as the film was moving at 0.16 cm/s speed on the semi-continuous film casting and drying line. As an example for NIR spectra changes with varying thickness, an average of 10 spectra for 30 wt% MC-FNB (wt%) loaded films with the average thicknesses varying from 23.3 to 112.2 µm are presented in Figure 6.5. O–H stretching and O–H 1st overtone bands increased as thickness increases. The thickness range considering all individual

measurements was 23 to 135 µm. Ortega-Zuniga et al. demonstrated that the penetration depth of NIR radiation in polymeric films could be as high as 3.04 mm [170]. Even though the depth of penetration changes depending on the material, the films used in this study were thin enough for NIR radiation to go through. Therefore, NIR spectra represented the whole sample in the thickness axis allowing thickness monitoring.

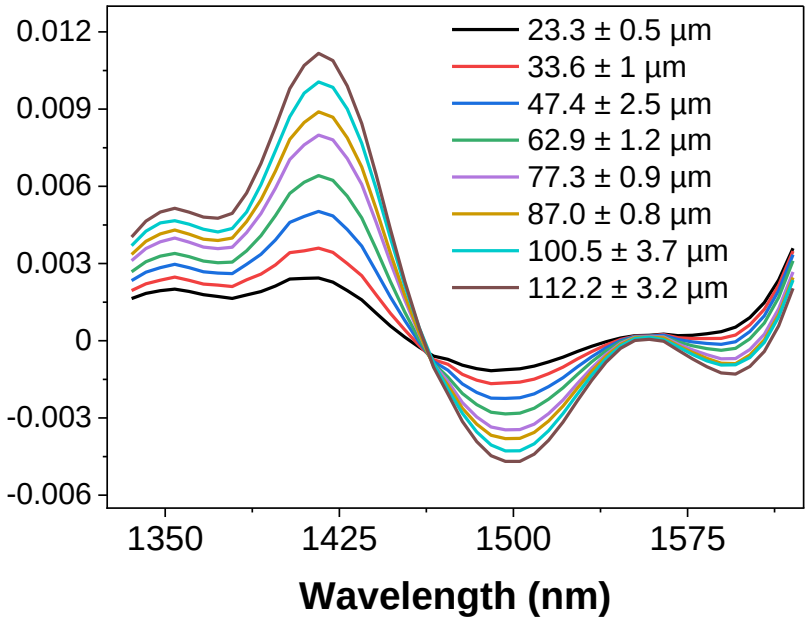

Figure 6.5 Pre-treatment (1st derivative) applied and averaged NIR spectra belonging to films with varying thickness, loaded with 30% MC-FNB.

PCA scores of NIR spectra belonging to films with different thicknesses were analyzed for 30 wt% AR-FNB, ARC-FNB, MUC-FNB, and MC-FNB loaded films (Figure 6.6). In all the cases, PC1 corresponded to the thickness of the film showing variability along PC1 axis and it was the only variable at fixed drug loading and particle type. PC2 most probably corresponded to thickness deviation along

with the film. PCA scores of NIR spectra belonging to films with varying thicknesses formed clusters for the same dry film thicknesses.

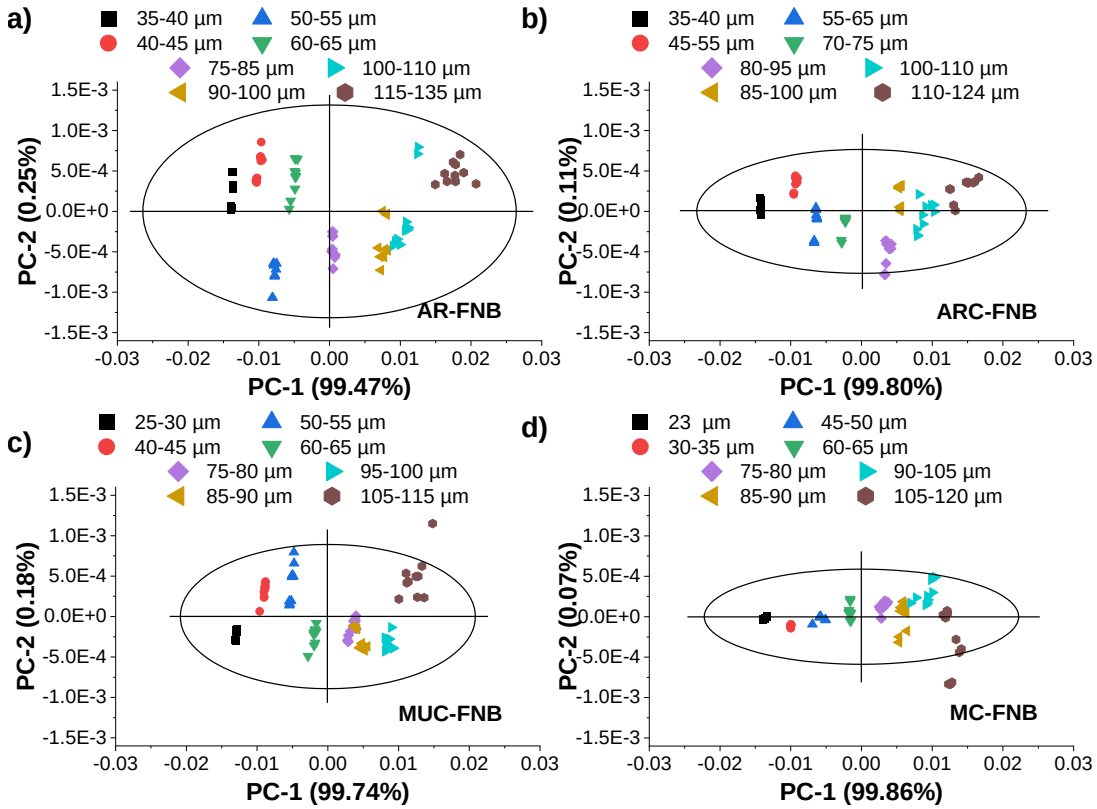

Figure 6.6 PCA score plots for NIR spectra belonging films loaded with 30% a) AR-FNB b) ARC-FNB c) MUC-FNB and d) MC-FNB.

Figure 6.6 demonstrates PCA score plots of the films loaded with either AR-FNB, ARC-FNB, MUC-FNB, or MC-FNB. Coated FNB loaded films (ARC-FNB or MC-FNB) (Figures 6.6. b and d) showed reduced variation within the replicates compared to their uncoated counterparts (AR-FNB or MUC-FNB) (Figures 6.6. a and c). Mostly, PCA scores for films loaded with micronized and/or dry coated FNB showed less variation within the same thickness measurements. The lower variation indicated that the dry coating of FNB allowed better drug distribution thus more uniform thickness. In the case of MC-FNB (Figure 6.6.d), 99.86% of the

spectral variation was explained with PC1 which corresponds to the thickness and had a narrower confidence ellipse confirming the uniformity enhancement via both micronization and coating of the FNB compared to other cases. In all cases, the variation among the samples with the same thickness increased as thickness was increased.

The effect of particle type in the film on the thickness was analyzed via NIR spectra scores (Figure 6.6). In order to analyze the variation in spectra between coated/uncoated or different particle size counterparts, spectra were further analyzed via PCA scores of paired sets. Effect of micronization and the coating of the FNB embedded in the film were analyzed by pairing the spectra belonging to films loaded with either the same size or same coating conditions (coated or uncoated).

The effect of micronization, i.e., particle size, was analyzed via PCA scores of NIR spectra belonging to films loaded with AR & MUC and ARC & MC (Figure 6.7.a and b). Films loaded with FNB in two different particle sizes with (d_{90} of 4.14 and 15.31 µm) or without coating (d_{90} of 7.38 and 15.86 µm) were compared. 99.31% and 99.6% of the spectral variation was explained by PC1 corresponding to thickness for PCA of AR & MUC and ARC & MC, respectively. Figures 6.7.a and b show a clear distinction between scores of ARC and MC compared to AR and MUC. It was due to the better distribution of coated particles compared to their uncoated counterparts leading to more differentiation in NIR spectra of the films loaded with different sized particles. It was stated that particle size could affect the interaction with NIR photons leading to an increase in absorbance [166]. However,

it was also shown that when larger particles are of a lower concentration in the blend, they could lead to inaccuracies [167]. The present results are also in line with previous results showing differentiation between different particle sizes.

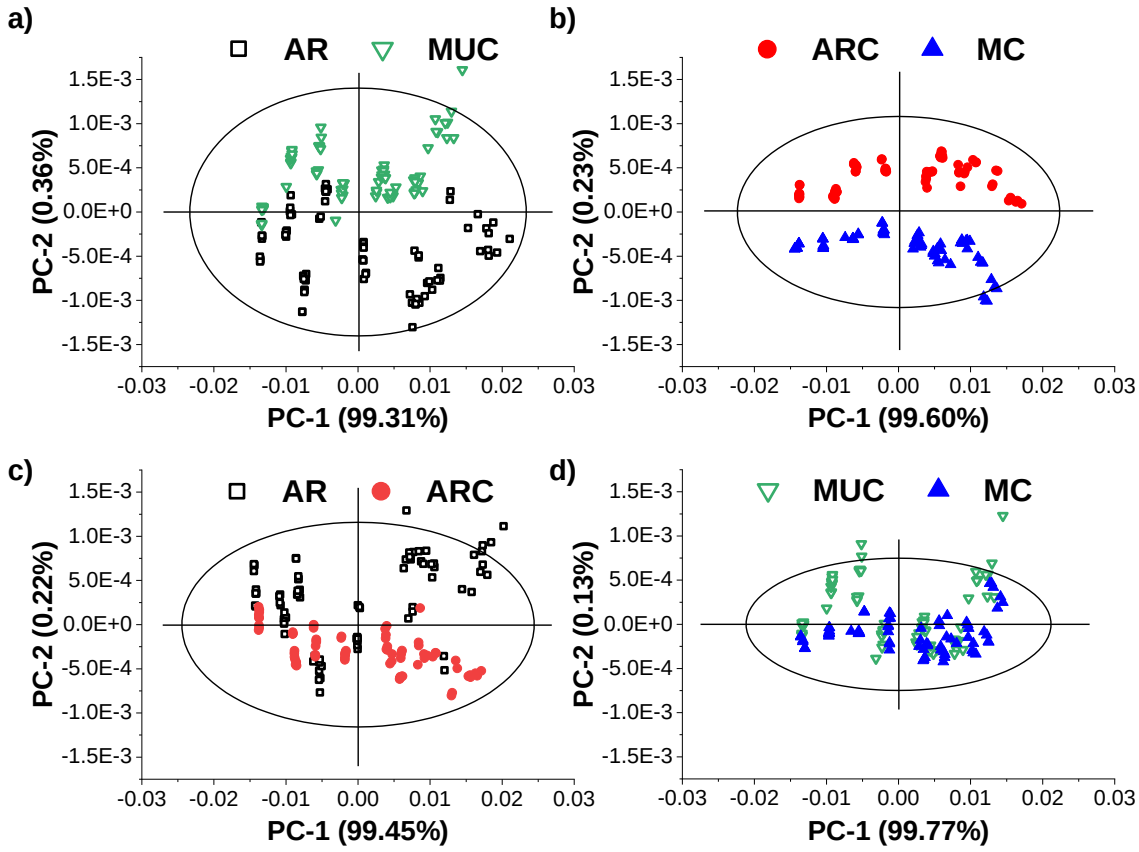

Figure 6.7 PCA score plots for NIR spectra belonging films loaded with 30% a) AR-FNB or MUC-FNB b) ARC-FNB or MC-FNB c) AR-FNB or ARC-FNB and d) MUC-FNB or MC-FNB.

The effect of dry coating of FNB was also analyzed via PCA scores of NIR spectra belonging to films loaded with AR & ARC and MUC & MC (Figure 6.7.c and d). PC1 corresponded to the thickness and PC2 thickness deviation in the film. The scores of the films loaded with the coated drug (ARC or MC) showed less variation (PC2 range of 0.001 and 0.0009, respectively) compared to their uncoated counterparts (AR or MUC) (PC2 range of 0.0021 and 0.0016,

respectively). Films loaded with the same type of FNB did not show clustering between the PCA scores belonging to films loaded with coated and uncoated FNB. This suggested that the coating of FNB did not interfere with NIR spectra and the same particle sizes resulted in similar spectra. PC1 explained 99.45% of the data for larger particles (AR or ARC) (Figure 6.7.c) while 99.77% of the data were explained by PC1 when smaller particles (MUC or MC) were used (Figure 6.7.d). As it was also shown in Figures 3 and 4, smaller MUC or MC particles (redispersed d_{90} of 7.38 and 4.14 µm, respectively) have better distribution especially at the surface of the film compared to larger, AR or ARC particles (d_{90} of 15.31 and 15.86 µm, respectively). This might have led to more repeatable NIR spectra acquisition.

All the NIR spectra-related analyses and discussions till this point were on the data taken while the film was moving on a belt at 0.16 cm/s. Since belt speed is one of the processing parameters, it was also examined to understand how it affects the NIR spectra of the films loaded with FNB. Figure 6.8 shows PCA scores of NIR spectra belonging to films loaded with 30% MC-FNB and with varying thicknesses where data were collected at two different belt speeds; 0.08 cm/s and 0.16 cm/s. PC1 explained 100% of the data. Figures 6.8.a and b present the same data but different grouping for better visualization. Different colors represent belt speed in Figure 6.8.a while Figure 6.8.b shows thickness grouping by colors. Less scattering of PCA scores was observed for higher belt speed, especially for thinner films. It may be due to faster movement of the film leading to more area coverage (increased sample size) during each NIR spectrum acquisition where 100 scans were averaged. Several studies are examining the effect of some of the processing

parameters in the spectral analysis leading to change in the sampling size [164, 171, 172]. Ortiz et al. showed that for an in-line NIR spectroscopy system on a tableting process, paddlewheel speed would affect the sampling size and middle speed generated more accurate predictions [171]. However, composite sampling is important for better representation of the material while eliminating the bias coming from the sampling procedure [173, 174]. The faster belt speed contributes to a larger composite sample.

PCA scores qualitatively demonstrated that particle size of FNB in the film and sampling size would potentially affect the thickness detection via NIR spectra. In addition, the coating agent did not interfere with the spectra thus multivariate analysis. Therefore, these results indicated that spectra of coated and uncoated FNB might be used in the same prediction model. This hypothesis is examined in the next section.

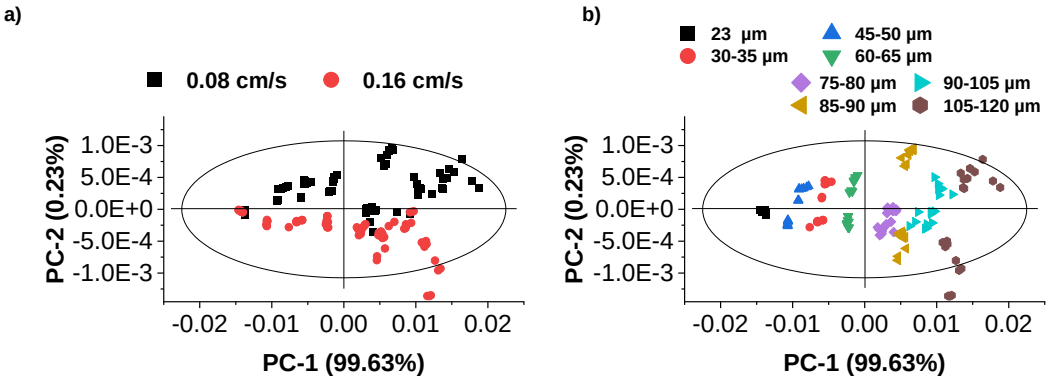

Figure 6.8 PCA score plots for NIR spectra belonging films loaded with 30% MC-FNB a) Belt speed grouping b) Dry film thickness grouping.

6.4.5 Development of the NIR calibration model and prediction

The predicted thicknesses using the developed models with optimized PLS factors as well as the measured thicknesses are presented in Table 6.4. All the models resulted in good predictions while predictions calculated using calibration model developed with all four formulations showed slightly higher differences compared to the measured value and other predictions in some cases. Overall, all the calibration models were able to predict the film thickness in a range of 23 – 124 µm. The effect of the dry coating was clearly seen on the calibration and prediction results by statistically improved models.

Statistics for all the calibration models, cross-validations, and predictions are presented for up to three PLS factors in Table 6.3. Considering lower RMSE, bias, the number of factors, and higher R^2, one PLS factor was selected as the optimized number of factors for each developed calibration model. The linearity of optimized calibration models where R^2 was found to be ≥ 0.99 for all the cases except for the model including all modification cases (Table 6.3). RMSE and bias for the prediction set were lower when micronization or dry coating was applied. As it was discussed via PCA scores in Section 3.4, the coating did not interfere with NIR data acquisition, it improved the uniformity of the films along with the reduced variation of NIR spectra belonging to the films loaded with micronized and/or dry coated FNB. This allowed to create better calibration models as sampling was improved [170].

Calibration models established using combined NIR spectra for same particle sizes (AR-ARC and MUC-MC) provided reasonable PLS statistics (Table

6.3) as well as comparable predictions to one type of FNB calibration (Table 6.4). Prediction results confirmed PCA results discussed in the previous section. PCA scores showed that the particle size would lead to differentiation in thickness detection while dry coating only improved the variation in the spectra (Figure 6.7).

Table 6.3 Statistics of PLS models for the Prediction of the Thickness (Films Loaded with 30 wt% FNB)

FNB in the Film	***Calibration***	***Cross-Validation***			***Prediction***	
	***RMSEC* (µm)**	***RMSECV* (µm)**	***Bias* (µm)**	***R^2***	***RMSEP* (µm)**	***Bias* (µm)**
AR	2.92	3.02	0.007	0.9899	4.06	-1.273
ARC	2.17	2.24	0.018	0.9930	2.23	-0.495
MUC	2.60	2.69	-0.011	0.9909	2.54	0.299
MC	2.24	2.28	-0.005	0.9944	2.17	-0.105
AR - ARC	2.62	2.66	0.005	0.9912	3.36	-0.864
MUC - MC	3.40	3.43	0.004	0.9861	3.21	0.096
ALL	4.31	4.33	0.001	0.9774	4.32	-0.314

In the case where all the data used in the calibration, RMSEs were higher than other models, and linearity was reduced (R^2 of 0.977) while comparable bias was obtained. Predicted thicknesses from the calibration curve including all four types of FNB deviated from measured thicknesses while predictions from one type FNB calibration curve were much closer to measured (Table 6.4).

Developed PLS models quantitatively demonstrated that the thickness of a film loaded with coated or uncoated FNB, in a d_{50} range of 2.5 to 6 µm, can be detected via inline NIR measurements. However, separate calibration models

were needed to be developed for FNB in different particle sizes loaded films. In addition, the coating agent did not adversely affect NIR acquisition and allowed usage of coated and uncoated FNB in the same calibration model with good prediction.

Table 6.4 Thickness Predictions using Selected PLS Models for Corresponding API(s) in the Film

Number of FNB types used in Calibration:		**One**	**Two**	**All types (4)**
Formulation	**Reference Film Thickness (µm) ± SD**	**Predicted Film Thickness (µm) ± SD**	**Predicted Film Thickness (µm) ± SD**	**Predicted Film Thickness (µm) ± SD**
AR	36.1 ± 0.9	35.8 ± 0.2	35.1 ± 0.2	29.8 ± 0.2
	42.5 ± 1	46.6 ± 0	46 ± 0	41.6 ± 0.1
	53.6 ± 1.2	52.4 ± 0.1	51.8 ± 0.1	48 ± 0.1
	60.5 ± 1.2	60.6 ± 1.2	60.1 ± 1.2	56.9 ± 1.3
	64.0 ± 1.6	64.7 ± 2.7	64.3 ± 2.7	61.4 ± 2.9
	79.9 ± 1.5	75.8 ± 0.1	75.5 ± 0.2	73.5 ± 0.2
	94.6 ± 2.5	98.3 ± 1.2	98.2 ± 1.2	98.1 ± 1.3
	99.8 ± 2	95.9 ± 0.3	95.8 ± 0.3	95.5 ± 0.4
	105.9 ± 2.8	103.2 ± 2.3	103.1 ± 2.3	103.4 ± 2.5
	124.1 ± 6.7	118.2 ± 7.6	118.2 ± 7.6	119.7 ± 8.3
ARC	35.0 ± 1.4	35.5 ± 0.4	36.5 ± 0.4	31.4 ± 0.4
	48.5 ± 2.5	49.1 ± 0.4	49.8 ± 0.4	45.8 ± 0.5
	53.4 ± 1.3	56.4 ± 0.2	57 ± 0.2	53.6 ± 0.3
	58.8 ± 2.3	58 ± 0.1	58.6 ± 0.1	55.3 ± 0.1
	70.2 ± 1.5	70.3 ± 0.2	70.7 ± 0.2	68.4 ± 0.2
	87.2 ± 3.6	86.4 ± 0.4	86.6 ± 0.4	85.6 ± 0.4
	93.8 ± 3.0	92.1 ± 0.4	92.2 ± 0.4	91.6 ± 0.5
	95.8 ± 2.2	92.1 ± 2	92.2 ± 2	91.6 ± 2.1
	104.7 ± 3.3	106 ± 0.9	105.9 ± 0.9	106.4 ± 0.9
	117.1 ± 3.7	113.3 ± 2.3	113.1 ± 2.2	114.2 ± 2.4

Table 6.4 (Continued): Thickness predictions using selected PLS models for corresponding API(s) in the film

Number of FNB types used in Calibration:	**One**	**Two**	**All types (4)**
Formulation	**Reference Film Thickness (µm) ± SD**	**Predicted Film Thickness (µm) ± SD**	**Predicted Film Thickness (µm) ± SD**	**Predicted Film Thickness (µm) ± SD**
MUC	26.9 ± 1	26.7 ± 0.2	24.3 ± 0.2	30.1 ± 0.2
	42.0 ± 1	40.2 ± 1.2	37.7 ± 1.2	42.4 ± 1.1
	45.5 ± 0.9	46 ± 1	43.6 ± 1	47.8 ± 0.9
	51.9 ± 0.9	52.3 ± 0.8	49.9 ± 0.9	53.5 ± 0.8
	62.0 ± 0.7	64.1 ± 0.4	61.7 ± 0.4	64.3 ± 0.4
	80.2 ± 0.9	82.5 ± 1.5	80.1 ± 1.5	81.1 ± 1.4
	80.3 ± 1.2	85.3 ± 1	83 ± 1	83.7 ± 0.9
	89.2 ± 0.8	85.8 ± 2	83.5 ± 2	84.2 ± 1.8
	100.1 ± 1.7	97.9 ± 0.7	95.6 ± 0.7	95.3 ± 0.7
	112.6 ± 2.2	112.7 ± 1.1	110.4 ± 1.2	108.8 ± 1.1
MC	23.3 ± 0.5	21.1 ± 0.5	23.8 ± 0.5	29.7 ± 0.5
	33.6 ± 1	34 ± 0.1	36.6 ± 0.1	41.3 ± 0.1
	47.4 ± 2.5	49.1 ± 1.5	51.6 ± 1.5	55 ± 1.4
	50.7 ± 0.5	50.9 ± 0.3	53.3 ± 0.3	56.7 ± 0.3
	62.9 ± 1.2	62.5 ± 0.3	64.9 ± 0.3	67.2 ± 0.3
	77.3 ± 0.9	79.6 ± 0.9	81.9 ± 0.9	82.8 ± 0.8
	80.8 ± 1.1	82.3 ± 1	84.6 ± 1	85.2 ± 0.9
	87.0 ± 0.8	87.7 ± 2.3	90 ± 2.3	90.1 ± 2.1
	100.5 ± 3.7	99.8 ± 1.5	102 ± 1.5	101.1 ± 1.4
	112.2 ± 3.2	108.8 ± 2.8	110.9 ± 2.8	109.2 ± 2.5

6.5 Conclusions

NIR spectroscopy as a PAT tool for monitoring the strip film manufacturing process was successfully applied for in-line quantification of film thickness. PCA was able to explain major contributions to the models, i.e., micronization, and dry coating. The effects of the micronization and dry coating of the API on the detection of the thickness were explained qualitatively and quantitatively. PCA analysis showed that modification of the API (micronization and dry coating) had no adverse effect on the NIR spectra of the films with varying thicknesses. Indeed, modification of API resulted in better uniformity (content and thickness) of the film leading to a better correlation between thickness and spectra. PLS models were developed by varying film thicknesses and R^2 was found to be ≥ 0.99 for individually investigated cases while modification of the API enabled either usage of fewer factors in the model, or lower RMSE or bias. Overall, it was shown that engineered particles led to uniform films enabling better chemometric analysis.

CHAPTER 7

OVERALL CONCLUSIONS AND FUTURE WORK

7.1 Conclusions

The overall objective of this dissertation was to provide fundamental knowledge towards a general design space on the path toward QbD with the specific objectives as outlined in Chapter 1.3. As part of the context of designed objectives, various formulation and process parameters were investigated in terms of relevant CQAs where CMA and CPP were identified.

The first major topic of investigation was regarding the combined effect of solvent, and cellulosic polymer on the pharmaceutical film quality attributes revealed the recrystallization problem and understanding the impact of the film structure on the dissolution rate. It was demonstrated that solvent not only affected the crystallinity but also affected the film structure due to the amount of solubilized drug and the conformation of the polymer chains in the analyzed solvent. Such combined effect of solvent on polymer and drug could lead to decreased dissolution rate with similar supersaturation capability for the crystal-free fresh films prepared with different solvents. It should be noted that the drug loading will be still limited due to the low solubility of the drug as well as the unstable nature of the amorphous drug. To have a significant advantage in dissolution rate with amorphous formulation over other bioavailability enhancement techniques, i.e., milled drug, the drug loading should be kept 10% or lower. Otherwise,

recrystallization in the product as well as during dissolution overcomes the increased solubility advantage of amorphous. This phenomenon led to films loaded with the crystalline drug having increased surface area (d_{50} of 3 µm) catching up with the amorphous drug-loaded films at 20 wt% drug loading in terms of dissolution rate and outperform at higher drug loadings (≥ 30 wt%).

An alternative solution for recrystallinity issues was proposed as a polymer coating of the top region which in turn would enhance the supersaturation capability. On the other hand, this extra layer slowed down the dissolution rate where a thickness optimization would be required.

In another bioavailability enhancement technique, slurry casting, the effect of particle size and drug loading on CQAs of the film was investigated. As particle size decreased, the increased total surface area of the drug enhanced the dissolution rate of a suspension containing drug particles. However, a similar trend between particle size and dissolution rate was not observed when a polymeric matrix was in question. As an important contribution to formulation development, it was proven that there is an optimum particle size for certain drug loadings. The smallest particle size did not result in the fastest dissolution for each drug loading due to the change in the matrix, i.e., low interparticle distance and enhanced mechanical properties.

Considering the findings from Chapters 2-4 together, it may be presumed that for the drug loadings 10% or lower, solution casting may be a better option while slurry casting with nano-sized particles may be used up to 20%. Also, at

higher drug loadings micronized-coated particles may be recommended for faster dissolution of poorly water-soluble drugs.

Drying was investigated as an important process step in terms of kinetics as well as the final product quality. It was shown that analysis of drying kinetics alone might not identify the failure modes. The drying kinetics analysis was combined with the identification of critical quality attributes affected by different drying modes and strengths. While the mechanical properties of the films did not vary among varying drying conditions, the crystallinity of the drug in the film was found to be strongly affected by film surface temperature during drying. In fact, the film surface temperature was found to be the most important criteria to design the drying process followed by the drying rate.

Finally, Near-IR Spectroscopy (NIRS) was found to be a useful tool to detect one of the most important product quality attributes for films, thickness. The utilization of NIRS not only helped to predict the thickness but also provided a better understanding of the effect of the particle modification, i.e., micronization and coating, on the thickness of the film.

Overall, this dissertation offered enhanced knowledge on solution and slurry casting techniques to link material properties with the performance of the product. Through the knowledge obtained from these studies, it is hoped that improved identification of design space including processing conditions for poorly water-soluble drug-loaded pharmaceutical film preparation methods may be developed towards implementing Quality by Design (QbD) into pharmaceutical film manufacturing.

7.2 Future Work

In Chapters 2 and 3, the critical importance of recrystallization was demonstrated by its adverse effect on the CQAs. Another polymer layer was shown to be preventing the initial crystallinity right after preparation. However, the long-term consequences of this solution should be further assessed as it was shown that low initial crystallinity does not guarantee better stability.

Another important part is to detect and control the product quality. Chapter 6 demonstrated the utilizing NIR for thickness detection for dry films. As the further steps, performing the thickness analysis right after the casting stage and in the middle of the process might save time and decrease the costs caused by waste by intervening in the process earlier in case of a failure. At an earlier stage, the water content will be different leading to changes in the spectra. In the relatively scarce literature, Hifumi et al.[175] and Kimber et al. [176] analyzed the drying process of films using off-line spectroscopic techniques mostly focusing on the mechanism. However, there is not any study showing an in-line analysis of the drug-loaded film thickness via spectroscopic techniques while moisture content is also changing simultaneously. In addition, determining the water content would allow better control over the process and another CQA i.e., residual water content.

In the context of this dissertation, CMAs and CPPs were investigated through CQAs of the films. However, there is also a gap in standardized characterization methods for pharmaceutical films. Most of the studies in the literature implement the dissolution techniques established for tablets to films. Aside from this, most of these methods implement sink conditions that use much

higher volume than the saliva in the mouth and most dissolution media are not related to bodily fluids. These misleading testing apparatus results in misinterpretation of the results and eventually makes the fair comparison between the studies quite difficult. In general, overestimation in the release kinetics and consequently underestimation in the complete drug release are some of the aforementioned misleading conclusions. These questionable behaviors should be addressed to result from the high volume or high agitation conditions in the testing methodologies. More importantly, dissolution testing under non-sink conditions should be investigated for film dosages. In the literature, a few studies used non-sink conditions for pharmaceutical films, even though it is a necessity for the amorphous drug-containing dosages [177, 178]. In Chapter 2, a dissolution test used under non-sink conditions was adapted from tablet testing. Even though the method used was appropriate for analyzing the supersaturation capabilities, it should be further evaluated to verify its discriminative potential for all related parameters such as thickness and drug loading. As FDA indicated, the dissolution tests used to evaluate any dosage forms should be developed to simulate the *in-vivo* behaviors [38]. For that matter, while developing such a method itself is important and challenging, it should be verified to be *in-vivo* related. While verifying the method, introducing *in vitro – in vivo* correlation (IVIVC) may help to decrease the need for *in-vivo* experiments on humans especially when these experiments are limited to specific patient groups i.e., pediatric patients. Many IVIVC methods can be found for tablets in the literature [179-182]. However, it is very limited for film dosages with very poor correlation [183].

APPENDIX A

SOLUTION CAST FILM PREPARATION

Ethanol (EtOH) was chosen as one of the solvents to examine since it is mostly used as a safe solvent for food and drug products. Methanol (MeOH) was another solvent considered. The model poorly-water soluble drug, fenofibrate (FNB), has similar solubilities in EtOH and MeOH. This allowed for examining solvents with similar solubilization effects on API but having different physical properties i.e., boiling point. In addition, acetone (Ace) and dichloromethane (DCM) were selected due to the higher solubility of FNB in them. The usage of DCM in pharmaceutical products should be limited according to FDA guidance for industry [70]. However, its alcoholic mixture is a good solvent for the polymers used, HPMC and HPC, as well as the drug, FNB. This allowed for preparing one of the formulations without any water in the solvent system, DCM:EtOH mixture, hence it was selected for research purpose.

HPMC is not soluble in pure organic solvents used in this study while it is in water-alcohol mixtures as well as DCM–alcohol mixtures [64]. HPC is soluble in pure organic solvents used in this study and DCM-alcohol mixtures. In order to keep the solvent same for both polymers as comparison, binary organic solvent mixture including water was used for both HPMC and HPC. First, a preliminary study was conducted to set the water/organic solvent (w:os) ratio with minimum water amount for preparation of the polymer solution a binary solvent. This part of the study was carried with HPMC since HPC is soluble in these organic solvents with or without water. Minimum water amount in the solvent mixture would allow

for maximizing FNB solubility while dissolving the HPMC. FNB loaded precursors (corresponding to 10% dug loading in the film) were prepared using ratios of 1:1, 1:2 and 1:4 of water:acetone (w:Ace) and water:ethanol (w:EtOH) solvent mixtures. The crystallinities of the film precursor solutions were analyzed via an optical microscope under the polarized light in the back-lighting mode (Figure A.1). Only 1:4 (w:os) mixture resulted in fully dissolved drug particles in the polymer solution for both acetone and ethanol. Consequently, 1:4 (w:os) ratio was chosen for further study. This ratio also worked for the second film former, HPC-L, and was used for all HPC-L formulations, which was expected since HPC-L is soluble in water also. In summary, in order to analyze solvent effects on different polymers, four solvent mixtures were used for HPMC formulations while two were selected for HPC formulations, of which one solvent mixture from lower solubility end (water-ethanol) and one from higher solubility end (water-acetone). The solubility of FNB in all these solvents and mixtures are listed in Table 2.1.

For the cellulosic polymer-based film-precursor formulation, Zhang et al. [30] suggested using 12% HPMC E15 (wt%) and 4% glycerin for a low viscosity aqueous polymer solution. However, 12% HPMC E15 solution in 1:4 (water:acetone) resulted in gelation (results are not shown). However, a slightly decreased amount of 10% (wt%) worked well, and correspondingly, the glycerin amount was decreased to 3.3% (wt%) to keep the plasticizer to polymer ratio the same (1:3). For HPC-L solutions, the polymer amount had to be doubled to 20 wt% because the viscosity of HPC-L (6-10 *cP*) is about half of HPMC E15 (12-18 *cP*). This was necessary because viscosity could have an impact on uniformity of the

films and it is better to keep it the same for both the polymers [30, 74]. Regarding the plasticizer to polymer ratio, when kept the same as HPMC formulations (1:3), HPC-L films were not peelable. It was found that to get peelable and non-sticky HPC-L films (prepared with organic solvents), the plasticizer amount had to be reduced, and the plasticizer to polymer ratio was 1:20.

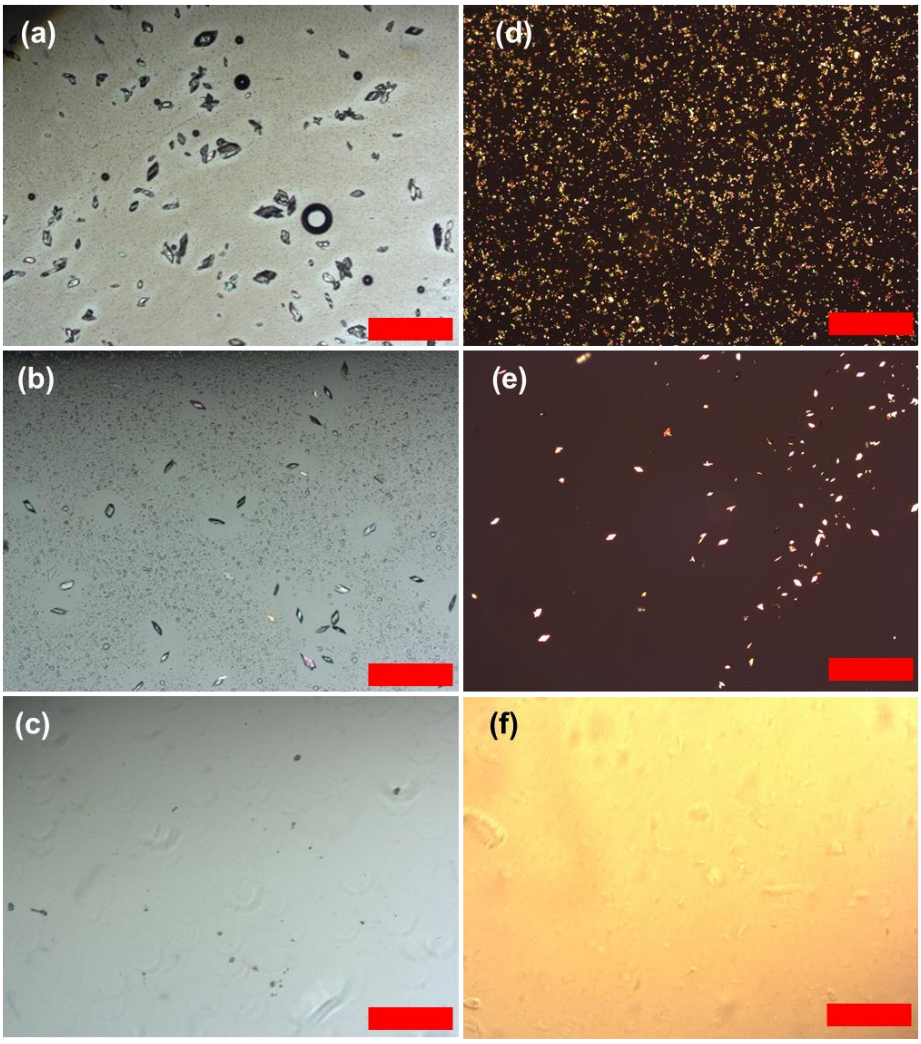

Figure A.1 Optical images of 10% FNB (in dry film) loaded HPMC precursors prepared with 1:1 (a and d), 1:2 (b and e), and 1:4 (c and f) ratios of w:Ace (a, b, and c) w:EtOH (d, e, and f) solvent mixtures. Scale bars on the images represents 400 µm.

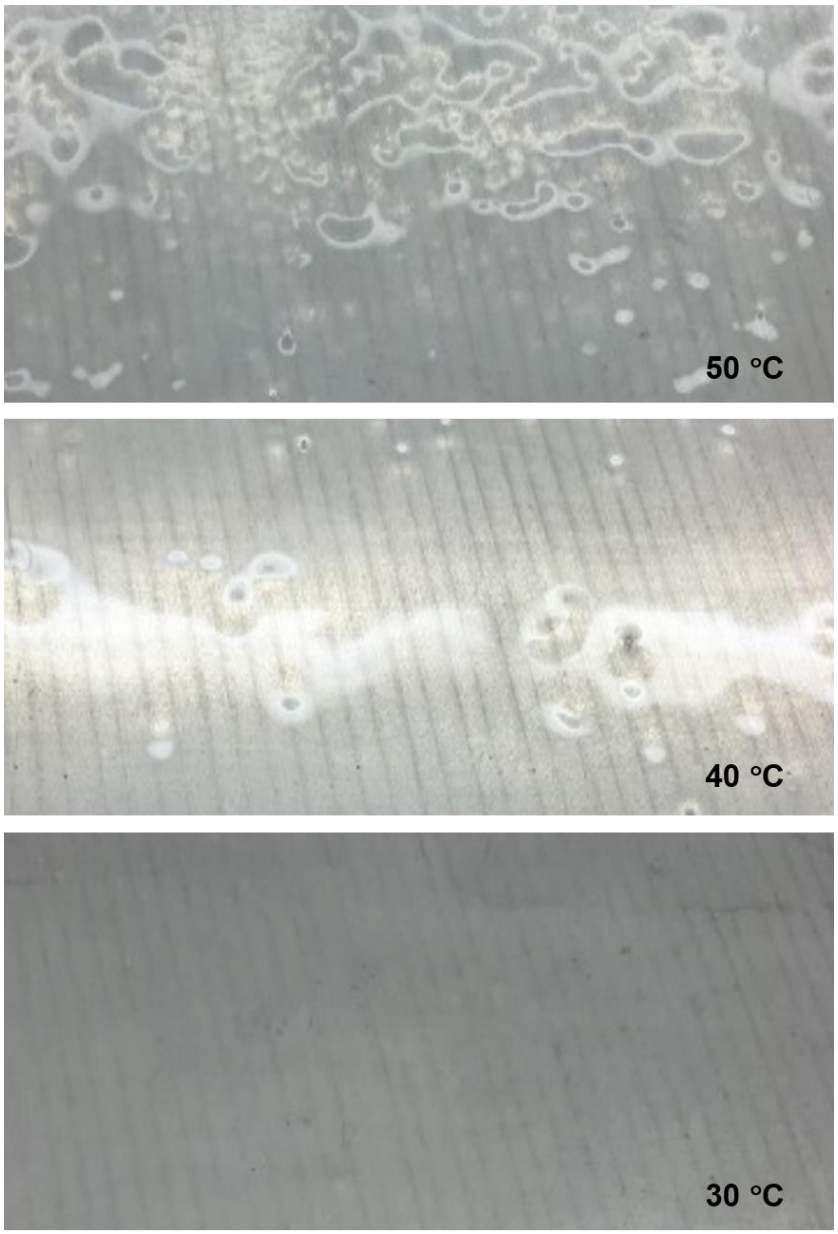

Figure A.2 Drying of the HPMC films made with 1:4 (water:ethanol) at different temperatures.

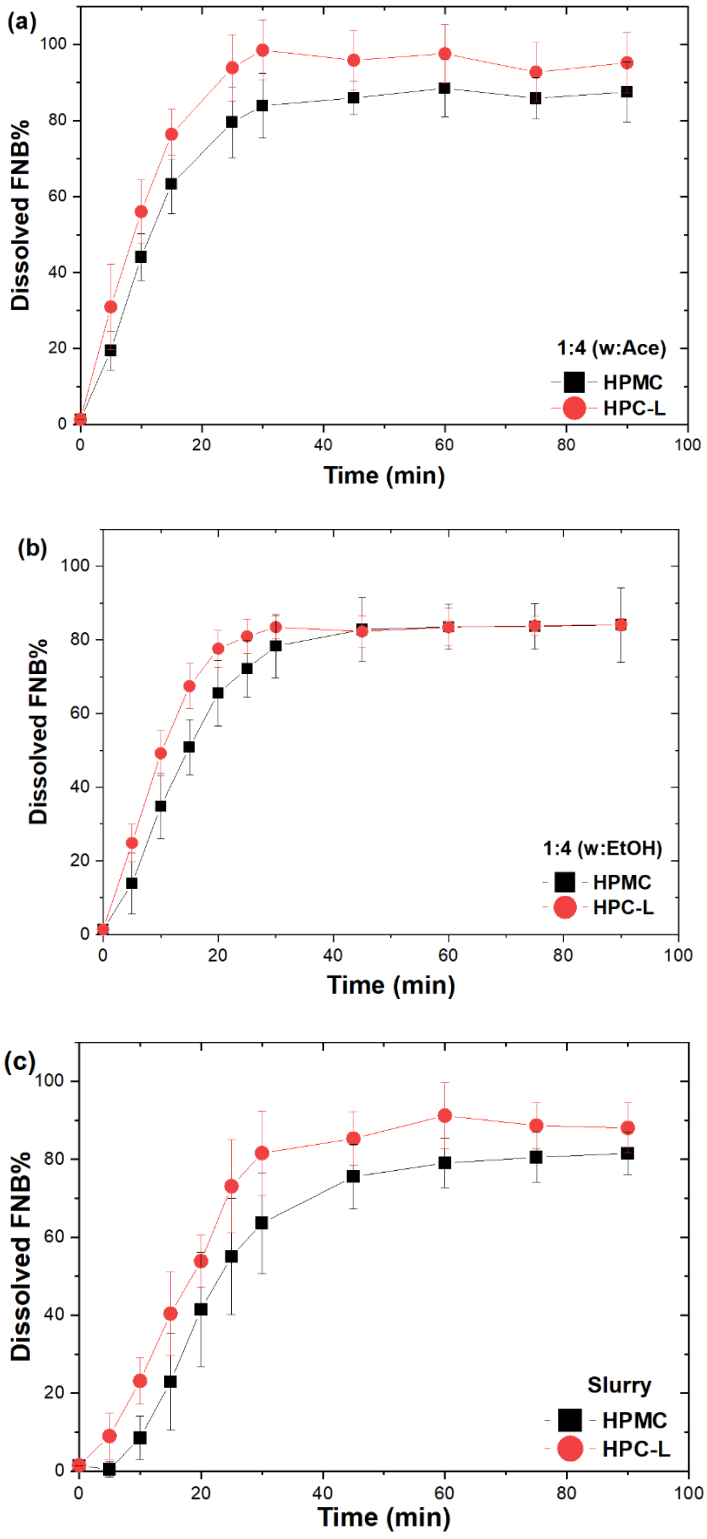

Figure A.3 Dissolution profiles under sink conditions - 10 % FNB loaded solution casting films made of HPMC and HPC-L (a) 1:4 (w:Ace), (b) 1:4 (w:EtOH), and (c) Slurry.

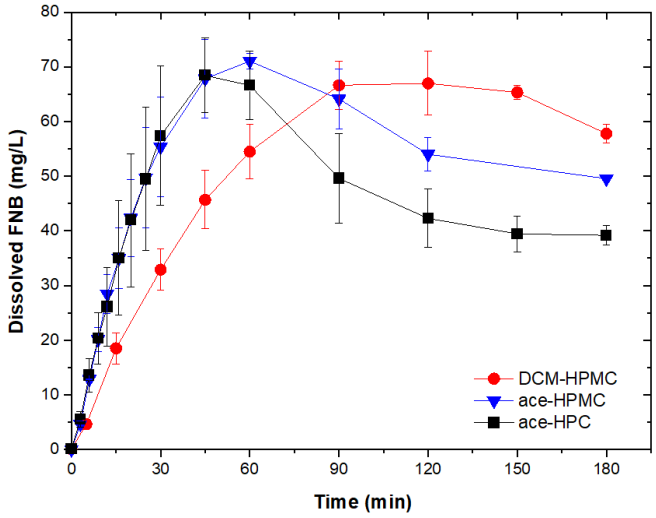

Figure A.4 Dissolution profiles under non-sink conditions for 10% FNB loaded solution casting films made of HPMC and HPC-L.

Table A.1 Statistical Analysis of Dissolution Profiles of HPMC Films under Sink Conditions

Ace-HPMC	f_2*	41.34			
	f_2*	40.85			
EtOH-HPMC	f_2*	43.08	57.77		
	f_2*	43.85	59.76		
MeOH-HPMC	f_2*	35.51	27.15	27.59	
	f_2*	35.35	27.38	27.97	
Slurry-HPMC	f_2*	60.52	38.84	40.29	34.43
	f_2*	61.06	39.73	40.69	34.57
		DCM-HPMC	**Ace-HPMC**	**EtOH-HPMC**	**MeOH-HPMC**

***f*₂*:** Bootstrap similarity factor

Table A.2 Statistical Analysis of Dissolution Profiles of HPC Films under Sink Conditions

Ace-HPMC	f_1	43	
	f_1	76	
	f_2	30	
EtOH-HPMC	f_1	34	16
	f_1	52	13
	f_2	37	54
		Slurry-HPMC	**Ace-HPMC**

***f*₁:** Difference factor
***f*₂:** Similarity factor

APPENDIX B

PREVENTION OF RE-CRYSTALLIZATION VIA BI-LAYER FILMS

B.1 Material and Methods

Film Preparation

Hydroxypropyl methyl cellulose (HPMC) solution for the drug loaded layer was prepared via previously established methods [29, 96]. Briefly, the required water-solvent mixture (1 to 4 ratio of water-ethanol) was heated up to 30 °C while stirring and the plasticizer (glycerin) was added. The solutions were continued to be heated up to 40–45 °C. Then, the polymer powder was added to the mixture slowly and the final solutions were cooled down to room temperature. The HPMC solution had 10 wt% HPMC, 3.3 wt% plasticizer and the rest was 1:4 (water: ethanol). The polymer solutions were also prepared using same technique except for plasticizer addition.

Polymer solution was mixed with FNB to obtain 10 wt% drug loading in the dry film using a planetary centrifugal mixer (Thinky Model ARE-310). Mixing was performed for 10 min at 2000 rpm and followed by defoaming for 2 min at 2200 rpm.

Precursor solution was cast onto a plastic substrate (Scotchpak TM 9744, 3M, MN, USA) with a doctor blade (Elcometer, Rochester Hills, MI) using a Lab-Cast Model TC-LC Tape Caster (HED International, Ringoes, NJ). Using a oil-sprayer bottle, polymer solution were sprayed on top of wet film loaded with FNB. Varying thicknesses were ensured by spraying different amounts of polymer solution per area. The films were dried at room temperature overnight. Following

the drying, films were peeled and stored in plastic bags until further analysis. More details on the selection of process parameters for mixing or drying can be found in [96].

Viscosity

The apparent shear viscosity of film precursor suspensions was tested with an R/S-CC+ Coaxial Cylinder Rheometer (Brookfield Engineering, Middleboro, MA, USA) combined with a shear rate controlled coaxial cylinder (CC25) and Lauda Eco water jacket assembly (Lauda-Brinkmann LP, Delran, NJ, USA) for temperature control. The viscosity of each polymer solution was recorded at shear rate of 1000 s^{-1} at 35 ± 0.5 °C. The test was performed with three replicates for each solution.

Raman Spectroscopy

Raman spectroscopy is measured with a Fergie Raman (Princeton Instruments) equipped with a fiber optic probe (785 nm laser, 475 mW). The spectral range was selected as 800 - 1720 cm^{-1}. In all cases, 1 scan is done with an acquisition time of 45 s.

Morphology of drug loaded films

The cross-section of films loaded with the drug was analyzed using an optical microscope with polarization mode (Carl Zeiss Microscopy, LLC. Germany). Film samples were cut into thin pieces and fixed onto a glass slide with the help of double-sided tape. Images were taken as representative of the sample.

Crystallinity of fenofibrate in the film

The crystallinity of fenofibrate in the film was analyzed using a differential scanning calorimeter (DSC, Mettler Toledo, Inc., Columbus, OH). An aluminum standard pan loaded with ~8 mg of the film was heated from 25 °C to 120 °C at a constant heating rate of 10 °C/min under a nitrogen flow and cooled down to 25 °C.

Fourier-transform infrared spectroscopy (FTIR)

FTIR spectra were measured for each film as well as pure as received drug powders and placebo films containing no drug using a Fourier transform infrared spectrometer (Agilent Cary 620) with an attached Attenuated Total Reflectance (ATR) accessory and a single reflection Diamond crystal. Samples were measured within the range from 400 to 4000 cm^{-1}. The spectral resolution of FTIR spectra was set to 4 cm^{-1}. Reported final spectra are an average of 32 scans.

Content uniformity

The uniformity of the dried films was analyzed in terms of content, i.e., drug loading and drug amount per area, and thickness via relative standard deviations. For each formulation randomly selected ten circular punches, ~0.7 cm^2 area, were dissolved in 20 mL of 7.2 g/L sodium dodecyl sulfate (SDS) solution following mass and thickness measurements. It should be noted that the small sample size used for the uniformity testing, which was about $1/10^{th}$ of the intended dosage size (2 cm x 3 cm), was for better discrimination between samples [27, 30]. The absorbance of each solution was measured via a UV-vis spectrophotometer (Thermo Fisher Scientific Inc., MA, USA) at the maximum wavelength for FNB (290 nm) and concentrations were calculated using a pre-prepared calibration curve. Relative standard deviations (RSD, average value divided by standard deviation) for drug

amount per area and drug loading% (FNB weight with respect to total weight) were calculated and reported.

Dissolution under non-sink conditions

Dissolution studies for non-sink conditions were conducted in USP II (Sotax, Switzerland). The procedure was adapted from an early study on the paddle method under sink conditions [75]. Experiments were conducted at 37 °C and paddles were rotated at 50 rpm. 500 mL of 3.6 g/L SDS solution was used as dissolution media. Film samples (amount corresponds to 100 mg FNB) were introduced to dissolution vessel in a sinker to prevent any floating sample and sticking of the sample to the vessel. Samples were taken at predetermined time intervals and replaced with the same amount of fresh medium. Taken samples were filtered using a syringe filter (pore size of 0.2 µm). After adequate dilutions, absorbances of the solutions were measured using UV-vis Spectroscopy. The dissolution results are reported as the concentration of FNB dissolved (mg/L) with respect to time. The supersaturation capability is characterized by calculating the area under the curve (AUC) for all dissolution curves.

B.2 Results and Discussion

Viscosity

The polymer concentration for top layer coating solutions was adjusted to be 10% for HPC-L and 5 % for HPMC, as the half of the polymer concentration of drug loaded layer to have sprayable solution. However, 10% solid concentration in the solution led fiber formation during the spraying. Similar behavior had been reported for spray drying processes in the literature (ref). Therefore, the polymer concentration for HPC-L solution was reduced to be 8 wt%. Since HPMC is

insoluble in pure organic solutions, a water-solvent mixture had to be used while HPC solutions were prepared both in pure organic solvent and water-organic solvent mixtures. The viscosities of polymer solutions are presented in Table B.1.

Table B.1 Viscosity of Polymer Solutions Used as A Second Layer

Name	**Viscosity *(cP)***
8% HPC in ace	59.6 ± 1.9
8% HPC in etOH	102.5 ± 0.5
5% HPC in etOH	15.8 ± 0.4
5% HPC in 1:4 (etOH)	32.2 ± 0.1
5% HPMC in 1:4 (etOH)	125.2 ± 1
5% HPMC in 1:4 (ace)	59.8 ± 1.4

Raman Spectroscopy

The drug loaded film without polymer layer on top was analyzed through Raman Spectroscopy to assess the solid-state change during the drying. The wavelength range of 1110 – 1205 cm^{-1} was analyzed for any solid-state changes of fenofibrate (FNB) since a strong peak for crystalline FNB was reported at 1148 cm^{-1} [164]. The second derivative of spectra were reported for better visualization (Figure B.1). Timely measurements showed that the peak corresponds to FNB shifts from 1158 cm^{-1} towards 1148 cm^{-1} but did not reach the 1148 cm^{-1}. The wavenumber shift indicated that a crystallization occurred during drying but FNB was not fully recrystallized and resulted in partially amorphous film. At the same time intensity of the peak was also increased since the concentration of FNB was increased during drying due to solvent evaporation.

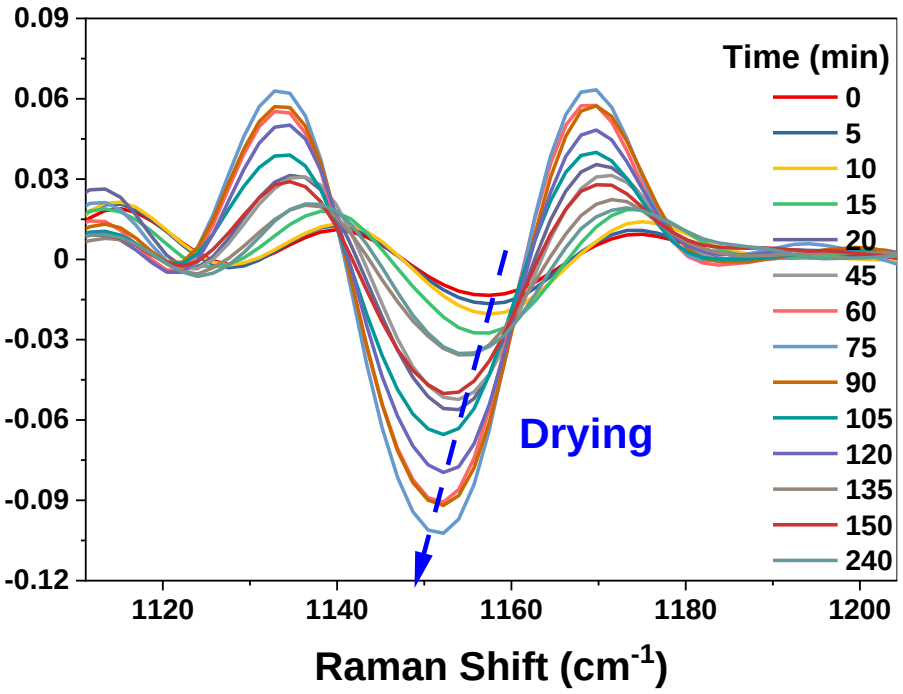

Figure B.1 The 2nd derivative of Raman spectra during drying of the film

Crystallinity of films loaded with drug

The cross-sections of the dried films were analyzed using polarized light microscopy (Figure B.2). The images revealed that the crystalline AR-FNB particles were uniformly distributed in the film (Figure B.2.a) while the recrystallized were mostly found on the top surface of solution cast film (Figure B.2.b). Coating prior to drying of 10% FNB loaded solution cast film led to much clear film (Figure B.2.c).

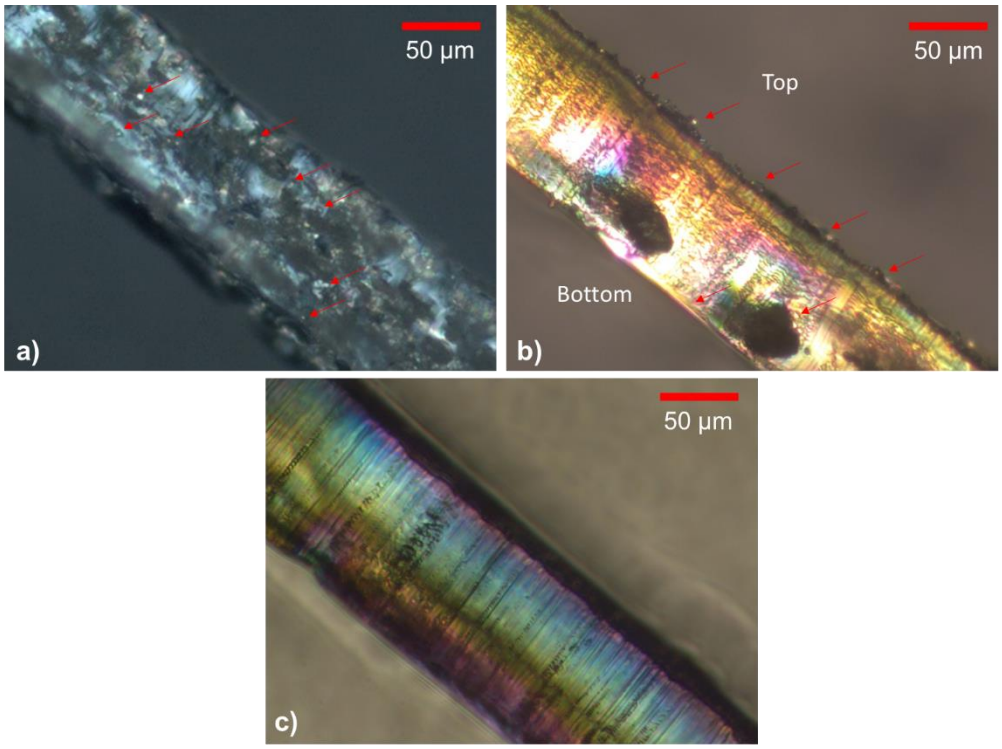

Figure B.2 Optical images of cross-section of the films loaded with FNB a) Slurry b) Uncoated Solution film c) Coated Solution film.

The FTIR spectra of all the films loaded with 10% FNB prepared via slurry or solution casting and the pure FNB powder are shown in Figure B.3. Spectra for top and bottom of the solution film (10% FNB – 1:4 (water: etOH)) were different from each other. Spectra belonging to Slurry film and bottom of Solution film had a broad peak around 1050 cm^{-1} corresponding to the polymer while it was lost for top of the Solution film. The peak for polymer was suppressed by the peaks for crystalline FNB. In fact, spectrum for bottom of Solution film had the most distinctive crystalline FNB peaks as it was in pure FNB powder. However, the Slurry film does not have all the peaks with similar pronounced intensity even though the drug is crystalline in the film. Since the recrystallization was on the surface of the solution film the FNB peaks were more pronounced due to low

penetration depth. However, the drug was embedded in the polymer matrix for slurry cast films leading more diluted FNB detection by FTIR.

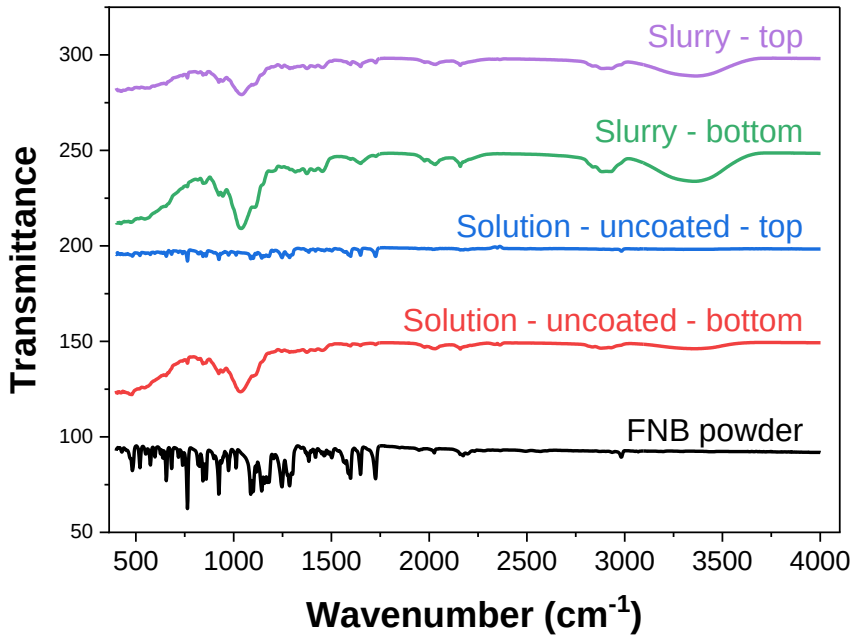

Figure B.3 Particle size distribution of re-dispersed particles from dry films with varying drug loadings and different preparation methods.

Table B.2 DSC Thermograms of Coated and Uncoated Films

Formulation	***Recrystallization %***
Uncoated	58.7 ± 5.3
Coated - 8% HPC in ace-1	6.6 ± 1.5
Coated - 8% HPC in ace-2	ND
Coated - 8% HPC in ace-3	ND
Coated - 8% HPC in etOH	3.4 ± 0.7
Coated - 8% HPC in etOH-2	ND
Coated - 5% HPC in 1:4 (etOH)	33 ± 14.3
Coated - 5% HPMC in 1:4 (etOH)	25.4 ± 1.1
Coated - 5% HPMC in 1:4 (ace)	49.9 ± 3.7

Content uniformity

The uniformity of the films was analyzed in terms of relative standard deviation (RSD) of drug loading and drug amount per area (Table B.3). In terms of drug loading, all the films were uniform (RSD<6%). As it was demonstrated on both solution and slurry casting formulations, adequate viscosity and mixing would lead good content uniformity regardless of solid-state, particle size and recrystallization [30, 96].

Table B.3 Drug Content Uniformity of Uncoated and Coated Films

Names	***RSD of drug amount per area***	***RSD of drug loading***	***Drug loading %***
Uncoated	6.3	1.4	10.2 ± 0.1
Coated - 8% HPC in ace-1	5.2	3.6	7.7 ± 0.3
Coated - 8% HPC in ace-2	3.8	5.1	7.6 ± 0.4
Coated - 8% HPC in ace-3	7.9	4.3	6.3 ± 0.3
Coated - 8% HPC in etOH	6.6	2.0	7.3 ± 0.1
Coated - 8% HPC in etOH-2	8.9	3.2	5.7 ± 0.2
Coated - 5% HPC in 1:4 (etOH)	22.7	2.4	8.5 ± 0.2
Coated - 5% HPMC in 1:4 (etOH)	17.0	3.7	8.1 ± 0.3
Coated - 5% HPMC in 1:4 (ace)	8.8	1.3	8.1 ± 0.1

Dissolution

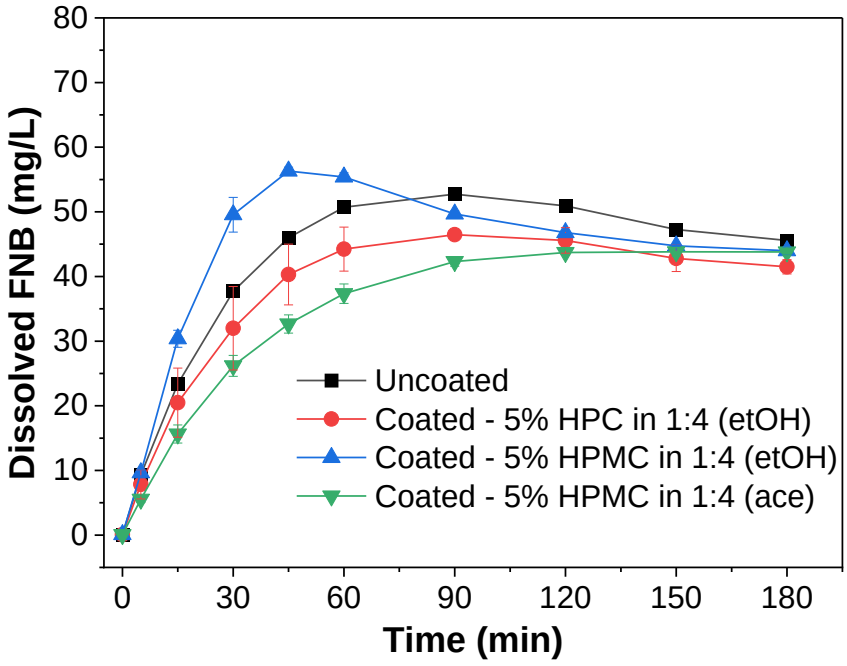

Figure B.4 Dissolution profiles under non-sink conditions for 10% FNB loaded films coated with 5% polymer solution.

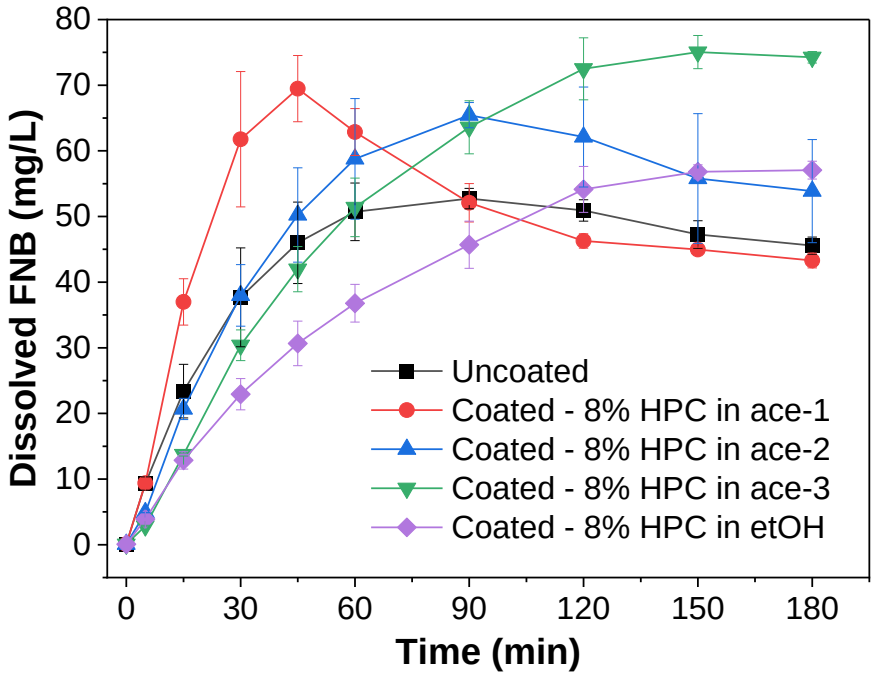

Figure B.5 Dissolution profiles under non-sink conditions for 10% FNB loaded films coated with 8% polymer solution.

B.3 Conclusions

Solution casting of FNB was investigated in terms of recrystallization issues during manufacturing. It was demonstrated that recrystallization started during drying and was mostly on the surface of the film. Another polymer layer coating on FNB loaded wet film was found to be preventing depending on the thickness. Prevented crystallization provided higher supersaturation extent while decreased the dissolution rate due to thicker film structure. Overall, supersaturation capability (AUC) was found to be improved even with slowed dissolution rate.

APPENDIX C

SOLUTION VS SLURRY CASTING

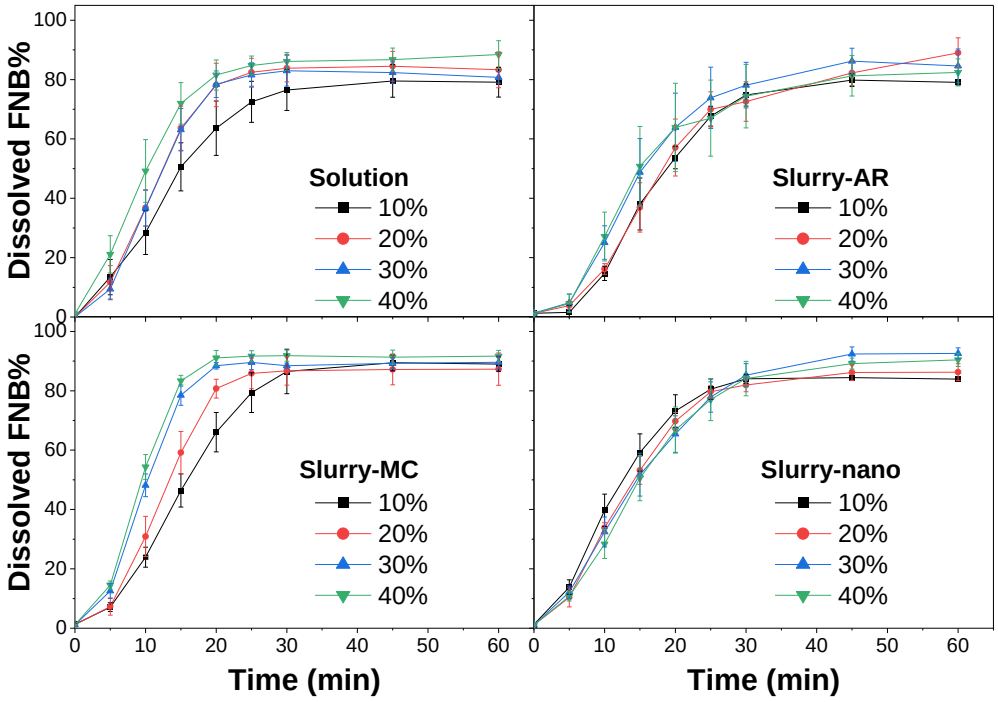

Figure C.1 Dissolution profiles of films prepared with different methods loaded with varying drug loadings, 10%, 20%, 30% and 40% FNB.

Table C.1 Statistical Analysis of Dissolution Profiles of Films Loaded with FNB at Varying Drug Loadings

Solution	f_2*	40.41		
	f_2*	40.71		
Slurry-AR	f_2*	30.86	37.22	
	f_2*	30.81	36.9	
Slurry-MC	f_2*	40.02	48.47	43.73
	f_2*	39.77	49.65	42.87
10% Drug loading		**Slurry-nano**	**Solution**	**Slurry-AR**
Solution	f_2*	45.17		
	f_2*	45.47		
Slurry-AR	f_2*	37.4	28.32	
	f_2*	37.92	27.84	
Slurry-MC	f_2*	53.77	43.57	33.16
	f_2*	53.8	42.37	32.78
20% Drug loading		**Slurry-nano**	**Solution**	**Slurry-AR**
Solution	f_2*	41.88		
	f_2*	43.11		
Slurry-AR	f_2*	43.18	33.81	
	f_2*	42.94	33.99	
Slurry-MC	f_2*	31.6	40.65	25.93
	f_2*	31.38	41.25	26.25
30% Drug loading		**Slurry-nano**	**Solution**	**Slurry-AR**
Solution	f_2*	30.53		
	f_2*	30.83		
Slurry-AR	f_2*	46.43	25.63	
	f_2*	46.45	25.67	
Slurry-MC	f_2*	28.37	43.84	23.78
	f_2*	28.4	43.56	22.91
40% Drug loading		**Slurry-nano**	**Solution**	**Slurry-AR**

APPENDIX D

EFFECT OF PARTICLE SIZE

Table D.1 Particle sizes of Redispersed FNB from Films.

Drug Loading%	Particle size in suspension (μm)	d_{10} (μm)	d_{50} (μm)	d_{90} (μm)	$d_{4,3}$ (μm)
2.5	8	3.33	8.407	19.4	10.54
2.5	5.5	2.282	5.347	10.87	6.142
2.5	0.7	0.247	1.063	2.818	1.317
2.5	0.4	0.202	0.388	1.675	0.587
2.5	0.16	0.106	0.162	0.245	0.17
10	8	3.621	8.557	18.25	9.833
10	5.5	1.997	4.255	8.549	4.813
10	0.7	0.246	0.921	2.857	1.293
10	0.4	0.187	0.361	1.496	0.528
10	0.16	0.104	0.157	0.24	0.165
25	8	3.405	7.767	15.92	8.807
25	5.5	2.019	4.364	8.727	4.916
25	0.7	0.231	0.718	2.68	1.189
25	0.4	0.183	0.355	1.441	0.517
25	0.16	0.104	0.162	0.244	0.169
40	8	3.309	7.621	15.69	8.669
40	5.5	1.801	3.706	7.512	4.221
40	0.7	0.235	0.875	3.012	1.323
40	0.4	0.196	0.378	1.668	0.578
40	0.16	0.102	0.16	0.251	0.169

Table D.2 Statistical Analysis of Dissolution Profiles of Films Loaded with FNB at Varying Particle Size and Drug Loadings

15 µm	f_2*	36.27			
	f_2*	36.21			
5.5 µm	f_2*	36.74	49.41		
	f_2*	36.58	49.35		
700 nm	f_2*	44.48	39.47	49.56	
	f_2*	44.48	39.33	49.01	
400 nm	f_2*	37.98	45.99	61	52.74
	f_2*	38.17	46.35	60.9	52.54
2.5% Drug loading		**160 nm**	**15 µm**	**5.5 µm**	**700 nm**
15 µm	f_2*	33.36			
	f_2*	33.36			
5.5 µm	f_2*	43.42	46.74		
	f_2*	43.1	46.58		
700 nm	f_2*	65.44	35.17	45.88	
	f_2*	65.6	35.17	46.01	
400 nm	f_2*	66.77	33.68	43.8	66.6
	f_2*	67.22	33.75	43.71	66.32
10% Drug loading		**160 nm**	**15 µm**	**5.5 µm**	**700 nm**
15 µm	f_2*	35.48			
	f_2*	37.17			
5.5 µm	f_2*	53.61	43.66		
	f_2*	53.82	43.37		
700 nm	f_2*	47.31	28.75	38.17	
	f_2*	49.64	28.98	38.75	
400 nm	f_2*	67.77	33.71	47.83	51.64
	f_2*	67.92	33.66	48	50.41
25% Drug loading		**160 nm**	**15 µm**	**5.5 µm**	**700 nm**
15 µm	f_2*	46.61			
	f_2*	46.28			
5.5 µm	f_2*	36.07	50.37		
	f_2*	36.58	50.57		
700 nm	f_2*	29.89	38.93	46.37	
	f_2*	29.87	39.27	46.63	
400 nm	f_2*	36.46	48.65	57.14	45.2
	f_2*	36.52	48.8	56.9	45.51
40% Drug loading		**160 nm**	**15 µm**	**5.5 µm**	**700 nm**

Table D.2 (Continued) Statistical Analysis of Dissolution Profiles of Films Loaded with FNB at Varying Particle Size and Drug Loadings

2.5% FNB	f_2*	38.27		
	f_2*	39.01		
10% FNB	f_2*	31.33	46.32	
	f_2*	31.19	52.6	
25% FNB	f_2*	41.29	53.15	41.77
	f_2*	41.24	53.43	41.99
15 µm		**40% FNB**	**2.5% FNB**	**10% FNB**
2.5% FNB	f_2*	34.67		
	f_2*	34.86		
10% FNB	f_2*	31.86	59.89	
	f_2*	32.35	58.51	
25% FNB	f_2*	46.31	46.02	41.73
	f_2*	47.36	46.42	42.41
5.5 µm		**40% FNB**	**2.5% FNB**	**10% FNB**
2.5% FNB	f_2*	33.32		
	f_2*	33.46		
10% FNB	f_2*	34.14	59	
	f_2*	34.24	58.47	
25% FNB	f_2*	55.87	35.09	35.94
	f_2*	56.26	35.65	36.5
700 nm		**40% FNB**	**2.5% FNB**	**10% FNB**
2.5% FNB	f_2*	35.34		
	f_2*	35.73		
10% FNB	f_2*	46.02	50.12	
	f_2*	45.73	49.32	
25% FNB	f_2*	62.74	36.92	48.08
	f_2*	62.05	36.29	48.08
400 nm		**40% FNB**	**2.5% FNB**	**10% FNB**
2.5% FNB	f_2*	44.38		
	f_2*	44.01		
10% FNB	f_2*	52.05	38.2	
	f_2*	50.76	51.78	
25% FNB	f_2*	41.06	55.23	48.54
	f_2*	40.22	60.71	49.75
160 nm		**40% FNB**	**2.5% FNB**	**10% FNB**

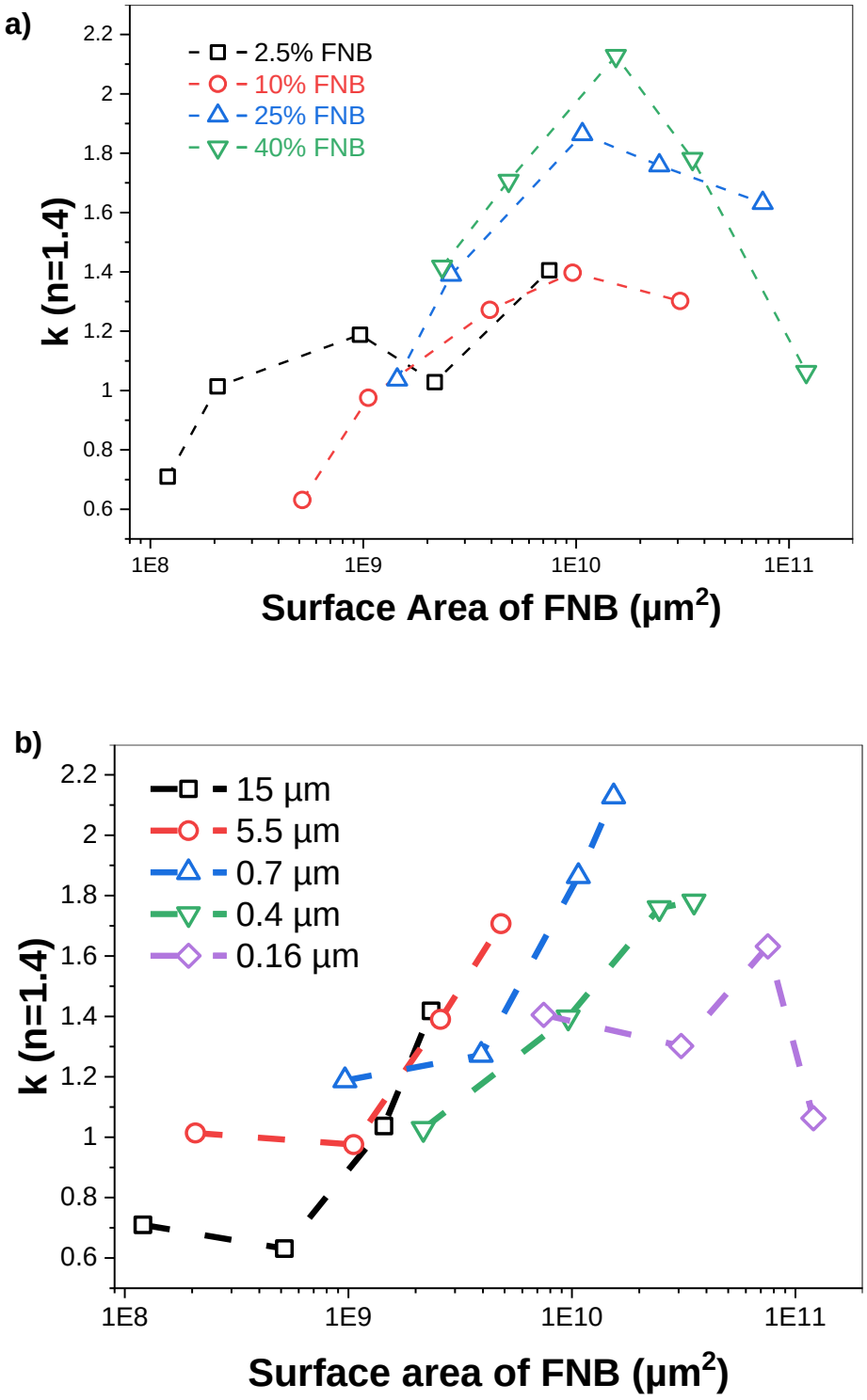

Figure D.1 Dissolution analysis with respect to total surface area of FNB a) drug loading and b) particle size grouping.

APPENDIX E

IN-LINE THICKNESS ANALYSIS

Table E.1 Statistics of PLS Models Developed Using Different Pre-Processing Methods (Films Loaded with 30 wt% AR-FNB)

Pre-treatment	RMSEC	RMSECV	Bias	R^2 (cross-validation)
Full range –1st derivative	2.47	2.59	0.015	0.9924
Reduced range – 1st derivative	2.92	2.98	0.001	0.9901
Reduced range – Baseline	4.88	5.00	0.020	0.9721
Reduced range – Baseline & Smoothing	4.90	5.03	0.022	0.9720
Reduced range – untreated	9.31	9.53	0.074	0.8993
Reduced range – Smoothing	9.32	9.50	0.024	0.8982
Full range – untreated	9.68	9.90	-0.004	0.8896
Reduced range – Smoothing & SNV	9.66	9.95	-0.076	0.8891
Full range –Smoothing	9.70	10.03	0.074	0.8870
Reduced range – Baseline & SNV	10.38	10.66	-0.045	0.8726
Reduced range – SNV	10.38	10.72	-0.163	0.8725
Full range – Baseline & Smoothing	10.04	11.42	-0.324	0.8553
Full range – Baseline	10.09	11.55	-0.173	0.8500
Full range –Smoothing & SNV	14.17	14.55	-0.113	0.7642
Full range –SNV	14.48	14.78	-0.095	0.7577
Full range – Baseline & SNV	14.48	14.81	-0.068	0.7568

SG: Savitzky Golay
SNV: Standard normal variate

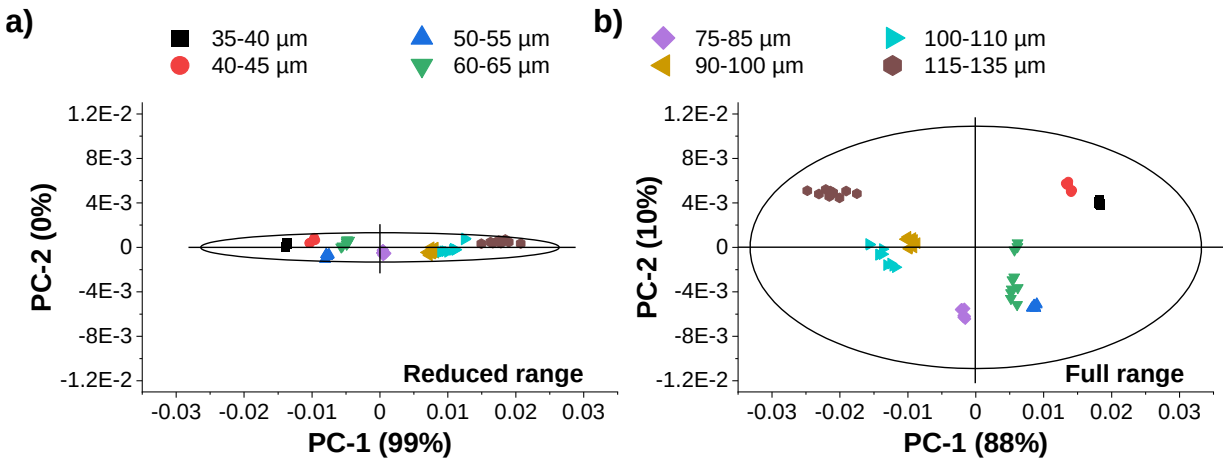

Figure E.1 PCA score plots for NIR spectra belonging films loaded with 30% AR-FNB a) Reduced (1304-1651 nm) and b) Full spectral range (908-1676 nm) were used.

REFERENCES

1. Borges, A.F., C. Silva, J.F. Coelho, and S. Simoes, *Oral films: Current status and future perspectives: I - galenical development and quality attributes.* Journal of Controlled Release, 2015. **206**: p. 1-19.

2. Dixit, R.P. and S.P. Puthli, *Oral strip technology: Overview and future potential.* Journal of Controlled Release, 2009. **139**(2): p. 94-107.

3. Hanif, M., M. Zaman, and V. Chaurasiya, *Polymers used in buccal film: A review.* Designed Monomers and Polymers, 2014. **18**(2): p. 105-111.

4. Gala, R.P., C. Popescu, G.T. Knipp, R.R. McCain, R.V. Ubale, R. Addo, T. Bhowmik, C.D. Kulczar, and M.J. D'Souza, *Physicochemical and preclinical evaluation of a novel buccal measles vaccine.* AAPS PharmSciTech, 2017. **18**(2): p. 283-292.

5. Mortazavian, E., F.A. Dorkoosh, and M. Rafiee-Tehrani, *Design, characterization and ex vivo evaluation of chitosan film integrating of insulin nanoparticles composed of thiolated chitosan derivative for buccal delivery of insulin.* Drug Development and Industrial Pharmacy, 2014. **40**(5): p. 691-8.

6. Cui, Z. and R.J. Mumper, *Bilayer films for mucosal (genetic) immunization via the buccal route in rabbits.* Pharmaceutical Research, 2002. **19**(7): p. 947-953.

7. Chatterjee, S. *Fda perspective on continuous manufacturing*. in *IFPAC Annual Meeting*. 2012. Baltimore.

8. Niese, S., J. Breitkreutz, and J. Quodbach, *Development of a dosing device for individualized dosing of orodispersible warfarin films.* International Journal of Pharmaceutics, 2019. **561**: p. 314-323.

9. Repka, M.A., S. Prodduturi, and S.P. Stodghill, *Production and characterization of hot-melt extruded films containing clotrimazole.* Drug Development and Industrial Pharmacy, 2003. **29**(7): p. 757-65.

10. Pimparade, M.B., A. Vo, A.S. Maurya, J. Bae, J.T. Morott, X. Feng, D.W. Kim, V.I. Kulkarni, R. Tiwari, K. Vanaja, R. Murthy, H.N. Shivakumar, D. Neupane, S.R. Mishra, S.N. Murthy, and M.A. Repka, *Development and evaluation of an oral fast disintegrating anti-allergic film using hot-melt extrusion technology.* European Journal of Pharmaceutics and Biopharmaceutics, 2017. **119**: p. 81-90.

11. Low, A.Q., J. Parmentier, Y.M. Khong, C.C. Chai, T.Y. Tun, J.E. Berania, X. Liu, R. Gokhale, and S.Y. Chan, *Effect of type and ratio of solubilising polymer on characteristics of hot-melt extruded orodispersible films.* International Journal of Pharmaceutics, 2013. **455**(1-2): p. 138-47.

12. Chen, M., J. Lu, W. Deng, A. Singh, N.N. Mohammed, M.A. Repka, and C. Wu, *Influence of processing parameters and formulation factors on the bioadhesive, temperature stability and drug release properties of hot-melt extruded films containing miconazole.* AAPS PharmSciTech, 2014. **15**(3): p. 522-9.

13. Palem, C.R., N.R. Dudhipala, S.K. Battu, M.A. Repka, and M. Rao Yamsani, *Development, optimization and in vivo characterization of domperidone-controlled release hot-melt-extruded films for buccal delivery.* Drug Development and Industrial Pharmacy, 2016. **42**(3): p. 473-84.

14. Palem, C.R., S. Kumar Battu, S. Maddineni, R. Gannu, M.A. Repka, and M.R. Yamsani, *Oral transmucosal delivery of domperidone from immediate release films produced via hot-melt extrusion technology.* Pharmaceutical Development and Technology, 2013. **18**(1): p. 186-95.

15. Prodduturi, S., R.V. Manek, W.M. Kolling, S.P. Stodghill, and M.A. Repka, *Solid-state stability and characterization of hot-melt extruded poly(ethylene oxide) films.* Journal of Pharmaceutical Sciences, 2005. **94**(10): p. 2232-45.

16. Repka, M.A., T.G. Gerding, S.L. Repka, and J.W. McGinity, *Influence of plasticizers and drugs on the physical-mechanical properties of hydroxypropylcellulose films prepared by hot melt extrusion.* Drug Development and Industrial Pharmacy, 1999. **25**(5): p. 625-33.

17. Tumuluri, S.V., S. Prodduturi, M.M. Crowley, S.P. Stodghill, J.W. McGinity, M.A. Repka, and B.A. Avery, *The use of near-infrared spectroscopy for the quantitation of a drug in hot-melt extruded films.* Drug Development and Industrial Pharmacy, 2004. **30**(5): p. 505-11.

18. Cilurzo, F., I.E. Cupone, P. Minghetti, F. Selmin, and L. Montanari, *Fast dissolving films made of maltodextrins.* European Journal of Pharmaceutics and Biopharmaceutics, 2008. **70**(3): p. 895-900.

19. Repka, M.A., K. Gutta, S. Prodduturi, M. Munjal, and S.P. Stodghill, *Characterization of cellulosic hot-melt extruded films containing lidocaine.* European Journal of Pharmaceutics and Biopharmaceutics, 2005. **59**(1): p. 189-96.

20. Woertz, C. and P. Kleinebudde, *Development of orodispersible polymer films containing poorly water soluble active pharmaceutical ingredients with focus on different drug loadings and storage stability.* International Journal of Pharmaceutics, 2015. **493**(1-2): p. 134-45.

21. Morales, J.O., R. Su, and J.T. McConville, *The influence of recrystallized caffeine on water-swellable polymethacrylate mucoadhesive buccal films.* AAPS PharmSciTech, 2013. **14**(2): p. 475-84.

22. Pechova, V., J. Gajdziok, J. Muselik, and D. Vetchy, *Development of orodispersible films containing benzydamine hydrochloride using a modified solvent casting method.* AAPS PharmSciTech, 2018. **19**(6): p. 2509-2518.

23. Senta-Loys, Z., S. Bourgeois, J.P. Valour, S. Briancon, and H. Fessi, *Orodispersible films based on amorphous solid dispersions of tetrabenazine.* International Journal of Pharmaceutics, 2017. **518**(1-2): p. 242-252.

24. Garsuch, V. and J. Breitkreutz, *Comparative investigations on different polymers for the preparation of fast-dissolving oral films.* Journal of Pharmacy and Pharmacology, 2010. **62**(4): p. 539-45.

25. Preis, M., C. Woertz, K. Schneider, J. Kukawka, J. Broscheit, N. Roewer, and J. Breitkreutz, *Design and evaluation of bilayered buccal film preparations for local administration of lidocaine hydrochloride.* European Journal of Pharmaceutics and Biopharmaceutics, 2014. **86**(3): p. 552-61.

26. Thabet, Y., D. Lunter, and J. Breitkreutz, *Continuous manufacturing and analytical characterization of fixed-dose, multilayer orodispersible films.* European Journal of Pharmaceutical Sciences, 2018. **117**: p. 236-244.

27. Krull, S.M., R. Susarla, A. Afolabi, M. Li, Y. Ying, Z. Iqbal, E. Bilgili, and R.N. Dave, *Polymer strip films as a robust, surfactant-free platform for delivery of bcs class ii drug nanoparticles.* International Journal of Pharmaceutics, 2015. **489**(1-2): p. 45-57.

28. Krull, S.M., Z. Ma, M. Li, R.N. Dave, and E. Bilgili, *Preparation and characterization of fast dissolving pullulan films containing bcs class ii drug nanoparticles for bioavailability enhancement.* Drug Development and Industrial Pharmacy, 2016. **42**(7): p. 1073-85.

29. Sievens-Figueroa, L., A. Bhakay, J.I. Jerez-Rozo, N. Pandya, R.J. Romanach, B. Michniak-Kohn, Z. Iqbal, E. Bilgili, and R.N. Dave, *Preparation and characterization of hydroxypropyl methyl cellulose films containing stable bcs class ii drug nanoparticles for pharmaceutical applications.* International Journal of Pharmaceutics, 2012. **423**(2): p. 496-508.

30. Zhang, L., Y. Li, M. Abed, and R.N. Dave, *Incorporation of surface-modified dry micronized poorly water-soluble drug powders into polymer strip films.* International Journal of Pharmaceutics, 2018. **535**(1-2): p. 462-472.

31. Brniak, W., E. Maslak, and R. Jachowicz, *Orodispersible films and tablets with prednisolone microparticles.* European Journal of Pharmaceutical Sciences, 2015. **75**: p. 81-90.

32. Steiner, D., J.H. Finke, and A. Kwade, *Instant odfs - development of an intermediate, nanoparticle-based product platform for individualized medication.* European Journal of Pharmaceutics and Biopharmaceutics, 2018. **126**: p. 149-158.

33. Krull, S.M., H.V. Patel, M. Li, E. Bilgili, and R.N. Dave, *Critical material attributes (CMAs) of strip films loaded with poorly water-soluble drug nanoparticles: I. Impact of plasticizer on film properties and dissolution.* European Journal of Pharmaceutical Sciences, 2016. **92**: p. 146-55.

34. Krull, S.M., J. Ammirata, S. Bawa, M. Li, E. Bilgili, and R.N. Dave, *Critical material attributes of strip films loaded with poorly water-soluble drug nanoparticles: II. Impact of polymer molecular weight.* Journal of Pharmaceutical Sciences, 2017. **106**(2): p. 619-628.

35. Krull, S.M., J. Moreno, M. Li, E. Bilgili, and R.N. Dave, *Critical material attributes (CMAs) of strip films loaded with poorly water-soluble drug nanoparticles: III. Impact of drug nanoparticle loading.* International Journal of Pharmaceutics, 2017. **523**(1): p. 33-41.

36. Vuddanda, P.R., M. Montenegro-Nicolini, J.O. Morales, and S. Velaga, *Effect of surfactants and drug load on physico-mechanical and dissolution properties of nanocrystalline tadalafil-loaded oral films.* European Journal of Pharmaceutical Sciences, 2017. **109**: p. 372-380.

37. Yu, L.X., G. Amidon, M.A. Khan, S.W. Hoag, J. Polli, G.K. Raju, and J. Woodcock, *Understanding pharmaceutical quality by design.* The AAPS Journal, 2014. **16**(4): p. 771-83.

38. Yu, L.X., *Pharmaceutical quality by design: Product and process development, understanding, and control.* Pharmaceutical Research, 2008. **25**(4): p. 781-91.

39. Lionberger, R.A., S.L. Lee, L. Lee, A. Raw, and L.X. Yu, *Quality by design: Concepts for andas.* The AAPS Journal, 2008. **10**(2): p. 268-76.

40. Visser, J.C., W.M. Dohmen, W.L. Hinrichs, J. Breitkreutz, H.W. Frijlink, and H.J. Woerdenbag, *Quality by design approach for optimizing the formulation and physical properties of extemporaneously prepared orodispersible films.* International Journal of Pharmaceutics, 2015. **485**(1-2): p. 70-6.

41. Zhang, L., J. Alfano, D. Race, and R.N. Dave, *Zero-order release of poorly water-soluble drug from polymeric films made via aqueous slurry casting.* European Journal of Pharmaceutical Sciences, 2018. **117**: p. 245-254.

42. Noyes, A.A. and W.R. Whitney, *The rate of solution of solid substances in their own solutions.* Journal of the American Chemical Society, 1897. **19**(12): p. 930-934.

43. Zhao, Y., P. Quan, and L. Fang, *Preparation of an oral thin film containing meclizine hydrochloride: In vitro and in vivo evaluation.* International Journal of Pharmaceutics, 2015. **496**(2): p. 314-22.

44. Prajapati, V.D., A.M. Chaudhari, A.K. Gandhi, and P. Maheriya, *Pullulan based oral thin film formulation of zolmitriptan: Development and optimization using factorial design.* International Journal of Biological Macromolecules, 2018. **107**: p. 2075-2085.

45. Visser, J.C., H.J. Woerdenbag, S. Crediet, E. Gerrits, M.A. Lesschen, W.L.J. Hinrichs, J. Breitkreutz, and H.W. Frijlink, *Orodispersible films in individualized pharmacotherapy: The development of a formulation for pharmacy preparations.* International Journal of Pharmaceutics, 2015. **478**(1): p. 155-163.

46. Park, D.M., Y.K. Song, J.P. Jee, H.T. Kim, and C.K. Kim, *Development of chitosan-based ondansetron buccal delivery system for the treatment of emesis.* Drug Development and Industrial Pharmacy, 2012. **38**(9): p. 1077-83.

47. Van Eerdenbrugh, B., J.A. Baird, and L.S. Taylor, *Crystallization tendency of active pharmaceutical ingredients following rapid solvent evaporation--classification and comparison with crystallization tendency from undercooled melts.* Journal of Pharmaceutical Sciences, 2010. **99**(9): p. 3826-38.

48. Baird, J.A., B. Van Eerdenbrugh, and L.S. Taylor, *A classification system to assess the crystallization tendency of organic molecules from undercooled melts.* Journal of Pharmaceutical Sciences, 2010. **99**(9): p. 3787-806.

49. Powell, C.T., H. Xi, Y. Sun, E. Gunn, Y. Chen, M.D. Ediger, and L. Yu, *Fast crystal growth in o-terphenyl glasses: A possible role for fracture and surface mobility.* The Journal of Physical Chemistry B, 2015. **119**(31): p. 10124-10130.

50. Kapourani, A., E. Vardaka, K. Katopodis, K. Kachrimanis, and P. Barmpalexis, *Crystallization tendency of apis possessing different thermal and glass related properties in amorphous solid dispersions.* International Journal of Pharmaceutics, 2020. **579**: p. 119149.

51. Wu, T., Y. Sun, N. Li, M.M. de Villiers, and L. Yu, *Inhibiting surface crystallization of amorphous indomethacin by nanocoating.* Langmuir, 2007. **23**(9): p. 5148-5153.

52. Cai, T., L. Zhu, and L. Yu, *Crystallization of organic glasses: Effects of polymer additives on bulk and surface crystal growth in amorphous nifedipine.* Pharmaceutical Research, 2011. **28**(10): p. 2458-66.

53. Huang, C., S. Ruan, T. Cai, and L. Yu, *Fast surface diffusion and crystallization of amorphous griseofulvin.* The Journal of Physical Chemistry B, 2017. **121**(40): p. 9463-9468.

54. Pattnaik, S., K. Swain, S. Mallick, and Z. Lin, *Effect of casting solvent on crystallinity of ondansetron in transdermal films.* International Journal of Pharmaceutics, 2011. **406**(1-2): p. 106-10.

55. Laitinen, R., K. Lobmann, C.J. Strachan, H. Grohganz, and T. Rades, *Emerging trends in the stabilization of amorphous drugs.* International Journal of Pharmaceutics, 2013. **453**(1): p. 65-79.

56. Yu, L., *Amorphous pharmaceutical solids: Preparation, characterization and stabilization.* Advanced Drug Delivery Reviews, 2001. **48**(1): p. 27-42.

57. Mugheirbi, N.A., P.J. Marsac, and L.S. Taylor, *Insights into water-induced phase separation in itraconazole–hydroxypropylmethyl cellulose spin coated and spray dried dispersions.* Molecular Pharmaceutics, 2017. **14**(12): p. 4387-4402.

58. Bain, D.F., D.L. Munday, and A. Smith, *Solvent influence on spray-dried biodegradable microspheres.* Journal of Microencapsulation, 1999. **16**(4): p. 453-74.

59. Raula, J., H. Eerikäinen, and E.I. Kauppinen, *Influence of the solvent composition on the aerosol synthesis of pharmaceutical polymer nanoparticles.* International Journal of Pharmaceutics, 2004. **284**(1-2): p. 13-21.

60. Ansari, M.T. and V.B. Sunderland, *Solid dispersions of dihydroartemisinin in polyvinylpyrrolidone.* Archives of Pharmaceutical Research, 2008. **31**(3): p. 390.

61. Al-Obaidi, H., S. Brocchini, and G. Buckton, *Anomalous properties of spray dried solid dispersions.* Journal of Pharmaceutical Sciences, 2009. **98**(12): p. 4724-4737.

62. Hugo, M., K. Kunath, and J. Dressman, *Selection of excipient, solvent and packaging to optimize the performance of spray-dried formulations: Case example fenofibrate.* Drug Development and Industrial Pharmacy, 2013. **39**(2): p. 402-412.

63. Mugheirbi, N.A., L.I. Mosquera-Giraldo, C.H. Borca, L.V. Slipchenko, and L.S. Taylor, *Phase behavior of drug-hydroxypropyl methylcellulose amorphous solid dispersions produced from various solvent systems: Mechanistic understanding of the role of polymer using experimental and theoretical methods.* Molecular Pharmaceutics, 2018. **15**(8): p. 3236-3251.

64. Rowe, R., P. Sheskey, and M. Quinn, *Handbook of pharmaceutical excipients 6th edition pharmaceutical press.* London, England, 2009. **637**.

65. Takeuchi, H., R. Yamakawa, T. Nishimatsu, Y. Takeuchi, K. Hayakawa, and N. Maruyama, *Design of rapidly disintegrating drug delivery films for oral doses with hydoxypropyl methylcellulose.* Journal of Drug Delivery Science and Technology, 2013. **23**(5): p. 471-475.

66. Carolina Visser, J., O.A.F. Weggemans, R.J. Boosman, K.U. Loos, H.W. Frijlink, and H.J. Woerdenbag, *Increased drug load and polymer compatibility of bilayered orodispersible films.* European Journal of Pharmaceutical Sciences, 2017. **107**: p. 183-190.

67. Dow, *Methocel cellulose ethers technical handbook*. 2002, The Dow Chemical Company USA.

68. Arca, H.C., L.I. Mosquera-Giraldo, V. Bi, D. Xu, L.S. Taylor, and K.J. Edgar, *Pharmaceutical applications of cellulose ethers and cellulose ether esters.* Biomacromolecules, 2018. **19**(7): p. 2351-2376.

69. Zhang, M., H. Li, B. Lang, K. O'Donnell, H. Zhang, Z. Wang, Y. Dong, C. Wu, and R.O. Williams, 3rd, *Formulation and delivery of improved amorphous fenofibrate solid dispersions prepared by thin film freezing.* European Journal of Pharmaceutics and Biopharmaceutics, 2012. **82**(3): p. 534-44.

70. FDA, *Q3c-tables and list guidance for industry.* 2017.

71. Müller, C.M., A.T. Pires, and F. Yamashita, *Characterization of thermoplastic starch/poly (lactic acid) blends obtained by extrusion and thermopressing.* Journal of the Brazilian Chemical Society, 2012. **23**(3): p. 426-434.

72. Tipduangta, P., K. Takieddin, L. Fábián, P. Belton, and S. Qi, *Towards controlling the crystallisation behaviour of fenofibrate melt: Triggers of crystallisation and polymorphic transformation.* RSC Advances, 2018. **8**(24): p. 13513-13525.

73. USPharmacopedia, < *905> uniformity of dosage units*, in *United States Pharmacopoeia*. 2006: Rockville, MD: United States Pharmacopeial Convention, Inc.

74. Susarla, R., L. Sievens-Figueroa, A. Bhakay, Y. Shen, J.I. Jerez-Rozo, W. Engen, B. Khusid, E. Bilgili, R.J. Romañach, K.R. Morris, B. Michniak-Kohn, and R.N. Davé, *Fast drying of biocompatible polymer films loaded with poorly water-soluble drug nano-particles via low temperature forced convection.* International Journal of Pharmaceutics, 2013. **455**(1–2): p. 93-103.

75. Sievens-Figueroa, L., N. Pandya, A. Bhakay, G. Keyvan, B. Michniak-Kohn, E. Bilgili, and R.N. Dave, *Using usp i and usp iv for discriminating dissolution rates of nano- and microparticle-loaded pharmaceutical strip-films.* AAPS PharmSciTech, 2012. **13**(4): p. 1473-82.

76. Tipduangta, P., K. Takieddin, L. Fabian, P. Belton, and S. Qi, *A new low melting-point polymorph of fenofibrate prepared via talc induced heterogeneous nucleation.* Crystal Growth & Design, 2015. **15**(10): p. 5011-5020.

77. Heinz, A., K.C. Gordon, C.M. McGoverin, T. Rades, and C.J. Strachan, *Understanding the solid-state forms of fenofibrate--a spectroscopic and computational study.* European Journal of Pharmaceutics and Biopharmaceutics, 2009. **71**(1): p. 100-8.

78. Warren, D.B., H. Benameur, C.J. Porter, and C.W. Pouton, *Using polymeric precipitation inhibitors to improve the absorption of poorly water-soluble drugs: A mechanistic basis for utility.* Journal of drug targeting, 2010. **18**(10): p. 704-731.

79. Mohapatra, S., S. Samanta, K. Kothari, P. Mistry, and R. Suryanarayanan, *Effect of polymer molecular weight on the crystallization behavior of indomethacin amorphous solid dispersions.* Crystal Growth & Design, 2017. **17**(6): p. 3142-3150.

80. Baghel, S., H. Cathcart, and N.J. O'Reilly, *Polymeric amorphous solid dispersions: A review of amorphization, crystallization, stabilization, solid-state characterization, and aqueous solubilization of biopharmaceutical classification system class ii drugs.* Journal of Pharmaceutical Sciences, 2016. **105**(9): p. 2527-44.

81. Klug, E. *Some properties of water-soluble hydroxyalkyl celluloses and their derivatives*. in *Journal of Polymer Science Part C: Polymer Symposia*. 1971. Wiley Online Library.

82. Mosquera-Giraldo, L.I., C.H. Borca, X. Meng, K.J. Edgar, L.V. Slipchenko, and L.S. Taylor, *Mechanistic design of chemically diverse polymers with applications in oral drug delivery.* Biomacromolecules, 2016. **17**(11): p. 3659-3671.

83. Schram, C.J., S.P. Beaudoin, and L.S. Taylor, *Impact of polymer conformation on the crystal growth inhibition of a poorly water-soluble drug in aqueous solution.* Langmuir, 2015. **31**(1): p. 171-9.

84. Ilevbare, G.A., H. Liu, K.J. Edgar, and L.S. Taylor, *Understanding polymer properties important for crystal growth inhibition—impact of chemically diverse polymers on solution crystal growth of ritonavir.* Crystal Growth & Design, 2012. **12**(6): p. 3133-3143.

85. Nair, A.B., R. Kumria, S. Harsha, M. Attimarad, B.E. Al-Dhubiab, and I.A. Alhaider, *In vitro techniques to evaluate buccal films.* Journal of Controlled Release, 2013. **166**(1): p. 10-21.

86. Repka, M.A. and J.W. McGinity, *Influence of chlorpheniramine maleate on topical hydroxypropylcellulose films produced by hot-melt extrusion.* Pharmaceutical Development and Technology, 2001. **6**(3): p. 297-304.

87. Chen, Y., W. Huang, J. Chen, H. Wang, S. Zhang, and S. Xiong, *The synergetic effects of nonpolar and polar protic solvents on the properties of felodipine and soluplus in solutions, casting films, and spray-dried solid dispersions.* Journal of Pharmaceutical Sciences, 2018. **107**(6): p. 1615-1623.

88. Xu, L.L., L.L. Shi, Q.R. Cao, W.J. Xu, Y. Cao, X.Y. Zhu, and J.H. Cui, *Formulation and in vitro characterization of novel sildenafil citrate-loaded polyvinyl alcohol-polyethylene glycol graft copolymer-based orally dissolving films.* International Journal of Pharmaceutics, 2014. **473**(1-2): p. 398-406.

89. Fakes, M.G., B.J. Vakkalagadda, F. Qian, S. Desikan, R.B. Gandhi, C. Lai, A. Hsieh, M.K. Franchini, H. Toale, and J. Brown, *Enhancement of oral bioavailability of an hiv-attachment inhibitor by nanosizing and amorphous formulation approaches.* International Journal of Pharmaceutics, 2009. **370**(1-2): p. 167-174.

90. Vogt, M., K. Kunath, and J.B. Dressman, *Dissolution enhancement of fenofibrate by micronization, cogrinding and spray-drying: Comparison with commercial preparations.* European Journal of Pharmaceutics and Biopharmaceutics, 2008. **68**(2): p. 283-8.

91. Sigfridsson, K., S. Forssén, P. Holländer, U. Skantze, and J. de Verdier, *A formulation comparison, using a solution and different nanosuspensions of a poorly soluble compound.* European Journal of Pharmaceutics and Biopharmaceutics, 2007. **67**(2): p. 540-547.

92. Sun, W., R. Ni, X. Zhang, L.C. Li, and S. Mao, *Spray drying of a poorly water-soluble drug nanosuspension for tablet preparation: Formulation and process optimization with bioavailability evaluation.* Drug Development and Industrial Pharmacy, 2015. **41**(6): p. 927-933.

93. Li, M., N. Ioannidis, C. Gogos, and E. Bilgili, *A comparative assessment of nanocomposites vs. Amorphous solid dispersions prepared via nanoextrusion for drug dissolution enhancement.* European Journal of Pharmaceutics and Biopharmaceutics, 2017. **119**: p. 68-80.

94. Quan, P., X. Wan, Q. Tian, C. Liu, and L. Fang, *Dicarboxylic acid as a linker to improve the content of amorphous drug in drug-in-polymer film: Effects of molecular mobility, electrical conductivity and intermolecular interactions.* Journal of Controlled Release, 2020. **317**: p. 142-153.

95. Liu, J., J. Guan, X. Wan, R. Shang, X. Shi, L. Fang, and C. Liu, *The improved cargo loading and physical stability of ibuprofen orodispersible film: Molecular mechanism of ion-pair complexes on drug-polymer miscibility.* Journal of Pharmaceutical Sciences, 2020. **109**(3): p. 1356-1364.

96. Cetindag, E., J. Pentangelo, T.A. Cespedes, and R.N. Davé, *Effect of solvents and cellulosic polymers on quality attributes of films loaded with a poorly water-soluble drug.* Carbohydrate Polymers, 2020. **250**: p. 117012.

97. Han, X., C. Ghoroi, D. To, Y. Chen, and R. Davé, *Simultaneous micronization and surface modification for improvement of flow and dissolution of drug particles.* International Journal of Pharmaceutics, 2011. **415**(1): p. 185-195.

98. Bilgili, E. and A. Afolabi, *A combined microhydrodynamics-polymer adsorption analysis for elucidation of the roles of stabilizers in wet stirred media milling.* International Journal of Pharmaceutics, 2012. **439**(1-2): p. 193-206.

99. Knieke, C., M.A. Azad, R.N. Davé, and E. Bilgili, *A study of the physical stability of wet media-milled fenofibrate suspensions using dynamic equilibrium curves.* Chemical Engineering Research and Design, 2013. **91**(7): p. 1245-1258.

100. Paixão, P., L.F. Gouveia, N. Silva, and J.A. Morais, *Evaluation of dissolution profile similarity–comparison between the f2, the multivariate statistical distance and the f2 bootstrapping methods.* European Journal of Pharmaceutics and Biopharmaceutics, 2017. **112**: p. 67-74.

101. Mendyk, A., A. Pacławski, J. Szlek, and R. Jachowicz, *Pheq_bootstrap: Open-source software for the simulation of f2 distribution in cases of large variability in dissolution profiles.* Dissolution Technology, 2013. **20**(1): p. 13-17.

102. Patel, D., S.S. Zode, and A.K. Bansal, *Formulation aspects of intravenous nanosuspensions.* International Journal of Pharmaceutics, 2020: p. 119555.

103. Da Silva, F.L.O., M.B.F. Marques, K.C. Kato, and G. Carneiro, *Nanonization techniques to overcome poor water-solubility with drugs.* Expert Opinion on Drug Discovery, 2020. **15**(7): p. 853-864.

104. Kalepu, S. and V. Nekkanti, *Insoluble drug delivery strategies: Review of recent advances and business prospects.* Acta Pharmaceutica Sinica B, 2015. **5**(5): p. 442-453.

105. Kumar, R., S.V. Dalvi, and P.F. Siril, *Nanoparticle-based drugs and formulations: Current status and emerging applications.* ACS Applied Nano Materials, 2020. **3**(6): p. 4944-4961.

106. Serajuddin, A.T., *Salt formation to improve drug solubility.* Advanced Drug Delivery Reviews, 2007. **59**(7): p. 603-616.

107. Bhakay, A., M. Rahman, R.N. Dave, and E. Bilgili, *Bioavailability enhancement of poorly water-soluble drugs via nanocomposites: Formulation–processing aspects and challenges.* Pharmaceutics, 2018. **10**(3): p. 86.

108. Rahman, M., A. Coelho, J. Tarabokija, S. Ahmad, K. Radgman, and E. Bilgili, *Synergistic and antagonistic effects of various amphiphilic polymer combinations in enhancing griseofulvin release from ternary amorphous solid dispersions.* European Journal of Pharmaceutical Sciences, 2020. **150**: p. 105354.

109. Shah, A.V., H.H. Desai, P. Thool, D. Dalrymple, and A.T.M. Serajuddin, *Development of self-microemulsifying drug delivery system for oral delivery of poorly water-soluble nutraceuticals.* Drug Development and Industrial Pharmacy, 2018. **44**(6): p. 895-901.

110. Dalvi, S.V. and R.N. Dave, *Controlling particle size of a poorly water-soluble drug using ultrasound and stabilizers in antisolvent precipitation.* Industrial & Engineering Chemistry Research, 2009. **48**(16): p. 7581-7593.

111. Kesisoglou, F., S. Panmai, and Y. Wu, *Nanosizing—oral formulation development and biopharmaceutical evaluation.* Advanced Drug Delivery Reviews, 2007. **59**(7): p. 631-644.

112. Kipp, J.E., *The role of solid nanoparticle technology in the parenteral delivery of poorly water-soluble drugs.* International Journal of Pharmaceutics, 2004. **284**(1-2): p. 109-22.

113. Woertz, C. and P. Kleinebudde, *Development of orodispersible polymer films with focus on the solid state characterization of crystalline loperamide.* European Journal of Pharmaceutics and Biopharmaceutics, 2015. **94**: p. 52-63.

114. Li, W., Y. Yang, Y. Tian, X. Xu, Y. Chen, L. Mu, Y. Zhang, and L. Fang, *Preparation and in vitro/in vivo evaluation of revaprazan hydrochloride nanosuspension.* International Journal of Pharmaceutics, 2011. **408**(1-2): p. 157-162.

115. Zuo, B., Y. Sun, H. Li, X. Liu, Y. Zhai, J. Sun, and Z. He, *Preparation and in vitro/in vivo evaluation of fenofibrate nanocrystals.* International Journal of Pharmaceutics, 2013. **455**(1-2): p. 267-75.

116. Murdande, S.B., D.A. Shah, and R.H. Dave, *Impact of nanosizing on solubility and dissolution rate of poorly soluble pharmaceuticals.* Journal of Pharmaceutical Sciences, 2015. **104**(6): p. 2094-2102.

117. Chaubal, M.V. and C. Popescu, *Conversion of nanosuspensions into dry powders by spray drying: A case study.* Pharmaceutical Research, 2008. **25**(10): p. 2302-2308.

118. Basa, S., T. Muniyappan, P. Karatgi, R. Prabhu, and R. Pillai, *Production and in vitro characterization of solid dosage form incorporating drug nanoparticles.* Drug Development and Industrial Pharmacy, 2008. **34**(11): p. 1209-1218.

119. Azad, M., A. Afolabi, A. Bhakay, J. Leonardi, R. Davé, and E. Bilgili, *Enhanced physical stabilization of fenofibrate nanosuspensions via wet co-milling with a superdisintegrant and an adsorbing polymer.* European Journal of Pharmaceutics and Biopharmaceutics, 2015. **94**: p. 372-385.

120. Van Eerdenbrugh, B., G. Van den Mooter, and P. Augustijns, *Top-down production of drug nanocrystals: Nanosuspension stabilization, miniaturization and transformation into solid products.* International Journal of Pharmaceutics, 2008. **364**(1): p. 64-75.

121. Choi, J.-Y., J.Y. Yoo, H.-S. Kwak, B.U. Nam, and J. Lee, *Role of polymeric stabilizers for drug nanocrystal dispersions.* Current Applied Physics, 2005. **5**(5): p. 472-474.

122. Verma, S., B.D. Huey, and D.J. Burgess, *Scanning probe microscopy method for nanosuspension stabilizer selection.* Langmuir, 2009. **25**(21): p. 12481-12487.

123. Braig, V., C. Konnerth, W. Peukert, and G. Lee, *Enhanced dissolution of naproxen from pure-drug, crystalline nanoparticles: A case study formulated into spray-dried granules and compressed tablets.* International Journal of Pharmaceutics, 2019. **554**: p. 54-60.

124. Van Eerdenbrugh, B., L. Froyen, J. Van Humbeeck, J.A. Martens, P. Augustijns, and G. Van Den Mooter, *Alternative matrix formers for nanosuspension solidification: Dissolution performance and x-ray microanalysis as an evaluation tool for powder dispersion.* European Journal of Pharmaceutical Sciences, 2008. **35**(4): p. 344-353.

125. Zhang, X., J. Guan, R. Ni, L.C. Li, and S. Mao, *Preparation and solidification of redispersible nanosuspensions.* Journal of Pharmaceutical Sciences, 2014. **103**(7): p. 2166-2176.

126. Mermet-Guyennet, M., J.G. De Castro, H.S. Varol, M. Habibi, B. Hosseinkhani, N. Martzel, R. Sprik, M. Denn, A. Zaccone, and S.H. Parekh, *Size-dependent reinforcement of composite rubbers.* Polymer, 2015. **73**: p. 170-173.

127. Fu, S.-Y., X.-Q. Feng, B. Lauke, and Y.-W. Mai, *Effects of particle size, particle/matrix interface adhesion and particle loading on mechanical properties of particulate–polymer composites.* Composites Part B: Engineering, 2008. **39**(6): p. 933-961.

128. Davris, T., M.R. Mermet-Guyennet, D. Bonn, and A.V. Lyulin, *Filler size effects on reinforcement in elastomer-based nanocomposites: Experimental and simulational insights into physical mechanisms.* Macromolecules, 2016. **49**(18): p. 7077-7087.

129. Moczo, J. and B. Pukanszky, *Polymer micro and nanocomposites: Structure, interactions, properties.* Journal of Industrial and Engineering Chemistry, 2008. **14**(5): p. 535-563.

130. Costa, P. and J.M. Sousa Lobo, *Modeling and comparison of dissolution profiles.* European Journal of Pharmaceutical Sciences, 2001. **13**(2): p. 123-33.

131. Gibaldi, M. and S. Feldman, *Establishment of sink conditions in dissolution rate determinations. Theoretical considerations and application to nondisintegrating dosage forms.* Journal of Pharmaceutical Sciences, 1967. **56**(10): p. 1238-1242.

132. Higuchi, T., *Rate of release of medicaments from ointment bases containing drugs in suspension.* Journal of Pharmaceutical Sciences, 1961. **50**(10): p. 874-875.

133. Peppas, N.A., *Analysis of fickian and non-fickian drug release from polymers.* Pharmaceutica Acta Helvetiae, 1985. **60**(4): p. 110-1.

134. Korsmeyer, R.W., R. Gurny, E. Doelker, P. Buri, and N.A. Peppas, *Mechanisms of solute release from porous hydrophilic polymers.* International Journal of Pharmaceutics, 1983. **15**(1): p. 25-35.

135. Hixson, A. and J. Crowell, *Dependence of reaction velocity upon surface and agitation.* Industrial and Engineering Chemistry, 1931. **23**(8): p. 923-931.

136. Mysiukiewicz, O., B. Gospodarek, P. Ławniczak, and T. Sterzyński, *Influence of the conductive network creation on electrical, rheological, and mechanical properties of composites based on ldpe and eva matrices.* Advances in Polymer Technology, 2018. **37**(8): p. 3542-3551.

137. Pastor, C., L. Sánchez-González, M. Cháfer, A. Chiralt, and C. González-Martínez, *Physical and antifungal properties of hydroxypropylmethylcellulose based films containing propolis as affected by moisture content.* Carbohydrate Polymers, 2010. **82**(4): p. 1174-1183.

138. De Moura, M.R., R.J. Avena-Bustillos, T.H. McHugh, D.F. Wood, C.G. Otoni, and L.H. Mattoso, *Miniaturization of cellulose fibers and effect of addition on the mechanical and barrier properties of hydroxypropyl methylcellulose films.* Journal of Food Engineering, 2011. **104**(1): p. 154-160.

139. Cascone, S., *Modeling and comparison of release profiles: Effect of the dissolution method.* European Journal of Pharmaceutical Sciences, 2017. **106**: p. 352-361.

140. Denavi, G., D. Tapia-Blácido, M. Añón, P. Sobral, A. Mauri, and F. Menegalli, *Effects of drying conditions on some physical properties of soy protein films.* Journal of Food Engineering, 2009. **90**(3): p. 341-349.

141. Allanic, N., P. Le Bideau, P. Glouannec, and R. Deterre, *An experimental study on infrared drying kinetics of an aqueous adhesive supported by polymer composite.* Heat and Mass Transfer, 2016. **53**(1): p. 223-231.

142. Ortiz, C.M., J.O. de Moraes, A.R. Vicente, J.B. Laurindo, and A.N. Mauri, *Scale-up of the production of soy (glycine max l.) protein films using tape casting: Formulation of film-forming suspension and drying conditions.* Food Hydrocolloids, 2017. **66**: p. 110-117.

143. Oliveira de Moraes, J., A.S. Scheibe, B. Augusto, M. Carciofi, and J.B. Laurindo, *Conductive drying of starch-fiber films prepared by tape casting: Drying rates and film properties.* LWT - Food Science and Technology, 2015. **64**(1): p. 356-366.

144. Mayachiew, P., S. Devahastin, B.M. Mackey, and K. Niranjan, *Effects of drying methods and conditions on antimicrobial activity of edible chitosan films enriched with galangal extract.* Food Research International, 2010. **43**(1): p. 125-132.

145. Le Person, S., J. Puiggali, M. Baron, and M. Roques, *Near infrared drying of pharmaceutical thin films: Experimental analysis of internal mass transport.* Chemical Engineering and Processing: Process Intensification, 1998. **37**(3): p. 257-263.

146. Velaga, S.P., D. Nikjoo, and P.R. Vuddanda, *Experimental studies and modeling of the drying kinetics of multicomponent polymer films.* AAPS PharmSciTech, 2018. **19**(1): p. 425-435.

147. Thabet, Y. and J. Breitkreutz, *Orodispersible films: Product transfer from lab-scale to continuous manufacturing.* International Journal of Pharmaceutics, 2018. **535**(1-2): p. 285-292.

148. Mazumder, S., N. Pavurala, P. Manda, X. Xu, C.N. Cruz, and Y.S.R. Krishnaiah, *Quality by design approach for studying the impact of formulation and process variables on product quality of oral disintegrating films.* International Journal of Pharmaceutics, 2017. **527**(1-2): p. 151-160.

149. Vuddanda, P.R., M. Montenegro-Nicolini, J.O. Morales, and S. Velaga, *Effect of plasticizers on the physico-mechanical properties of pullulan based pharmaceutical oral films.* European Journal of Pharmaceutical Sciences, 2017. **96**: p. 290-298.

150. Panda, B., A.S. Parihar, and S. Mallick, *Effect of plasticizer on drug crystallinity of hydroxypropyl methylcellulose matrix film.* International Journal of Biological Macromolecules, 2014. **67**: p. 295-302.

151. Sayed, S., H.K. Ibrahim, M.I. Mohamed, and M.F. El-Milligi, *Fast-dissolving sublingual films of terbutaline sulfate: Formulation and in vitro/in vivo evaluation.* Molecular Pharmaceutics, 2013. **10**(8): p. 2942-7.

152. Preis, M., D. Gronkowsky, D. Grytzan, and J. Breitkreutz, *Comparative study on novel test systems to determine disintegration time of orodispersible films.* Journal of Pharmacy and Pharmacology, 2014. **66**(8): p. 1102-11.

153. Bonhoeffer, B., A. Kwade, and M. Juhnke, *Alternative manufacturing concepts for solid oral dosage forms from drug nanosuspensions using fluid dispensing and forced drying technology.* Journal of Pharmaceutical Sciences, 2018. **107**(3): p. 909-921.

154. Page, G.E., *Factors influencing the maximum rates of air drying shelled corn in thin layers*. 1949: Purdue University.

155. FDA, *Guidance for industry: Pat – a framework for innovative pharmaceutical development, manufacture, and quality assurance*. 2004.

156. De Beer, T., A. Burggraeve, M. Fonteyne, L. Saerens, J.P. Remon, and C. Vervaet, *Near infrared and raman spectroscopy for the in-process monitoring of pharmaceutical production processes.* International Journal of Pharmaceutics, 2011. **417**(1-2): p. 32-47.

157. Nieuwmeyer, F.J., M. Damen, A. Gerich, F. Rusmini, K. van der Voort Maarschalk, and H. Vromans, *Granule characterization during fluid bed drying by development of a near infrared method to determine water content and median granule size.* Pharmaceutical Research, 2007. **24**(10): p. 1854-61.

158. Andersson, M., S. Folestad, J. Gottfries, M.O. Johansson, M. Josefson, and K.G. Wahlund, *Quantitative analysis of film coating in a fluidized bed process by in-line nir spectrometry and multivariate batch calibration.* Analytical Chemistry, 2000. **72**(9): p. 2099-108.

159. Gendre, C., M. Genty, M. Boiret, M. Julien, L. Meunier, O. Lecoq, M. Baron, P. Chaminade, and J.M. Pean, *Development of a process analytical technology (pat) for in-line monitoring of film thickness and mass of coating materials during a pan coating operation.* European Journal of Pharmaceutical Sciences, 2011. **43**(4): p. 244-50.

160. Prats-Montalbán, J.M., J.I. Jerez-Rozo, R.J. Romañach, and A. Ferrer, *Multivariate image analysis and near infrared chemical imaging for characterisation of micro-mixing in polymeric thin films.* NIR news, 2014. **25**(6): p. 4-7.

161. Vakili, H., H. Wickstrom, D. Desai, M. Preis, and N. Sandler, *Application of a handheld nir spectrometer in prediction of drug content in inkjet printed orodispersible formulations containing prednisolone and levothyroxine.* International Journal of Pharmaceutics, 2017. **524**(1-2): p. 414-423.

162. Foo, W.C., E. Widjaja, Y.M. Khong, R. Gokhale, and S.Y. Chan, *Application of miniaturized near-infrared spectroscopy for quality control of extemporaneous orodispersible films.* Journal of Pharmaceutical and Biomedical Analysis, 2018. **150**: p. 191-198.

163. Hammes, F., T. Hille, and T. Kissel, *Reflectance infrared spectroscopy for in-line monitoring of nicotine during a coating process for an oral thin film.* Journal of Pharmaceutical and Biomedical Analysis, 2014. **89**: p. 176-82.

164. Zhang, J., Y. Ying, B. Pielecha-Safira, E. Bilgili, R. Ramachandran, R. Romanach, R.N. Dave, and Z. Iqbal, *Raman spectroscopy for in-line and off-line quantification of poorly soluble drugs in strip films.* International Journal of Pharmaceutics, 2014. **475**(1-2): p. 428-37.

165. Inoue, M., O. Kiefer, B. Fischer, and J. Breitkreutz, *Raman monitoring of semi-continuously manufactured orodispersible films for individualized dosing.* Journal of Drug Delivery Science and Technology, 2020: p. 102224.

166. Dahm, D.J., E.W. Ciurczak, and K.H. Norris, *Effect of particle size on absorbance (for real).* NIR news, 2005. **16**(4): p. 4-5.

167. Duy, P.K., S. Chun, Y. Lee, and H. Chung, *Investigation of the particle size-dependent near-infrared spectral features of binary mixture samples in conjunction with monte carlo simulation and the influence of particle size on the accuracy of quantitative analysis.* Analyst, 2018. **143**(18): p. 4306-4315.

168. Ghoroi, C., L. Gurumurthy, D.J. McDaniel, L.J. Jallo, and R.N. Davé, *Multi-faceted characterization of pharmaceutical powders to discern the influence of surface modification.* Powder Technology, 2013. **236**: p. 63-74.

169. Centkowska, K., E. Lawrecka, and M. Sznitowska, *Technology of orodispersible polymer films with micronized loratadine-influence of different drug loadings on film properties.* Pharmaceutics, 2020. **12**(3).

170. Ortega-Zuñiga, C., K. Reyes-Maldonado, R. Méndez, and R.J. Romañach, *Study of near infrared chemometric models with low heterogeneity films: The role of optical sampling and spectral preprocessing on partial least squares errors.* Journal of Near Infrared Spectroscopy, 2017. **25**(2): p. 103-115.

171. Mateo-Ortiz, D., Y. Colon, R.J. Romañach, and R. Méndez, *Analysis of powder phenomena inside a fette 3090 feed frame using in-line nir spectroscopy.* Journal of Pharmaceutical and Biomedical Analysis, 2014. **100**: p. 40-49.

172. Martínez, L., A. Peinado, L. Liesum, and G. Betz, *Use of near-infrared spectroscopy to quantify drug content on a continuous blending process: Influence of mass flow and rotation speed variations.* European Journal of Pharmaceutics and Biopharmaceutics, 2013. **84**(3): p. 606-615.

173. Esbensen, K.H., A.D. Román-Ospino, A. Sanchez, and R.J. Romañach, *Adequacy and verifiability of pharmaceutical mixtures and dose units by variographic analysis (theory of sampling)–a call for a regulatory paradigm shift.* International Journal of Pharmaceutics, 2016. **499**(1-2): p. 156-174.

174. Razuc, M., A. Grafia, L. Gallo, M.V. Ramirez-Rigo, and R.J. Romanach, *Near-infrared spectroscopic applications in pharmaceutical particle technology.* Drug Development and Industrial Pharmacy, 2019. **45**(10): p. 1565-1589.

175. Hifumi, H., A.V. Ewing, and S.G. Kazarian, *Atr-ftir spectroscopic imaging to study the drying and dissolution of pharmaceutical polymer-based films.* International Journal of Pharmaceutics, 2016. **515**(1-2): p. 57-68.

176. Kimber, J.A., M. Gerst, and S.G. Kazarian, *Fast drying and film formation of latex dispersions studied with ftir spectroscopic imaging.* Langmuir, 2014. **30**(45): p. 13588-95.

177. Domokos, A., A. Balogh, D. Denes, G. Nyerges, L. Zodi, B. Farkas, G. Marosi, and Z.K. Nagy, *Continuous manufacturing of orally dissolving webs containing a poorly soluble drug via electrospinning.* European Journal of Pharmaceutical Sciences, 2019. **130**: p. 91-99.

178. Alhayali, A., P.R. Vuddanda, and S. Velaga, *Silodosin oral films: Development, physico-mechanical properties and in vitro dissolution studies in simulated saliva.* Journal of Drug Delivery Science and Technology, 2019. **53**.

179. Buch, P., P. Holm, J.Q. Thomassen, D. Scherer, R. Branscheid, U. Kolb, and P. Langguth, *Ivivc for fenofibrate immediate release tablets using solubility and permeability as in vitro predictors for pharmacokinetics.* Journal of Pharmaceutical Sciences, 2010. **99**(10): p. 4427-36.

180. Gaynor, C., A. Dunne, and J. Davis, *A comparison of the prediction accuracy of two ivivc modelling techniques.* Journal of Pharmaceutical Sciences, 2008. **97**(8): p. 3422-32.

181. Sankalia, J.M., M.G. Sankalia, and R.C. Mashru, *Drug release and swelling kinetics of directly compressed glipizide sustained-release matrices: Establishment of level a ivivc.* Journal of controlled release, 2008. **129**(1): p. 49-58.

182. Buchwald, P., *Direct, differential-equation-based in-vitro-in-vivo correlation (ivivc) method.* Journal of Pharmacy and Pharmacology, 2003. **55**(4): p. 495-504.

183. Vetchý, D., H. Landová, J. Gajdziok, P. Doležel, Z. Daněk, and J. Štembírek, *Determination of dependencies among in vitro and in vivo properties of prepared mucoadhesive buccal films using multivariate data analysis.* European Journal of Pharmaceutics and Biopharmaceutics, 2014. **86**(3): p. 498-506.